

Unified Fracture Design

Bridging the gap between theory and practice



Michael Economides, Ronald Oligney, Peter Valkó

Unified Fracture Design
Bridging the Gap Between Theory and Practice

Unified Fracture Design

Bridging the Gap Between Theory and Practice

Michael Economides

Ronald Oligney

Peter Valkó

Orsa Press

Alvin, Texas

Unified Fracture Design

Copyright © 2002 by Orsa Press

All rights, including reproduction by photographic or electronic process and translation into other languages are fully reserved under the International Copyright Union, the Universal Copyright Convention, and the Pan-American Copyright Convention. Reproduction of this book in whole or in part in any manner without written permission from the publisher is prohibited.

Orsa Press
P.O. Box 2569
Alvin, TX 77512

10 9 8 7 6 5 4 3 2 1

Library of Congress Cataloging-in-Publication Data

Economides, Michael J.

Unified fracture design : bridging the gap between theory and practice / Michael Economides, Ronald Oligney, Peter Valkó
p. cm.

Includes bibliographical references and index.

ISBN 0-9710427-0-5 (alk. paper)

1. Oil wells—Hydraulic fracturing. I. Oligney, Ronald E.
II. Valkó, Peter, 1950- III. Title.

TN871.E335 2002
622'.3382—dc21

2002025793

Printed in the United States of America

Contents

CHAPTER 1

Hydraulic Fracturing for Production or Injection Enhancement 1

- **FRACTURING AS COMPLETION OF CHOICE 1**
- **BASIC PRINCIPLES OF UNIFIED FRACTURE DESIGN 4**
 - Fractured Well Performance 5
 - Sizing and Optimization 7
 - Fracture-to-Well Connectivity 8
- **THE TIP SCREENOUT CONCEPT AND OTHER ISSUES
IN HIGH PERMEABILITY FRACTURING 9**
 - Tip Screenout Design 10
 - Net Pressure and Leakoff in the High Permeability Environment 11
 - Candidate Selection 12
- **“BACK OF THE ENVELOPE” FRACTURE DESIGN 14**
 - Design Logic 14
 - Fracture Design Spreadsheet 14

CHAPTER 2

How To Use This Book 17

- **STRUCTURE OF THE BOOK 17**
- **WHICH SECTIONS ARE FOR YOU 18**
 - Fracturing Crew 19

CHAPTER 3

Well Stimulation as a Means to Increase the Productivity Index 23

- PRODUCTIVITY INDEX 23
- THE WELL-FRACTURE-RESERVOIR SYSTEM 26
 - PROPPANT NUMBER 27
- Well Performance for Low and Moderate Proppant Numbers 32
 - OPTIMUM FRACTURE CONDUCTIVITY 35
 - DESIGN LOGIC 38

CHAPTER 4

Fracturing Theory 39

- LINEAR ELASTICITY AND FRACTURE MECHANICS 39
 - FRACTURING FLUID MECHANICS 42
- LEAKOFF AND VOLUME BALANCE IN THE FRACTURE 46
 - Formal Material Balance: The Opening-Time Distribution Factor 46
 - Constant Width Approximation (Carter Equation II) 48
 - Power Law Approximation to Surface Growth 48
 - Detailed Leakoff Models 50
- BASIC FRACTURE GEOMETRIES 50
 - Perkins-Kern Width Equation 51
 - Khrstianovich-Zhel'tov-Geertsma-deKlerk Width Equation 53
 - Radial (Penny-shaped) Width Equation 54

CHAPTER 5

Fracturing of High Permeability Formations 57

- THE EVOLUTION OF THE TECHNIQUE 57
- HPF IN VIEW OF COMPETING TECHNOLOGIES 60
 - Gravel Pack 60
 - High-Rate Water Packs 62
- PERFORMANCE OF FRACTURED HORIZONTAL WELLS
IN HIGH PERMEABILITY FORMATIONS 62

- **DISTINGUISHING FEATURES OF HPF** 63
 - The Tip Screenout Concept 63
 - Net Pressure and Fluid Leakoff 66
 - Net Pressure, Closure Pressure, and Width in Soft Formations 66
 - Fracture Propagation 66
- **LEAKOFF MODELS FOR HPF** 67
 - Fluid Leakoff and Spurt Loss as Material Properties: The Carter Leakoff Model with Nolte's Power Law Assumption 67
 - Filter Cake Leakoff Model According to Mayerhofer, et al. 68
 - Polymer-Invaded Zone Leakoff Model of Fan and Economides 70
- **FRACTURING HIGH PERMEABILITY GAS CONDENSATE RESERVOIRS** 72
 - Optimizing Fracture Geometry in Gas Condensate Reservoirs 74
 - **EFFECT OF NON-DARCY FLOW IN THE FRACTURE** 76
 - Definitions and Assumptions 77
 - Case Study for the Effect of Non-Darcy Flow 80

CHAPTER 6

Fracturing Materials 83

- **FRACTURING FLUIDS** 84
 - **FLUID ADDITIVES** 85
 - **PROPPANTS** 87
 - Calculating Effective Closure Stress 88
- **FRACTURE CONDUCTIVITY AND MATERIALS SELECTION IN HPF** 91
 - Fracture Width as a Design Variable 91
 - Proppant Selection 93
 - Fluid Selection 94

CHAPTER 7

Fracture Treatment Design 101

- **MICROFRACTURE TESTS** 101
 - **MINIFRACS** 102
- **TREATMENT DESIGN BASED ON THE UNIFIED APPROACH** 109
 - Pump Time 110
 - Proppant Schedule 113
 - Departure from the Theoretical Optimum 118
 - TSO Design 119

- PUMPING A TSO TREATMENT 120
 - Swab Effect Example 121
 - Perforations for HPF 122
- PRE-TREATMENT DIAGNOSTIC TESTS FOR HPF 122
 - Step-Rate Tests 123
 - Minifrac 125
 - Pressure Falloff Tests 126
 - Bottomhole Pressure Measurements 126

CHAPTER 8

Fracture Design and Complications 129

- FRACTURE HEIGHT 129
 - Fracture Height Map 132
 - Practical Fracture Height Determination 133
- TIP EFFECTS 134
- NON-DARCY FLOW IN THE FRACTURE 135
- COMPENSATING FOR FRACTURE FACE SKIN 136
- EXAMPLES OF PRACTICAL FRACTURE DESIGN 137
 - A Typical Preliminary Design—Medium Permeability Formation: MPF01 137
 - Pushing the Limit—Medium Permeability Formation: MPF02 142
 - Proppant Embedment: MPF03 145
 - Fracture Design for High Permeability Formation: HPF01 148
 - Extreme High Permeability: HPF02 152
 - Low Permeability Fracturing: LPF01 157
- SUMMARY 162

CHAPTER 9

Quality Control and Execution 163

- FRACTURING EQUIPMENT 164
 - EQUIPMENT LIST 166
 - Water Transfer and Storage 166
 - Proppant Supply 167
 - Slurrification and Blending 168
 - Pumping 169
 - Monitoring and QA/QC 172
 - Miscellaneous 174
- SPECIAL INSTRUCTIONS ON HOOK-UP 174
 - Spotting the Equipment 174

- Fluid Supply-to-Blender 177
 - Proppant Supply 177
 - Frac Pumps 177
 - Manifold-to-Well 178
- Monitoring/Control Equipment and Support Personnel 179
- STANDARD FRACTURING QA PROCEDURES 180
 - FORCED CLOSURE 181
 - QUALITY CONTROL FOR HPF 183

CHAPTER 10

Treatment Evaluation 185

- REAL-TIME ANALYSIS 185
- HEIGHT CONTAINMENT 186
- LOGGING METHODS AND TRACERS 188
- A WORD ON FRACTURE MAPPING 189
 - WELL TESTING 190
- EVALUATION OF HPF TREATMENTS—A UNIFIED APPROACH 193
 - Production Results 193
 - Evaluation of Real-Time HPF Treatment Data 194
 - Post-Treatment Well Tests in HPF 195
 - Validity of the Skin Concept in HPF 197
 - SLOPES ANALYSIS 197
 - Assumptions 198
 - Restricted Growth Theory 199
 - Slopes Analysis Algorithms 201

Appendices

- A: NOMENCLATURE 207
- B: GLOSSARY 211
- C: BIBLIOGRAPHY 219
- D: FRACTURE DESIGN SPREADSHEET 227
- E: MINIFRAC SPREADSHEET 233
- F: STANDARD PRACTICES AND QC FORMS 239
- G: SAMPLE FRACTURE PROGRAM 251

Index 259

Preface

The purpose of writing this book is to establish a unified design methodology for hydraulic fracture treatments, a long established well stimulation activity in the petroleum and related industries. Few activities in the industry hold such potential to improve well performance both profitably and reliably.

The word “unified” has been selected deliberately to denote both the integration of all the highly diverse technological aspects of the process, but also to dispel the popular notion that there is one type of treatment that applies to low-permeability and another to high-permeability reservoirs. It is natural, even for experienced practitioners to think so because traditional targets have been low-permeability reservoirs while the fracturing of high-permeability formations has sprung from the gravel pack, sand control practice.

The key idea is that treatment sizes can be unified because they can be best characterized by the dimensionless Proppant Number, which determines the theoretically optimum fracture dimensions at which the maximum productivity or injectivity index can be obtained. Technical constraints should be satisfied in such a way that the design departs from the theoretical optimum only to the necessary extent. With this approach, difficult topics such as high- versus low-permeability fracturing, extensive height growth, non-Darcy flow, and proppant embedment are treated in a transparent and unified way, providing the engineer with a logical and coherent design procedure.

A design software package is included with the book.

The authors' backgrounds span the entire spectrum of technical, research, development, and field applications in practically all geographic and reservoir type settings. It is their desire that this book finds its appropriate place in everyday practice.

1

Hydraulic Fracturing for Production or Injection Enhancement

FRACTURING AS COMPLETION OF CHOICE

This book has the ambition to do something that has not been done properly before: to unite the gap between theory and practice in what is arguably the most common stimulation/well completion technique in petroleum production. Even more important, the book takes a new and ascendant position on the most critical link in the sequence of events in this type of well stimulation—the sizing and the design of hydraulic fracture treatments.

Fracturing was first employed to improve production from marginal wells in Kansas in the late 1940s (Figure 1-1). Following an explosion of the practice in the mid-1950s and a considerable surge in the mid-1980s, massive hydraulic fracturing (MHF) grew to become a dominant completion technique, primarily for low permeability reservoirs in North America. By 1993, 40 percent of new oil wells and 70 percent of gas wells in the United States were fracture treated.

With improved modern fracturing capabilities and the advent of high permeability fracturing (HPF), which in the vernacular has been referred to as “frac & pack” or variants, fracturing has expanded further to become the completion of choice for all types of wells in the United States, but particularly natural gas wells (see Figure 1-2).

2 ■ *Unified Fracture Design*



FIGURE 1-1. An early hydraulic fracture treatment, circa. 1949. (*Source:* Halliburton.)

The tremendous advantage in fracturing most wells is now largely accepted. Even near water or gas contacts, considered the bane of fracturing, HPF is finding application because it offers controlled fracture extent and limits drawdown (Mullen et al., 1996; Martins et al., 1992). The rapid ascent of high permeability fracturing from a few isolated treatments before 1993 (Martins et al., 1992; Grubert, 1991; Ayoub et al., 1992) to some 300 treatments per year in the United States by 1996 (Tiner et al., 1996) was the start to HPF becoming a dominating optimization tool for integrated well completion and production. Today, it is established as one of the major recent developments in petroleum production.

The philosophy of this book hinges on the overriding commonality in fracture design that transcends the value of the reservoir permeability. There is a strong theoretical foundation to this approach, which will be outlined in this book. Hence the title, *Unified Fracture Design*, which suggests the connection between theory and practice, but also that the design process cuts across all petroleum reservoirs—low permeability to high permeability, hard rock to soft rock. And indeed, it is common to all.

There is substantial room for additional growth of hydraulic fracturing in the worldwide petroleum industry, as well as other industries. It is estimated that hydraulic fracturing may add several hundred thousand barrels per day from existing wells in a number of countries.

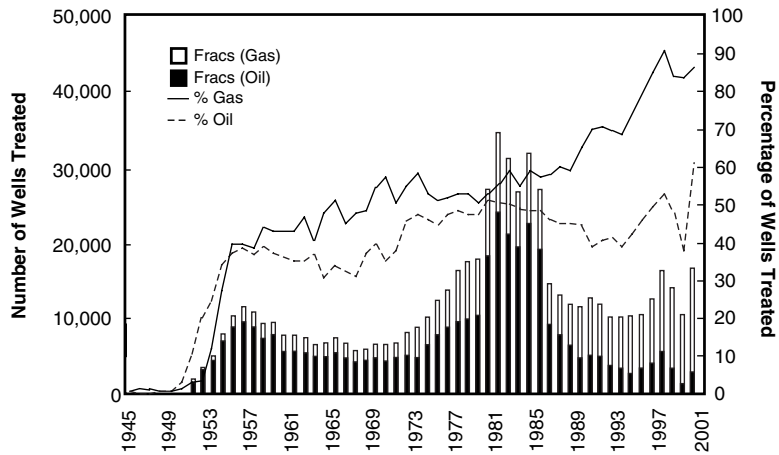


FIGURE 1-2. Fracturing as “completion of choice” in U.S. oil and gas wells. (Source: Schlumberger.)

This can be accomplished if the process is undertaken in a serious and concerted way so that the economy of scale influences the cost of the treatments and, hence, the overall economics.

There are two frequently encountered impediments to substantial applications of hydraulic fracturing:

1. A widespread misunderstanding that the process is still only for low permeability reservoirs (e.g., less than 1 md), or that it is the last refuge for enhancing well production or injection performance, to be tried only if everything else fails. The latter carries along with it an often unjustifiable phobia that hydraulic fracturing is dangerous, that it accelerates the onset of water production, that it increases the water cut or affects zonal isolation, and so on. The more serious associated problem is that using fracturing as a last, at times desperate, resort implies unplanned stimulation that may suffer from a number of problems (such as well deviation and inadequate perforating), which, in turn, may almost guarantee disappointing results. A final related problem is the notion that high permeability fracturing applies only to those reservoirs that need sand production control. This is clearly not the case, and reservoirs with permeabilities of several hundred millidarcies are now routinely fractured.
2. At times, engineers in various companies outside of North America may actually try fracturing, but a treatment is done so rarely

4 ■ *Unified Fracture Design*

and so haphazardly that it is bound to be expensive, such that the cost cannot be justified even if the incremental production is substantial. Hydraulic fracturing is a massive operation with a very large complement of equipment, complicated and demanding fluids and proppants, and a wide spectrum of ancillary and people-intensive engineering and operational demands. Costs assigned to individual, isolated jobs—e.g., one or two treatments carried out every three to six months—are essentially prohibitive. Coupled with an occasional job failure, sketchy and spotty application of hydraulic fracturing is almost assured of economic failure and the dampening of any desire to apply it further.

Virtually no petroleum operation carries such a differential price tag among areas where it is applied in a widespread and massive way, such as North America and offshore in the North Sea, and elsewhere. In North America, over 60 percent of all oil wells and 85 percent of all gas wells are hydraulically fractured, and the percentages are still increasing. Yet, consider this: a 100-ton proppant treatment in the United States, at the time of this writing, costs less than \$100,000. Exactly the same treatment, with the same equipment and the same service company, for example in Venezuela or Oman, is likely to cost at least \$1 million, and it can cost as much as \$2 million.

At the same time, virtually no other petroleum technology carries a larger incremental asset. The hundreds-of-thousands to millions of barrels per day of worldwide production increase that we project assumes that the percentage of existing wells being hydraulically fractured approaches that of oil wells in the United States (60 percent), and the incremental production realized from each well is just 25 percent over the pre-treatment state. The latter implies the very modest assumptions that all existing wells continue to produce, and that fracturing would result in a very achievable average “skin” equal to -2 . In fact, the incremental production capacity from a massive stimulation campaign with adequate equipment and well-trained people is likely to be much higher.

BASIC PRINCIPLES OF UNIFIED FRACTURE DESIGN

Hydraulic fracturing entails injecting fluids in an underground formation at a pressure that is high enough to induce a parting of the formation.

Granulated materials—called “proppants,” which range from natural sands to rather expensive synthetic materials—are pumped into the created fracture as a slurry. They hold open, or “prop,” the created fracture after the injection pressure used to generate the fracture has been relieved.

The fracture, filled with proppant, creates a narrow but very conductive flow path toward the wellbore. This flow path has a very large permeability, frequently five to six orders of magnitude larger than the reservoir permeability. It is most often narrow in one horizontal direction, but can be quite long in the other horizontal direction and can cover a significant height. Typical intended propped widths in low permeability reservoirs are on the order of 0.25 cm (0.1 in.), while the length can be several hundred meters. In high permeability reservoirs, the targeted fracture width (deliberately affected by the design and execution) is much larger, perhaps as high as 5 cm (2 in.), while the length might be as short as 10 meters (30 ft).

In almost all cases, an overwhelming part of the production comes into the wellbore through the fracture; therefore, the original near-wellbore damage is “bypassed,” and the pre-treatment skin does not affect the post-treatment well performance.

Fractured Well Performance

The performance of a fractured well can be described in many ways. One common way is to forecast the production of oil, gas, and even water as a function of time elapsed after the fracturing treatment. However, post-treatment production is influenced by many decisions that are not crucial to the treatment design itself. The producing well pressure, for example, may or may not be the same as the pre-treatment pressure, and may or may not be held constant over time. Even if, for the sake of evaluation, an attempt is made to set all well operating parameters the same before and after the treatment, comparison over time is still obfuscated by the accelerated nature of reservoir depletion in the presence of a hydraulic fracture.

Thus, in a preliminary sizing and optimization phase, it is imperative to use a simple performance index that describes the expected and actual improvement in well performance due to the treatment.

In unified fracture design, we consider a very simple and straightforward performance indicator: the *pseudo-steady state productivity index*. The improvement in this variable describes the actual effect of the propped fracture on well performance. Realizing the maximum

possible pseudo-steady state productivity index, for all practical purposes, means that the fracture will not under-perform any other possible realization of the same propped volume, even if the well produces for a considerable time period in the so-called “transient” regime. While this statement might not appear plausible at first, the experienced production engineer will understand it by thinking of the transient flow period as a continuous increase in *drainage area* in which the pseudo-steady state has already been established. Considerable cumulative production can only come from a large drained area, and hence that pseudo-steady state productivity index must be maximized, which corresponds to the finally formed drainage area.

Fracture length and *dimensionless fracture conductivity* are the two primary variables that control the productivity index of a fractured well. Dimensionless fracture conductivity is a measure of the relative ease with which produced fluids flow inside the fracture compared to the ability of the formation to feed fluids *into* the fracture. It is calculated as the product of fracture permeability and fracture width, divided by the product of reservoir permeability and fracture (by convention, half-) length.

In low permeability reservoirs, the fracture conductivity is *de facto* large, even if only a narrow propped fracture has been created and a long fracture length is needed. A post-treatment skin can be as negative as -7 , leading to several folds-of-increase in well performance compared to the unstimulated well.

For high permeability reservoirs, a large fracture width is essential for adequate fracture performance. Over the last several years, a technique known as tip screenout (TSO) has been developed, which allows us to deliberately arrest the lateral growth of a hydraulic fracture and subsequently inflate its width, exactly to affect a larger conductivity.

For a fixed volume of proppant placed in the formation, a well will deliver the maximum production or injection rate when the dimensionless fracture conductivity is near unity. In other words, a dimensionless fracture conductivity around one (or more precisely, 1.6, as shown in Chapter 3) is the physical optimum, at least for treatments not involving extremely large quantities of proppant. Larger values of the dimensionless fracture conductivity would mean relatively shorter-than-optimum fracture lengths and, thus, the flow from the reservoir into the fracture would be unnecessarily restricted. Dimensionless fracture conductivity values *smaller* than unity would mean less-than-optimum fracture *width*, rendering the fracture as a bottleneck to optimum production.

There are a number of secondary issues that complicate the picture—early time transient flow regime, influence of reservoir boundaries, non-Darcy flow effects, and proppant embedment, just to mention a few. Nevertheless, these effects can be correctly taken into account only if the role of dimensionless fracture conductivity is understood.

It is possible that in certain theaters of operation the practical optimum may be different than the physical optimum. In some cases, the theoretically indicated fracture geometry may be difficult to achieve because of physical limitations imposed either by the available equipment, limits in the fracturing materials, or the mechanical properties of the rock to be fractured. However, aiming to maximize the well productivity or injectivity is an appropriate first step in the fracture design.

Sizing and Optimization

The term “optimum” as used above means the maximization of a well’s productivity, within the constraint of a certain treatment size. Hence, a decision on treatment size should actually precede (or go hand-in-hand with) an optimization based on the dimensionless fracture conductivity criterion.

For a long time, practitioners considered fracture half-length as a convenient variable to characterize the size of the created fracture. That tradition emerged because it was not possible to independently change fracture length and width, and because length had a primary effect on productivity in low permeability formations. In unified fracture design, where both low and high permeability formations are considered, the best single variable to characterize the size of a created fracture is the *volume of proppant* placed in the productive horizon, or “pay.”

Obviously, the total volume of proppant placed in the pay interval is always less than the total proppant injected. From a practical point of view, treatment sizing means deciding how much proppant to inject. When sizing the treatment, an engineer must be aware that increasing the injected amount of proppant by a certain quantity x will not necessarily increase the amount of proppant reaching the pay layer by the same quantity, x . We will refer to the ratio of the two proppant volumes (i.e., the volume of proppant placed in the pay interval divided by the total volume injected into the well) as the *volumetric proppant efficiency*.

By far the most critical factor in determining volumetric proppant efficiency is the ratio of created fracture height to the net pay thickness.

Extensive height growth limits the volumetric proppant efficiency, and is something that we generally try to avoid. (The possibility of intersecting a nearby water table is another important reason to avoid excessive height growth.)

Actual selection of the amount of proppant indicated for injection is primarily based on economics, the most commonly used criterion being the net present value (NPV). As with most engineering activities, costs increase almost linearly with the size of the treatment, but after a certain point, the revenues increase only marginally. Thus, there is an optimum treatment size, the point at which the NPV of incremental revenue, balanced against treatment costs, is a maximum.

The optimum size can be determined if some method is available to predict the maximum possible productivity increase achievable with a certain amount of proppant. Unified fracture design makes extensive use of this fact, given that the maximum achievable productivity increase is already determined by the volume of proppant in the pay. Many of the operational details are subsumed by the basic decision on treatment size, making possible a simple yet robust design process.

Therefore, we employ the concept of “volume of proppant reaching the pay” or simply “propped volume in the pay” as the key decision variable in the sizing phase of the unified fracture design procedure. To handle it correctly, the amount of proppant indicated for injection and the volumetric proppant efficiency must be determined.

Fracture-to-Well Connectivity

While the maximum achievable improvement of productivity is determined by the propped volume in the pay, several additional conditions must be satisfied *en route* to a fracture that actually realizes this potential improvement. One of the crucial factors is to establish an optimum compromise between the length and width (or to depart from the optimum only as much as necessary, if required by operational constraints). As previously explained, the optimum dimensionless fracture conductivity is the variable that helps us to find the right compromise. However, another condition is equally important. It is related to the connectivity of the fracture to the well.

A reservoir at depth is under a state of stress that can be characterized by three principal stresses: one vertical, which in almost all cases of deep reservoirs (depth greater than 500 meters, 1500 ft) is the largest of the three, and two horizontal, one minimum and one maximum. A hydraulic fracture will be normal to the smallest stress,

leading to vertical hydraulic fractures in almost all petroleum production applications. The azimuth of these fractures is pre-ordained by the natural state of earth stresses. As such, deviated or horizontal wells that are to be fractured should be drilled in an orientation that agrees with this azimuth. Vertical wells, of course, naturally coincide with the fracture plane.

If the well azimuth does not coincide with the fracture plane, the fracture is likely to initiate in one plane and then twist, causing considerable “tortuosity” *en route* to its final azimuth—normal to the minimum stress direction. Vertical wells with vertical fractures or perfectly horizontal wells drilled deliberately along the expected fracture plane result in the best aligned well-fracture systems. Other well-fracture configurations are subject to “choke effects,” unnecessarily decreasing the productivity of the fractured well. Perforations and their orientation may also be a source of problems during the execution of a treatment, including multiple fracture initiations and premature screenouts caused by tortuosity effects.

The dimensionless fracture conductivity in low permeability reservoirs is naturally high, so the impact of choke effects from the phenomena described above is generally minimized; to avoid tortuosity, point source fracturing is frequently employed.

Fracture-to-well connectivity is considered today as a critical point in the success of high permeability fracturing, often dictating the well azimuth (e.g., drilling S-shape vertical wells) or indicating horizontal wells drilled longitudinal to the fracture direction. Perforating is being revisited, and alternatives, such as hydro-jetting of slots, are considered by the most advanced practitioners. While some models incorporate complex well-fracture geometries with choke and other effects, the many uncertainties prevent us from predicting performance. Rather, we are limited to *explain* the performance once post-treatment well test and production information become available. In the design phase, we try to make decisions that minimize the likelihood of such unnecessary reductions in productivity.

THE TIP SCREENOUT CONCEPT AND OTHER ISSUES IN HIGH PERMEABILITY FRACTURING

Because high permeability fracturing has the most fertile possibility for expansion in petroleum operations worldwide, key issues for this

type of well completion are described below. The purpose is to identify those features that distinguish high permeability fracturing from conventional hydraulic fracturing.

Tip Screenout Design

The critical elements of high permeability fracturing treatment design, execution and treatment behavioral interpretation are substantially different than for conventional fracturing treatments. In particular, HPF relies on a carefully timed “tip screenout,” or TSO, to limit fracture growth and allow for fracture inflation and packing. The TSO occurs when sufficient proppant has concentrated at the leading edge of the fracture to prevent further fracture extension. Once the fracture growth has been arrested (and assuming the pump rate is larger than the rate of leakoff to the formation), continued pumping will inflate the fracture, i.e., increase the fracture width. Tip screenout and fracture inflation should be accompanied by an increase in net fracturing pressure. Thus, the treatment can be conceptualized in two distinct stages: fracture creation (equivalent to conventional designs) and fracture inflation/packing (after tip screenout).

Creation of the fracture and arrest of its growth (i.e., the tip screenout) is accomplished by injecting a relatively small “pad” of clean fluid (no sand) followed by a “slurry” containing 1–4 lbs of sand per gallon of fluid (ppg). Once the fracture growth has been arrested, further injection builds fracture width and allows injection of a high-concentration slurry (e.g., 10–16 ppg). Final *areal proppant concentrations* of 20 lb_m/sq ft are possible. A usual practice is to retard the injection rate near the end of the treatment (coincidental with opening the annulus to flow) to dehydrate and pack the fracture near the well. Rate reductions may also be used to force a tip screenout in cases where no TSO event is observed on the downhole pressure record.

Frequent field experience suggests that the tip screenout can be difficult to model, affect, or even detect. There are many reasons for this, including a tendency toward overly conservative design models (resulting in no TSO), partial or multiple tip screenout events, and inadequate pressure monitoring practices.

Accurate bottomhole measurements are imperative for meaningful treatment evaluation and diagnosis. Calculated bottomhole pressures are unreliable because of the sizeable and complex friction pressure effects associated with pumping high proppant slurry concentrations through small diameter tubulars and service tool crossovers.

Surface data may indicate that a TSO event has occurred when the bottomhole data shows no evidence, and vice versa.

Net Pressure and Leakoff in the High Permeability Environment

The entire HPF process is dominated by *net pressure* and *fluid leakoff* considerations. First, high permeability formations are typically soft and exhibit low elastic modulus values, and second, the fluid volumes are relatively small and leakoff rates high (high permeability, compressible reservoir fluids and non-wall building fracturing fluids). While traditional practices applicable to design, execution, and evaluation in hydraulic fracturing continue to be used in HPF, these are frequently not sufficient.

Net Pressure

Net pressure is the difference between the pressure at any point in the fracture and the pressure at which the fracture will close. This definition implies the existence of a unique *closure pressure*. Whether the closure pressure is a constant property of the formation or depends heavily on the pore pressure (or rather on the disturbance of the pore pressure relative to the long-term steady value) is an open question.

In high-permeability, soft formations it is difficult (if not impossible) to suggest a simple recipe to determine the closure pressure as classically derived from shut-in pressure decline curves. Furthermore, because of the low elastic modulus values, even small induced uncertainties in the net pressure are amplified into large uncertainties in the calculated fracture width.

Fracture propagation, the availability of sophisticated 3D models notwithstanding, is a very complex process and difficult to describe, even in the best of cases, because of the large number and often competing physical phenomena. The physics of fracture propagation in soft rock is even more complex, but it is reasonably expected to involve incremental energy dissipation and more severe tip effects when compared to hard rock fracturing. Again, because of the low modulus values, an inability to predict net pressure behavior may lead to a significant departure between predicted and actual treatment performance. Ultimately, the classic fracture propagation models may not reflect even the main features of the propagation process in high permeability rocks.

It is common practice for some practitioners to “predict” fracture propagation and net pressure features *ex post facto* using a computer fracture simulator. The tendency toward substituting clear models and physical assumptions with “knobs”—e.g., arbitrary stress barriers, friction changes (attributed to erosion if decreasing and sand resistance if increasing) and less than well understood properties of the formation expressed as dimensionless factors—does not help to clarify the issue. Other techniques are warranted and several are under development.

Leakoff

Considerable effort has been expended on laboratory investigation of the fluid leakoff process for high permeability cores. The results raise some questions about how effectively fluid leakoff can be limited by filtercake formation. In all cases, but especially in high permeability formations, the quality of the fracturing fluid is only one of the factors that influence leakoff, and often not the determining one. Transient fluid flow in the formation might have an equal or even larger impact. Transient flow cannot be understood by simply fitting an empirical equation to laboratory data. The use of models based on solutions to the fluid flow in porous media is an unavoidable step, and one that has already been taken by many.

Candidate Selection

The utility of high permeability fracturing extends beyond the obvious productivity benefits associated with bypassing near-well damage to include *sand control*. However, in HPF the issue is not mere sand control, which implies most often mechanical retention of migrating sand particles (and plugging), but rather sand *deconsolidation* control.

Increasingly, wellbore stability should be viewed in a holistic approach with horizontal wells and hydraulic fracture treatments. Proactive well completion strategies are critical to wellbore stability and sand-production control to reduce pressure drawdown while obtaining economically attractive rates. Reservoir candidate recognition for the correct well configurations is the key element. Necessary steps in candidate selection include appropriate reservoir engineering, formation characterization, wellbore stability calculations, and the combining of production forecasts with assessments of sand-production potential.

Complex Well-Fracture Configurations

Vertical wells are not the only candidates for hydraulic fracturing. Figure 1-3 shows some basic single-fracture configurations for vertical and horizontal wells. Horizontal wells that employ conventional or especially high permeability fracturing with the well drilled in the expected fracture azimuth (accepting a longitudinal fracture) appear to have, at least conceptually, a very promising prospect as discussed in Chapter 5. However, a horizontal well intended for a longitudinal fracture configuration would have to be drilled along the maximum horizontal stress. And this, in addition to well-understood drilling problems, may contribute to long-term formation stability problems.

Figure 1-4 illustrates two multi-fracture configurations. A rather sophisticated conceptual configuration would involve the combination of HPF with multiple-fractured vertical branches emanating from a horizontal “mother” well drilled above the producing formation. Of course, horizontal wells, being normal to the vertical stress, are generally more prone to wellbore stability problems. Such a configuration would allow for placement of the horizontal borehole in a competent, non-producing interval. There are other advantages to fracture treating a vertical section over a highly deviated or horizontal section: multiple starter fractures, fracture turning, and tortuosity problems are avoided; convergence-flow skins (choke effects) are much less of a concern; and the perforating strategy is simplified.

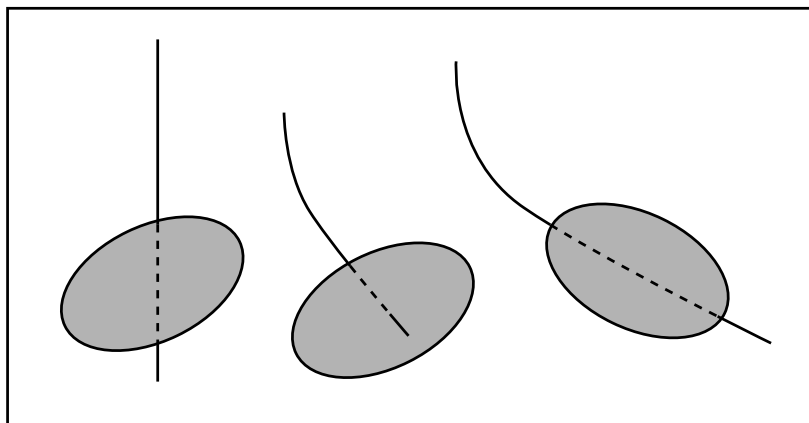


FIGURE 1-3. Single-fracture configurations for vertical and horizontal wells.

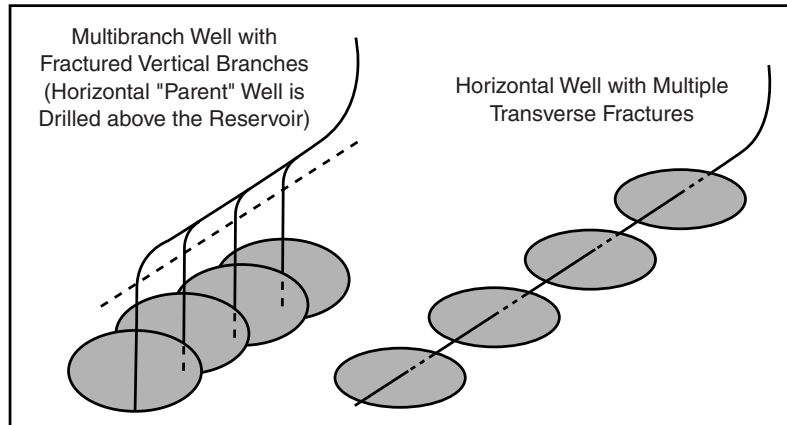


FIGURE 1-4. Multibranched, multiple-fracture configurations for horizontal wells.

“BACK OF THE ENVELOPE” FRACTURE DESIGN

Design Logic

In unified fracture design, we consider treatment size, specifically propped volume in the pay, as the primary decision variable. Once the basic decision on size is made, the optimum length and width are determined. These parameters are then revised in view of the technical constraints, and the target dimensions of the created fracture are set. A preliminary injection schedule is calculated that realizes the target dimensions and assures uniform placement of the indicated amount of proppant. If the optimum placement cannot be realized by traditional means, a TSO treatment is indicated. Even if the injected amount of proppant is already fixed, the volumetric proppant efficiency may change during the design process. It is extremely important that the basic decisions be made in an iterative manner, but without going into unnecessary details of fracture mechanics, fluid rheology, or reservoir engineering.

Fracture Design Spreadsheet

A simple spreadsheet, based on a transparent design logic, is an ideal tool to make preliminary design decisions and a primary evaluation of the executed treatment. The CD attached to the back cover of the

book contains such a spreadsheet, named HF2D. The HF2D Excel spreadsheet is a fast 2D software package for the design of traditional (moderate permeability and hard rock) and frac & pack (higher permeability and soft rock) fracture treatments.

Readers are strongly encouraged to use the spreadsheet while reading the book. By modifying various input parameters, an intuitive feel for their relative importance in treatment design and final fractured well performance can be rapidly acquired, an important but uncommon prospect in the era of complex 3D fracture simulators. The spreadsheet will help readers make the most important decisions and be aware of their consequences.

The attached spreadsheet is not necessarily intended as a substitute for more sophisticated software tools, but the rapid “back of the envelope” calculations that it affords can provide substantive fracture designs. In many cases, by virtue of restricting the analysis to important first-order considerations, the spreadsheet results are more robust than those provided by highly involved 3D fracture simulators. It is suggested that readers run parallel cases with one or more 3D simulators, if available, as an interesting exercise.

2

How To Use This Book

The purpose of this book is to transfer hydraulic fracturing technology and, especially, facilitate its execution. The various chapters supply information on candidate recognition, fracture treatment design, execution and evaluation, materials selection, quality control, and equipment specifications.

While the book includes late developments from some of the most respected practitioners of hydraulic fracturing in the world—genuine state-of-the-art technology—the entry point is deliberately low. That is, the book can also serve as a very useful primer for those being exposed to fracturing technology for the first time.

STRUCTURE OF THE BOOK

Chapters 1 through 10 provide a detailed narrative of the most important aspects across the spectrum of hydraulic fracturing activities.

Appendices A through G are reference material, including a glossary of fracturing terms; an extensive bibliography; data requirements and user instructions for the included design software; standard quality control practices and forms; and example fracturing procedures.

The CD attached to the back cover of the book contains two spreadsheets:

1. The HF2D Excel spreadsheet is a fast 2D software package for the design of traditional (moderate permeability and hard rock) and frac & pack (higher permeability and soft rock) fracture treatments.
2. The MF Excel spreadsheet is a minifrac (calibration test) evaluation package. Its main purpose is to extract the leakoff coefficient from pressure fall-off data.

Two industry-leading references are strongly recommended as addenda to this book:

- *Hydraulic Fracture Mechanics*, by Peter Valkó and Michael Economides, addresses the theoretical background of this seminal technology. It provides a fundamental treatment of basic phenomena such as elasticity, stress distribution, fluid flow, and the dynamics of the rupture process. Contemporary design and analysis techniques are derived and improved using a comprehensive and unified approach.
- *Stimulation Engineering Handbook*, by John Ely, aptly covers many issues of fracture treatment implementation and quality control. This is a very hands-on book, intended to drive execution performance and quality control.

Other reference books that contain abundant information by dozens of experts in the field include *Petroleum Well Construction*, edited by Michael Economides, Larry Watters, and Shari Dunn-Norman; *Reservoir Stimulation, Third Edition*, by Michael Economides and Ken Nolte; and the somewhat dated but classic volume, *SPE Monograph No. 12: Advances in Hydraulic Fracturing*, edited by John Gidley, Steve Holditch, Dale Nierode, and Ralph Veatch. While these books provide historical perspective as well as in-depth discussion and opinions (some controversial) on various details of the fracturing process, they are not recommended for a first reading because of the highly technical language and compartmentalized style of presentation.

WHICH SECTIONS ARE FOR YOU

Which sections of the book that you will use—whether it’s a quick review of the introductory material or a check of the glossary, reading

the chapter on fracturing fluids, only, or hands-on use of the design theory and software—depends on your role in the fracturing operation.

Neither this book nor any other technology transfer mechanism is useful apart from capable people. The following key personnel comprise the fracturing team and the targeted readership of this book.

Fracturing Crew

A fracturing crew is the absolute minimum and basic unit required for a fracturing treatment. The crew may consist of anywhere from 7 to 15 people, depending on the number of pumping units and the monitoring capability on location. Many of these people are trained to do multiple jobs, such as driving trucks, hooking up equipment, and installing and maintaining the monitoring instruments.

In addition to being trained on each piece of equipment that they will operate, each member of the fracturing crew should be conversant with the material in Chapter 10, On-Site Quality Control, and the accompanying Appendix F, Standard Practices and QC Forms.

The key people in any fracturing operation, in order of critical importance, are:

Frac-Crew Chief—Sometimes known as the *field engineer*, this is the person responsible on-site for proper execution of the job. He is a highly experienced person, either an engineer that has reverted into a field service manager position, or a highly gifted operator who has been promoted to the job. The crew chief directs fracturing operations from the monitoring van (“frac van”) and has complete responsibility for the operation, including safety. He communicates constantly by two-way radio with all pumping, blender, and proppant storage operators. He is certified to operate high pressure equipment. He understands the fracture design and is responsible for its implementation. He has complete authority to continue or shut down a job. (Note that while the pronoun “he” is used for clarity, there are several highly capable women currently practicing as fracturing engineers.)

This is not a job that can be learned gradually in a start-up operation. This individual must be identified through a careful search among qualified candidates. Extensive and relevant hands-on experience in fracture execution is a must. The frac-crew chief should be highly conversant with *Unified Fracture Design* in its entirety.

Desk Engineer—The desk engineer concept is practiced by many companies, within and external to the petroleum industry. Simply put, the

fracturing service company places one of its full-time staff permanently on location in each client producing company. The client is responsible to furnish a space (desk) at which the external employee (engineer) can sit and work, giving rise to the term *desk engineer*. This constant accessibility and the cross-pollination of needs (producing company) and capabilities (service company) can dramatically improve the range and success of application of a technology, and could be especially important for the rapid and necessarily massive introduction of hydraulic fracturing in a new operating area or country.

This individual will have the same aptitude as the frac-crew chief, but typically with somewhat less experience. Like the frac-crew chief, the desk engineer should become highly conversant with the entire fracturing book.

QA/QC Chemist—Any fracturing operation requires a chemist who is well versed in the chemistry and physics (rheology) of fracturing fluids and additives. This person operates a specially outfitted laboratory. The laboratory includes, in addition to all basic implements and working spaces (e.g., hoods), a Fann 50 high-pressure/high-temperature viscometer and possibly a fluid shear-history simulator. The chemist should have a background in polymer chemistry, or at least a good understanding of the subject matter, and should be trained in detecting the quality of proppant (visually, with a 100-magnification microscope).

The chemist is the field quality assurance/quality control (QA/QC) officer. Prior to the fracture treatment, he inspects the make-up water, fluid additives, and proppant to ensure that they are appropriate and that they are of high quality. During the treatment, he makes sure that the fracturing materials are blended in the correct proportions and at the proper time (e.g., in the case of delayed crosslinkers). He continues to spot check and approve the proppant quality in real-time for the duration of the treatment.

It is almost entirely the responsibility of the QC/QA chemist to understand Chapter 6 and Chapter 9 of this book, as well as Appendix F, and to revise them for company-specific needs. In addition, this person should fully digest the *Stimulation Engineering Handbook*.

Fracture Design Engineer—As the title suggests, this individual is responsible for design of the fracturing treatment. The fracture design engineer must master the basics of hydraulic fracturing, as included in Chapters 4 through 9, and should be proficient to run the included fracture design software. Depending on the magnitude of the fracturing activity, there could be several people trained to perform this task. In

small operations, the same person may double-up as the field engineer that performs real-time analysis of the treatment from the frac van (Chapter 10).

The fracture design engineer must have an engineering background, preferably petroleum engineering, and be dedicated to study the subtle and sometimes complex aspects of fracture design. Experience in the industry is desirable, but not necessary. With proper training, a gifted person can start functioning properly after several jobs. Ultimately, the fracturing engineer should be broadly conversant in fracture execution, fracturing fluid chemistry, and well completions. He should be able to make critical use of the additional literature recommended above.

3

Well Stimulation as a Means to Increase the Productivity Index

The primary goal of well stimulation is to increase the productivity of a well by removing damage in the vicinity of the wellbore or by superimposing a highly conductive structure onto the formation. Commonly used stimulation techniques include hydraulic fracturing, frac & pack, carbonate and sandstone matrix acidizing, and fracture acidizing. Any of these stimulation techniques can be expected to generate some increase in the productivity index, which, in turn, can be used either to increase the production rate or decrease the pressure drawdown. There is no need to explain the benefits of increasing the production rate. The benefits of decreased pressure drawdown are less obvious, but include minimizing sand production and water coning and/or shifting the phase equilibrium in the near-well zone to reduce condensate formation. Injection wells also benefit from stimulation in a similar manner.

To understand how stimulation increases productivity, basic production and reservoir engineering concepts are presented below.

PRODUCTIVITY INDEX

In discussing the productivity of a specific well, we think of a linear relation between the production rate and the driving force (pressure drawdown),

24 ■ Unified Fracture Design

$$q = J\Delta p \quad (3-1)$$

where the proportionality “constant” J is called the productivity index (PI). During its lifespan, a well is subject to several changes in flow conditions, but the two most important idealizations are constant production rate,

$$\Delta p = \frac{\alpha_1 B q \mu}{2\pi k h} p_D \quad (3-2)$$

and constant drawdown pressure,

$$q = \frac{2\pi k h \Delta p}{\alpha_1 B \mu} q_D \quad (3-3)$$

where k is the formation permeability, h is the pay thickness, B is the formation volume factor, μ is the fluid viscosity, and α_1 is a conversion constant (equal to 1 for a coherent system). Either the production rate (q) or the drawdown (Δp) are specified, and therefore used to define the dimensionless variables. Table 3-1 lists some of the well-known solutions to the radial diffusivity equation.

Because of the radial nature of flow, most of the pressure drop occurs near the wellbore, and any damage in this region significantly increases the pressure loss. The impact of damage near the well can be represented by the skin factor, s , added to the dimensionless pressure in the expression of the PI:

$$J = \frac{2\pi k h}{B\mu(p_D + s)} \quad (3-4)$$

The skin is another idealization, capturing the most important aspect of near-wellbore damage: the additional pressure loss caused by the

TABLE 3-1. Flow into an Undamaged Vertical Well

Flow Regime	Δp	p_D ($\approx 1/q_D$)
Transient (infinite acting reservoir)	$p_i - p_{wf}$	$p_D = -\frac{1}{2} Ei\left(-\frac{1}{4t_D}\right)$, where $t_D = \frac{kt}{\phi\mu c_r r_w^2}$
Steady state	$p_e - p_{wf}$	$p_D = \ln(r_e/r_w)$
Pseudo-steady state	$\bar{p} - p_{wf}$	$p_D = \ln(0.472r_e/r_w)$

damage is proportional to the production rate. Even with best drilling and completion practices, some kind of near-well damage is present in most cases. The skin can be considered as the measure of the “goodness” of a well. Other mechanical factors, not caused by damage *per se* may add to the skin effect. These may include bad perforations, partial well penetration, or undersized well completion equipment, and so on. If the well is damaged (or its productivity is less than the ideal reference value for any other reason), the skin factor is positive.

Well stimulation increases the productivity index. It is reasonable to look at any type of stimulation as an operation to reduce the skin factor. With the generalization to negative values of skin factor, even such stimulation treatments—which not only remove damage but also superimpose some new or improved conductivity paths—can be put into this framework. In the latter case, it is more correct to speak about *pseudo-skin factor*, indicating that stimulation causes some structural changes in the fluid flow path as well as removing damage.

As we explained in Chapter 1, crucial from the fracture design viewpoint is the pseudo-steady state productivity index:

$$J = \frac{q}{\bar{p} - p_{wf}} = \frac{2\pi kh}{\alpha_1 B \mu} J_D \quad (3-5)$$

where J_D is called the dimensionless productivity index.

For a well located in the center of a circular drainage area, the dimensionless productivity index in pseudo-steady state reduces to

$$J_D = \frac{1}{\ln \left[\frac{0.472 r_e}{r_w} \right] + s} \quad (3-6)$$

In the case of a propped fracture, there are several ways to incorporate the stimulation effect into the productivity index. One can use the pseudo-skin concept,

$$J_D = \frac{1}{\ln \left[\frac{0.472 r_e}{r_w} \right] + s_f} \quad (3-7)$$

or the equivalent wellbore radius concept,

$$J_D = \frac{1}{\ln \left[\frac{0.472 r_e}{r'_w} \right]} \quad (3-8)$$

or one can just provide the dimensionless productivity index as a function of the fracture parameters,

$$J_D = \begin{array}{l} \text{function of drainage-volume geometry} \\ \text{and fracture parameters} \end{array} \quad (3-9)$$

All three options give exactly the same results (if done in coherent terms). The last option is the most general and convenient, especially if we wish to consider fractured wells in more general drainage areas (not necessarily circular).

Many authors have provided charts and correlations in one form or another to handle special geometries and reservoir types. Unfortunately, most of the results are less obvious or difficult to apply in higher permeability cases. Even for the simplest possible case, a vertical fracture intersecting a vertical well, there are quite large discrepancies (see, for instance, Figure 12-13 of *Reservoir Stimulation, Third Edition*).

THE WELL-FRACTURE-RESERVOIR SYSTEM

We consider a fully penetrating vertical fracture in a pay layer of thickness h , as shown in Figure 3-1.

Note that in reality the drainage area is neither circular nor rectangular, however, for most drainage shapes these geometries are reasonable approximations. Using r_e or x_e is only a matter of convenience. The relation between the drainage area A , the drainage radius r_e and the drainage side length, x_e , is given by

$$A = r_e^2 \pi = x_e^2 \quad (3-10)$$

For a vertical well intersecting a rectangular vertical fracture that penetrates fully from the bottom to the top of the rectangular drainage

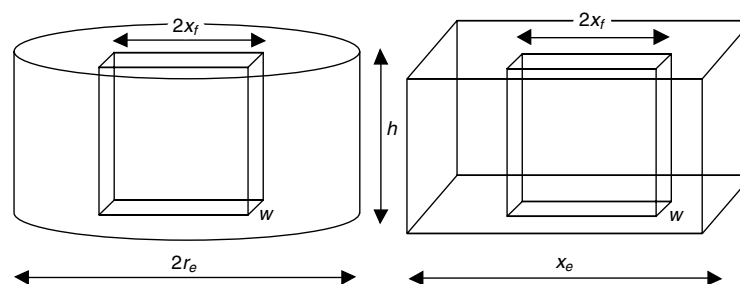


FIGURE 3-1. Notation for fracture performance.

volume, the performance is known to depend on the penetration ratio in the x direction,

$$I_x = \frac{2x_f}{x_e} \quad (3-11)$$

and on the dimensionless fracture conductivity,

$$C_{fD} = \frac{k_f w}{k x_f} \quad (3-12)$$

where x_f is the fracture half length, x_e is the side length of the square drainage area, k is the formation permeability, k_f is the proppant pack permeability, and w is the average (propped) fracture width.

PROPPANT NUMBER

The key to formulating a meaningful technical optimization problem is to realize that the fracture penetration and the dimensionless fracture conductivity (through width) are competing for the same resource: the propped volume. Once the reservoir and proppant properties and the amount of proppant are fixed, one has to make the optimal compromise between width and length. The available propped volume puts a constraint on the two dimensionless numbers. To handle the constraint easily, we introduce the dimensionless proppant number:

$$N_{prop} = I_x^2 C_{fD} \quad (3-13)$$

The proppant number as defined above is just a combination of the other two dimensionless parameters: penetration ratio and dimensionless fracture conductivity. Substituting the definition of the penetration ratio and dimensionless fracture conductivity into Equation 3-13, we obtain

$$N_{prop} = \frac{4k_f x_f w}{k x_e^2} = \frac{4k_f x_f w h}{k x_e^2 h} = \frac{2k_f}{k} \frac{V_{prop}}{V_{res}} \quad (3-14)$$

where N_{prop} is the proppant number, dimensionless; k_f is the effective proppant pack permeability, md; k is the formation permeability, md; V_{prop} is the propped volume in the pay (two wings, including void

space between the proppant grains), ft^3 ; and V_{res} is the drainage volume (i.e., drainage area multiplied by pay thickness), ft^3 . (Of course, any other coherent units can be used, because the proppant number involves only the ratio of permeabilities and the ratio of volumes.)

Equation 3-14 plainly reveals the meaning of the proppant number: it is the weighted ratio of propped fracture volume (two wings) to reservoir volume, with a weighting factor of two times the proppant-to-formation permeability contrast. Notice, only the proppant that reaches the pay layer is counted in the propped volume. If, for instance, the fracture height is three times the net pay thickness, then V_{prop} can be estimated as the bulk (packed) volume of injected proppant divided by three. In other words, the packed volume of the injected proppant multiplied by the volumetric proppant efficiency yields the V_{prop} used in calculating the proppant number.

The dimensionless proppant number, N_{prop} , is by far the most important parameter in unified fracture design.

Figure 3-2 shows J_D represented in a traditional manner, as a function of dimensionless fracture conductivity, C_{fD} , with I_x as a parameter. Similar graphs showing productivity increase are common in the published literature.

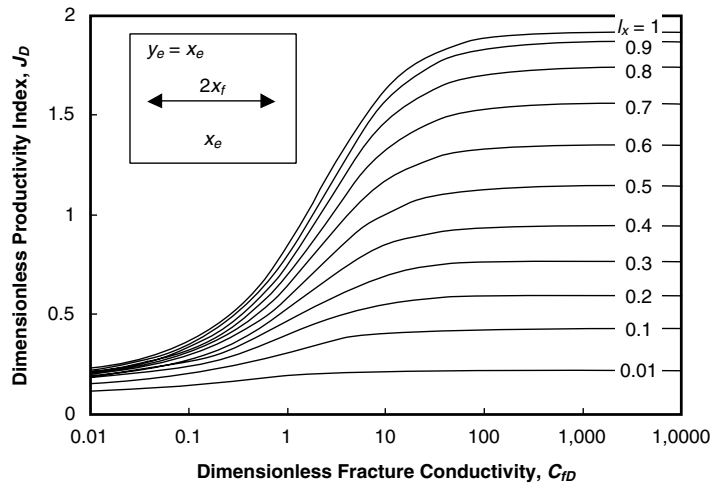


FIGURE 3-2. Dimensionless productivity index as a function of dimensionless fracture conductivity, with I_x as a parameter (McGuire-Sikora type representation).

However, Figure 3-2 is not very helpful in solving an optimization problem involving a fixed amount of proppant. For this purpose, in Figures 3-3 and 3-4, we present the same results, but now with the proppant number, N_{prop} , as a parameter. The individual curves correspond to J_D at a fixed value of the proppant number.

As seen from Figures 3-3 and 3-4, for a given value of N_{prop} , the maximum productivity index is achieved at a well-defined value of the dimensionless fracture conductivity. Because a given proppant number represents a fixed amount of proppant reaching the pay, the best compromise between length and width is achieved at the dimensionless fracture conductivity located under the peaks of the individual curves.

One of the main results seen from the figures is, that at proppant numbers less than 0.1, the optimal compromise occurs always at $C_{fD} = 1.6$. When the propped volume increases, the optimal compromise happens at larger dimensionless fracture conductivities, simply because the dimensionless penetration cannot exceed unity (i.e., once a fracture reaches the reservoir boundary, additional proppant is allocated only to fracture width). This effect is shown in Figure 3-4, as is the absolute maximum achievable dimensionless productivity index of 1.909. The maximum value of PI, equal to $6/\pi$, is the productivity index corresponding to perfect linear flow in a square reservoir.

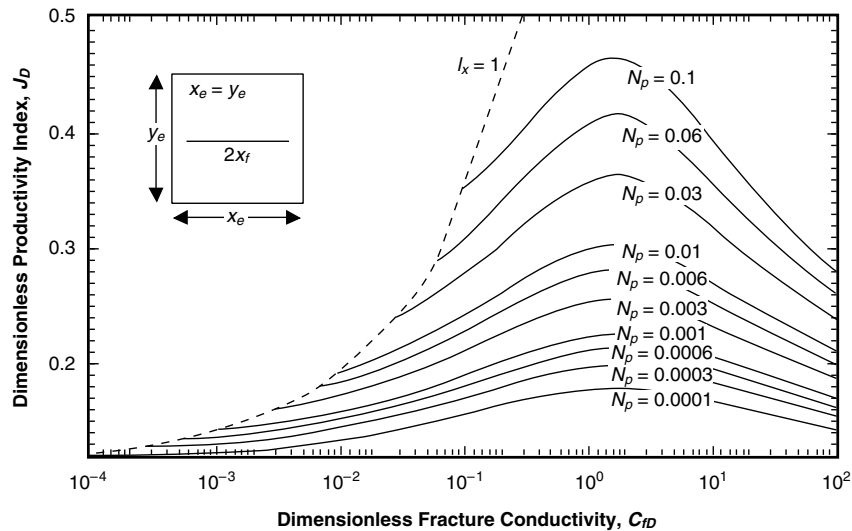


FIGURE 3-3. Dimensionless productivity index as a function of dimensionless fracture conductivity, with proppant number as a parameter (for $N_{prop} < 0.1$).

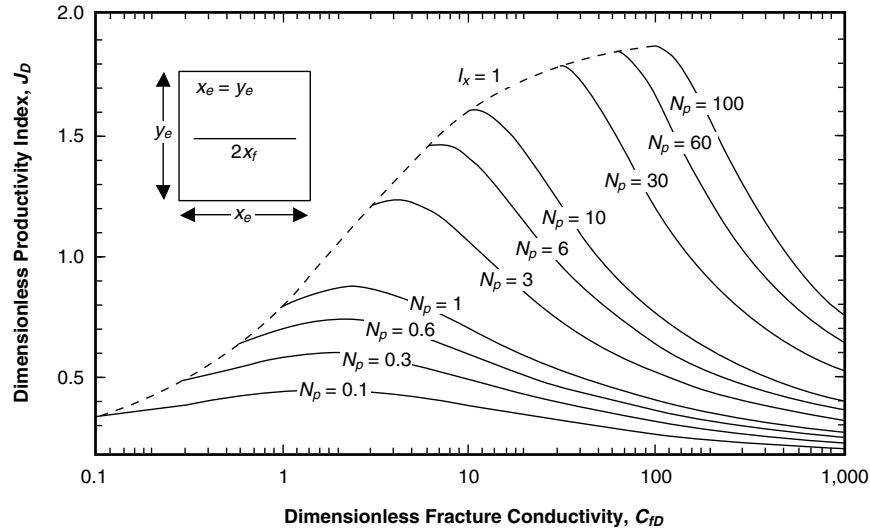


FIGURE 3-4. Dimensionless productivity index as a function of dimensionless fracture conductivity, with proppant number as a parameter (for $N_{prop} > 0.1$).

In medium and high permeability formations (above 50 md), it is practically impossible to achieve a proppant number larger than 0.1. For frac & pack treatments, typical proppant numbers range between 0.0001 and 0.01. Thus, for medium to high permeability formations, the optimum dimensionless fracture conductivity is always $C_{fDopt} = 1.6$.

In “tight gas” reservoirs, it is possible to achieve large dimensionless proppant numbers, at least in principle. Proppant numbers calculated for a limited drainage area—and not questioning the portion of proppant actually contained in the pay layer—can be as high as 1 to 10. However, in practice, proppant numbers larger than 1 may be difficult to achieve. For large treatments, the proppant can migrate upward, creating excessive and unplanned fracture height, or it might penetrate laterally outside of the assigned drainage area.

The situation is more complex for an individual well in a larger area. In this case, a (hypothetical) large fracture length tends to increase the drained reservoir volume, and the proppant number decreases. Ultimately, the large fracture is beneficial, but the achievable proppant number remains limited.

In reality, even trying to achieve proppant numbers larger than unity would be extremely difficult. Indeed, for a large proppant number, the optimum C_{fD} determines an optimum penetration ratio near unity. This can be easily seen from Figure 3-5, where the penetration

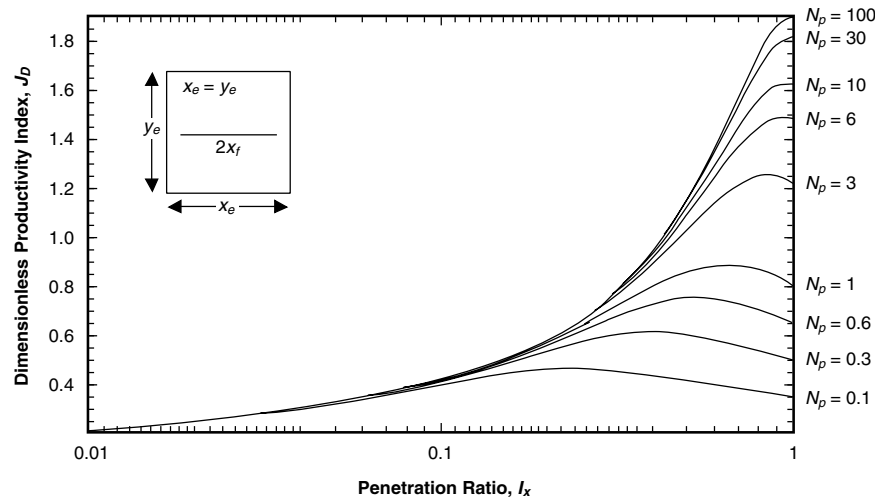


FIGURE 3-5. Dimensionless productivity index as a function of penetration ratio, with proppant number as a parameter (for $N_{prop} > 0.1$).

ratio is shown on the x -axis. To place the proppant “wall-to-wall” while keeping it inside the drainage volume would require a precision in the fracturing operation that is practically impossible to achieve.

The maximum possible dimensionless productivity index for $N_{prop} = 1$ is about $J_D = 0.9$. The dimensionless productivity index of an undamaged vertical well is between 0.12 and 0.14, depending on the well spacing and assumed well radius. Hence, there is a realistic maximum for the “folds of increase” in the pseudo-steady state productivity index (with respect to the zero skin case), i.e., 0.9 divided by 0.13 is approximately equal to 7. Larger folds of increase are not likely. Of course, larger folds of increase can be achieved with respect to an originally damaged well where the pre-treatment skin factor has a large and positive value.

Another common misunderstanding is related to the transient flow period. Under transient flow, the productivity index (and hence the production rate) is larger than in the pseudo-steady state case. With this qualitative picture in mind, it is easy to discard the pseudo-steady state optimization procedure and to “shoot for” very high dimensionless fracture conductivities and/or to anticipate many more folds of increase in the productivity. In reality, the existence of a transient flow period does not change the previous conclusions on optimal

dimensions. Our calculations show that there is no reason to depart from the optimum compromise derived for the pseudo-steady state case, even if the well will produce in the transient regime for a considerable time (say months or even years). Simply stated, what is good for maximizing pseudo-steady state flow is also good for maximizing transient flow.

In the definition of proppant number, k_f is the effective (or equivalent, as it is sometimes called) permeability of the proppant pack. This parameter is crucial in design. Current fracture simulators generally provide a nominal value for the proppant pack permeability (supplied by the proppant manufacturer) and allow it to be reduced by a factor that the user selects. The already-reduced value should be used in the proppant number calculation.

There are numerous reasons why the actual (or equivalent) proppant pack permeability will be lower than the nominal value. The main reasons are as follows:

- Large closure stresses crush the proppant, reducing the average grain size, grain uniformity, and porosity.
- Fracturing fluid residue decreases the permeability in the fracture.
- High fluid velocity in the proppant pack creates “non-Darcy effects,” resulting in additional pressure loss. This phenomenon can be significant when gas is produced in the presence of a liquid (water and/or condensate). The non-Darcy effect is caused by the periodic acceleration-deceleration of the liquid droplets, effectively reducing the permeability of the proppant pack. This reduced permeability can be an order of magnitude lower than the nominal value presented by the manufacturer.

During the fracture design, considerable attention must be paid to the effective permeability of the proppant pack and to the permeability of the formation. Knowledge of the effective permeability contrast is crucial, and cannot be substituted by qualitative reasoning.

Well Performance for Low and Moderate Proppant Numbers

By low and moderate proppant numbers, we mean anything less than 0.1. The most dynamic fracturing activities (frac & pack, for example) fall into this category—making it extremely important from a design standpoint.

The optimum treatment design for moderate proppant numbers can be simply and concisely presented in an analytical form. In the process, we will show how the proppant number and dimensionless productivity index relate to some other popular performance indicators, such as the Cinco-Ley and Samaniego *pseudo-skin function* and Prats' *equivalent wellbore radius*. In fact, fracture designs based on these related performance indicators are just the moderate (low) proppant number limit of the more comprehensive unified fracture design.

Prats (1961) introduced the concept of equivalent wellbore radius resulting from a fracture treatment. He also showed that, except for the fracture extent, all fracture variables affect well performance only through the combined quantity of dimensionless fracture conductivity. When the dimensionless fracture conductivity is high (e.g., greater than 100), the behavior is similar to that of an infinite conductivity fracture. The behavior of infinite conductivity fractures was studied later by Gringarten and Ramey (1974). To characterize the impact of a finite-conductivity vertical fracture on the performance of a vertical well, Cinco-Ley and Samaniego (1981) introduced a pseudo-skin function which is strictly a function of dimensionless fracture conductivity.

According to the definition of pseudo-skin factor, the dimensionless pseudo-steady state productivity index can be given as

$$J_D = \frac{1}{\ln 0.472 \frac{r_e}{r_w} + s_f} \quad (3-15)$$

where s_f is the pseudo-skin. In Prats' notation the same productivity index is described by

$$J_D = \frac{1}{\ln 0.472 \frac{r_e}{r'_w}} \quad (3-16)$$

where r'_w is the equivalent wellbore radius. Prats also used the *relative equivalent wellbore radius* defined by r'_w / x_f .

In the Cinco-Ley formalism, the productivity index is described as

$$J_D = \frac{1}{\ln 0.472 \frac{r_e}{x_f} + f} \quad (3-17)$$

where f is the pseudo-skin function with respect to the fracture half-length.

Table 3-2 shows the relations between these quantities.

The advantage of the Cinco-Ley and Samaniego formalism (f -factor) is that, for moderate (and low) proppant numbers, the quantity f depends only on the dimensionless fracture conductivity. The solid line in Figure 3-6 shows the Cinco-Ley and Samaniego f -factor as a function of dimensionless fracture conductivity.

Note that for large values of C_{fd} , the f -factor expression approaches $\ln(2)$, indicating that the production from an infinite conductivity fracture is equivalent to the production of $\pi/2$ times *more* than the production from the same surface arranged cylindrically (like the wall of a huge wellbore). In calculations, it is convenient to use an explicit expression of the form

$$f = \frac{1.65 - 0.328u + 0.116u^2}{1 + 0.18u + 0.064u^2 + 0.005u^3}, \quad \text{where } u = \ln C_{fd} \quad (3-18)$$

Because the relative wellbore radius of Prats can be also expressed by the f -factor (see Table 3-2), we obtain the equivalent result:

$$\frac{r'_w}{x_f} = \exp\left[-\frac{1.65 - 0.328u + 0.116u^2}{1 + 0.18u + 0.064u^2 + 0.005u^3}\right], \quad \text{where } u = \ln C_{fd} \quad (3-19)$$

The simple curve-fits represented by Equations 3-18 and 3-19 are only valid over the range indicated in Figure 3-6. For very large values of C_{fd} , one can simply use the limiting value for Equation 3-19, which is 0.5, showing that the infinite conductivity fracture has a productivity similar to an imaginary (huge) wellbore with radius $x_f/2$.

Interestingly enough, infinite conductivity behavior does not mean that we have selected the optimum way to place a given amount of proppant into the formation.

TABLE 3-2. Relations Between Various Performance Indicators

$f = s_f + \ln\left[\frac{x_f}{r_w}\right]$	$s_f = \ln\left[\frac{r_w}{r'_w}\right]$
$r'_w = r_w \exp[-s_f]$	$r'_w = x_f \exp[-f]$
$\frac{r'_w}{x_f} = \exp[-f]$	$\frac{r'_w}{x_f} = \frac{r_w}{x_f} \exp[-s_f]$

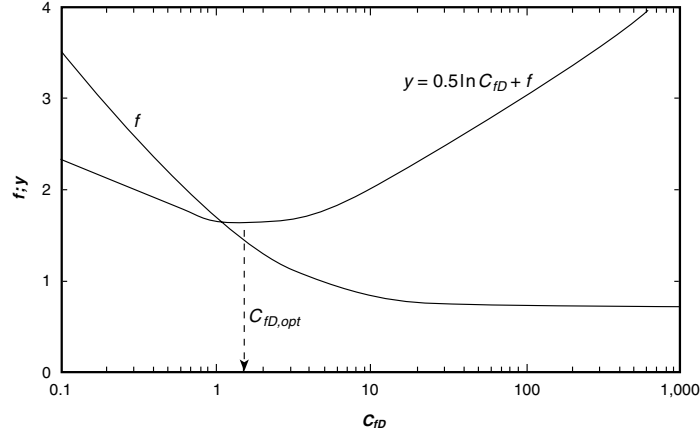


FIGURE 3-6. Cinco-Ley and Samaniego f -factor and the y -function.

OPTIMUM FRACTURE CONDUCTIVITY

In this context ($N_{prop} < 0.1$), a strictly physical optimization problem can be formulated: How should we select the length and width if the propped volume of one fracture wing, $V_f = w \times h \times x_f$, is given as a constraint, and we wish to maximize the PI in the pseudo-steady state flow regime. It is assumed that the formation thickness, drainage radius, and formation and proppant pack permeabilities are known, and that the fracture is vertically fully penetrating (i.e., $h_f = h$).

Selecting C_{fD} as the decision variable, the length is expressed as

$$x_f = \left(\frac{V_f k_f}{C_{fD} h k} \right)^{1/2} \tag{3-21}$$

Substituting Equation 3-21 into 3-17, the dimensionless productivity index becomes

$$J_D = \frac{1}{\ln 0.472 r_e + 0.5 \ln \frac{h k}{V_f k_f} + (0.5 \ln C_{fD} + f)} \tag{3-22}$$

where the only unknown variable is C_{fD} . Because the drainage radius, formation thickness, the two permeabilities, and the propped volume are fixed, the maximum PI occurs when the quantity in parentheses,

$$y = 0.5 \ln C_{fD} + f \quad (3-23)$$

reaches a minimum. That quantity is also shown in Figure 3-6. Because the above expression depends only on C_{fD} , the optimum, $C_{fD,opt} = 1.6$ is a given constant for any reservoir, well, and proppant volume.

This result provides a deeper insight to the real meaning of dimensionless fracture conductivity. The reservoir and the fracture can be considered as a system working in series. The reservoir can feed more fluids into the fracture if the length is larger, but (since the volume is fixed) this means a narrower fracture. In a narrow fracture, the resistance to flow may be significant. The optimum dimensionless fracture conductivity corresponds to the best compromise between the requirements of the two subsystems. Once it is found, the optimum fracture half-length can be calculated from the definition of C_{fD} as

$$x_f = \left(\frac{V_f k_f}{1.6 h k} \right)^{1/2} \quad (3-24)$$

and consequently, the optimum propped average width should be

$$w = \left(\frac{1.6 V_f k}{h k_f} \right)^{1/2} = \frac{V_f}{h x_f} \quad (3-25)$$

Notice that V_f is $V_{prop}/2$ because it is only one half of the propped volume.

The most important implication of the above results is that *there is no theoretical difference between low and high permeability fracturing*. In all cases, there exists a physically optimal fracture that should have a C_{fD} near unity. In low permeability formations, this requirement results in a long and narrow fracture; in high permeability formations, a short and wide fracture provides the same dimensionless conductivity.

If the fracture length and width are selected according to the optimum compromise, the dimensionless productivity index will be

$$J_{D,max} = \frac{1}{0.99 - 0.5 \ln N_{prop}} \quad (3-26)$$

Of course, the indicated optimal fracture dimensions may not be technically or economically feasible. In low permeability formations,

the indicated fracture length may be too large, or the extreme narrow width may mean that the assumed constant proppant permeability is no longer valid. In high permeability formations, the indicated large width might be impossible to create. For more detailed calculations, all the constraints must be taken into account, but, in any case, a dimensionless fracture conductivity far from the optimum indicates that either the fracture is a relative “bottleneck” ($C_{fD} \ll 1.6$) or that it is too “short and wide” ($C_{fD} \gg 1.6$).

The reader should not forget that the results of this section—including the Cinco-Ley and Samaniego graph and its curve fit, the optimum dimensionless fracture conductivity of 1.6, and Equation 3-26—are valid only for proppant numbers less than 0.1. This can be easily seen by comparing Figures 3-3 and 3-4. In Figure 3-3, the curves have their maximum at $C_{fD} = 1.6$, and the maximum J_D corresponds to the simple Equation 3-26. In Figure 3-4, however, where the proppant numbers are larger than 0.1, the location of the maximum is shifted, and the simple calculations based on the f -factor (Equation 3-18) or on the equivalent wellbore radius (Equation 3-19) are no longer valid.

Optimization routines found on the CD that accompanies this book are based on the full information contained in Figures 3-3 and 3-4, and formulas developed for moderate proppant numbers are used only in the range of their validity.

DESIGN LOGIC

We wish to place a certain amount of proppant in the pay interval and to place it in such a way that the maximum possible productivity index is realized. The key to finding the right balance between size and productivity improvement is in the proppant number. Since V_{prop} includes only that part of the proppant that reaches the pay, and hence is dependent on the volumetric proppant efficiency, the proppant number cannot be simply fixed during the design procedure.

In unified fracture design, we specify the amount of proppant indicated for injection and then proceed as follows:

1. Assume a volumetric proppant efficiency and determine the proppant number. (Once the treatment details are obtained, the assumed volumetric proppant efficiency related to created fracture height may be revisited and the design process may be repeated in an iterative manner.)

38 ■ *Unified Fracture Design*

2. Use Figure 3-3 or Figure 3-4 (or rather the design spreadsheet) to calculate the maximum possible productivity index, J_{Dmax} , and also the optimum dimensionless fracture conductivity, C_{fDopt} , from the proppant number.
3. Calculate the optimum fracture half-length. Denoting the volume of one propped wing (in the pay) by V_f , the optimum fracture half-length can be calculated as

$$x_f = \left(\frac{V_f k_f}{C_{fD,opt} h k} \right)^{1/2} \quad (3-27)$$

4. Calculate the optimum averaged propped fracture width as

$$w = \left(\frac{C_{fD,opt} V_f k}{h k_f} \right)^{1/2} = \frac{V_f}{x_f h} \quad (3-28)$$

In the above two equations, V_f and h must correspond to each other. If total fracture height is used for h , which is often denoted by h_f , then the proppant volume V_f must be the total propped volume of one wing. However, if the selected V_f corresponds only to that portion of one wing volume that is contained in the pay layer, then h should be the net thickness of the pay. The final result for optimum length and width will be the same in either case. It is a better practice, however, to use net thickness and net volume (contained in the pay) because those variables are also used to calculate the proppant number.

Once reservoir engineering and economic considerations have dictated the fracture dimensions to be created, the next issue is how to achieve that goal. From this point, design of the fracture treatment can be viewed as adjusting treatment details (pumping time and proppant schedule) to achieve the desired final fracture dimensions.

In the next chapter, we outline the mechanics of fracture creation in some detail. This theoretical basis is needed before we can proceed to design the fracture treatment, our ultimate goal.

4

Fracturing Theory

In the following, we briefly summarize the most important mechanical concepts related to hydraulic fracturing.

LINEAR ELASTICITY AND FRACTURE MECHANICS

Elasticity implies reversible changes. The initiation and propagation of a fracture means that the material has responded in an inherently non-elastic way, and an *irreversible* change has occurred. Nevertheless, linear elasticity is a useful tool when studying fractures because both the stresses and strains (except perhaps in the vicinity of the fracture face, and especially the tip) may still be adequately described by elasticity theory.

A linear elastic material is characterized by elastic constants that can be determined in static or dynamic loading experiments. For an isotropic material, where the properties are independent of direction, two constants are sufficient to describe the behavior.

Figure 4-1 is a schematic representation of a static experiment with uniaxial loading. The two parameters obtained from such an experiment are the Young's modulus (E) and the Poisson ratio (ν). They are

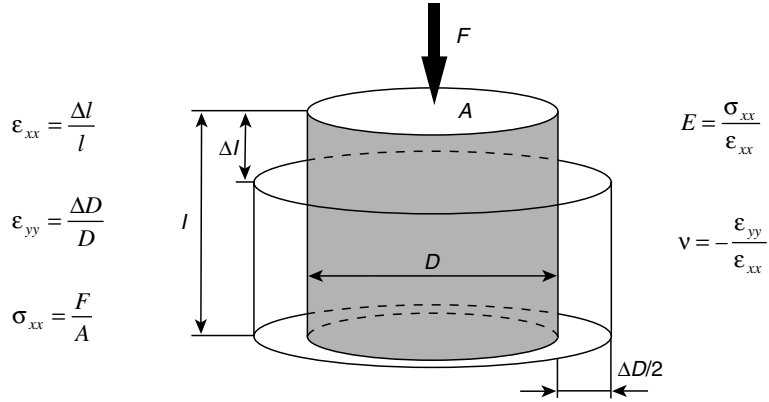


FIGURE 4-1. Uniaxial loading experiment.

calculated from the vertical stress (σ_{xx}) vertical strain (ϵ_{xx}) and horizontal strain (ϵ_{yy}), as shown in the figure.

Table 4-1 shows the interrelation of those constants most often used in hydraulic fracturing. The plane strain modulus (E') is the only elastic constant really needed in our equations.

In linear elastic theory, the concept of *plane strain* is often used to reduce the dimensionality of a problem. It is assumed that the body is infinite in at least one direction, and external forces (if any) are applied parallel to this direction (i.e., “infinitely repeated” in every cross section). In such case, it is intuitively obvious that the state of strain also repeats itself infinitely.

TABLE 4-1. Interrelation of Various Properties of a Linear Elastic Material

Required/Known	E, ν	G, ν	E, G
Shear modulus, G	$\frac{E}{2(1+\nu)}$	G	G
Young's modulus, E	E	$2G(1+\nu)$	E
Poisson ratio, ν	ν	ν	$\frac{E-2G}{2G}$
Plane strain modulus, E'	$\frac{E}{1-\nu^2}$	$\frac{2G}{1-\nu}$	$\frac{4G^2}{4G-E}$

Plane strain is a reasonable approximation in a simplified description of hydraulic fracturing. The main question is how to select the plane. Two possibilities arise, and, in turn, this has given rise to two different approaches to fracture modeling. The state of plane strain was assumed in the horizontal plane by Khristianovitch and Zheltov (1955) and by Geertsma and de Klerk (1969), while plane strain in the vertical plane (normal to the direction of fracture propagation) was assumed by Perkins and Kern (1961) and Nordgren (1972).

Often, in the hydraulic fracturing literature, the term “KGD” geometry is used interchangeably to the horizontal plane-strain assumption and “PKN” geometry is used as a substitute for postulating plane strain in the vertical plane.

Exact mathematical solutions are available for the problem of a pressurized crack in the state of plane strain. In particular, it is well known that the pressurized line crack has an elliptical width distribution (Sneddon, 1973):

$$w(x) = \frac{4p_0}{E'} \sqrt{c^2 - x^2} \quad (4-1)$$

where x is the distance from the center of the crack, c is the half-length (the distance of the tip from the center) and p_0 is the constant pressure exerted on the crack faces from inside. From Equation 4-1, the maximum width at the center is

$$w_0 = \frac{4cp_0}{E'} \quad (4-2)$$

indicating that a linear relationship is maintained between the crack opening induced and the pressure exerted. When the concept of pressurized line crack is applied for a real situation, p_0 is substituted with the net pressure, p_n , defined as the difference of the inner pressure and the minimum principal stress acting from outside, trying to close the fracture (Hubbert and Willis, 1957; Haimson and Fairhurst, 1967).

Fracture mechanics has emerged from the observation that any existing discontinuity in a solid deteriorates its ability to carry loads. A (possibly small) hole may give rise to high local stresses compared to the ones being present without the hole. The high stresses, even if they are limited to a small area, may lead to the rupture of the material. It is often convenient to look at material discontinuities as stress concentrators which locally increase the otherwise present stresses.

Two main cases must be distinguished. If the form of discontinuity is smooth (e.g., a circular borehole in a formation), then the maximum stress around the discontinuity is higher than the virgin stress by a finite factor, which depends on the geometry. For example, the stress concentration factor for a circular borehole is three.

The situation is different in the case of sharp edges, such as at the tip of a fracture. Then the maximum stress at the tip becomes infinite. In fracture mechanics, we have to deal with singularities. Two different loadings (pressure distributions) of a line crack result in two different stress distributions. Both cases may yield infinite stresses at the tip, but the “level of infinity” is different. We need a quantity to characterize this difference. Fortunately, all stress distributions near the tip of any fracture are similar in the sense that they decrease according to $r^{-1/2}$, where r is the distance from the tip. The quantity used to characterize the “level of infinity” is the stress intensity factor, K_I , defined as the multiplier to the $r^{-1/2}$ function. For the idealization of a pressurized line crack with half-length, c , and constant pressure, p_0 , the stress intensity factor is given by

$$K_I = p_0 c^{1/2} \quad (4-3)$$

In other words, the stress intensity factor at the tip is proportional to the constant pressure opening up the crack and to the square root of the crack half-length (characteristic dimension).

According to the key postulate of linear elastic fracture mechanics (LEFM), for a given material there is a critical value of the stress intensity factor, K_{IC} , called fracture toughness. If the stress intensity factor at the crack tip is above the critical value, the crack will propagate; otherwise it will not. Fracture toughness is a useful quantity for safety calculations, when the engineer’s only concern is to avoid fracturing. In well stimulation, where the engineer’s primary goal is to create and propagate a fracture, the concept has been found somewhat controversial because it predicts that less and less effort is necessary to propagate a fracture with increasing extent. In the large scale, however, the opposite is usually true.

FRACTURING FLUID MECHANICS

Fluid materials deform continuously (in other words, flow) without rupture when subjected to a constant stress. Solids generally will assume

a static equilibrium deformation under the same stresses. Crosslinked fracturing fluids usually behave as viscoelastic fluids. Their stress-strain material functions fall between those of pure fluids and solids.

From our point of view, the most important property of fluids is their resistance to flow. The local intensity of flow is characterized by the shear rate, $\dot{\gamma}$, measured in 1/s. It can be considered as the rate of change of velocity with the distance between sliding layers. The stress emerging between the layers is the shear stress, τ . Its dimension is force per unit area (in SI units, Pa). The material function relating shear stress and shear rate is the *rheological curve*. This information is necessary to calculate the pressure drop (actually, energy dissipation) for a given flow situation, such as flow in pipe or flow between parallel plates.

Apparent viscosity is defined as the ratio of stress to shear rate. Generally, the apparent viscosity varies with shear rate, except in the case of a Newtonian fluid—a very specific fluid in which the viscosity is a constant. The rheological curve and the apparent viscosity curve contain the same information and are used interchangeably. Figure 4-2 shows typical rheological curves, and Table 4-2 lists some commonly used rheological constitutive equations.

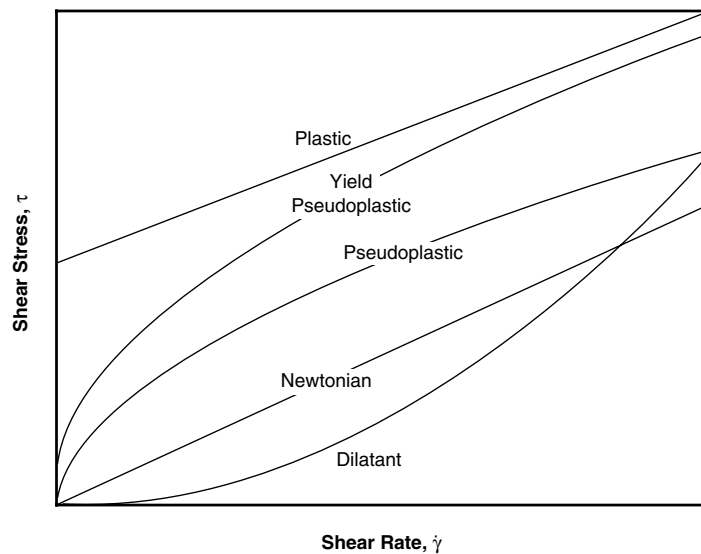


FIGURE 4-2. Typical rheological curves.

TABLE 4-2. Commonly Used Rheological Constitutive Equations

$\tau = \mu \dot{\gamma}$	Newtonian
$\tau = K \dot{\gamma}^n$	Power law
$\tau = \tau_y + \mu_p \dot{\gamma}$	Bingham plastic
$\tau = \tau_y + K \dot{\gamma}^n$	Yield power law

The model parameters vary with chemical composition, temperature and, to a lesser extent, many other factors including shear history. In the case of foams, the volumetric ratio between the gas and liquid phases plays an important role (Reidenbach, 1985; Winkler, 1995).

Most fracturing gels exhibit significant shear thinning (i.e., loss of viscosity with increasing shear rate). A constitutive equation that captures this primary aspect of their flow behavior is the Power law model. The flow behavior index, n , usually ranges from 0.3 to 0.6.

All fluids exhibit some finite limiting viscosity at high shear rates. The build-up of very high apparent viscosity at low shear might be approximated by the inclusion of a yield stress for certain fluids. Many fluids demonstrate what appears to be Newtonian behavior at low shear rates.

Much of the current rheology research focuses on building more realistic apparent viscosity models that effectively incorporate each of the previously mentioned characteristics as well as the nonlinear, time-dependent viscoelastic effects of crosslinked gels.

A rheological model is used to predict the pressure losses (gradient) associated with an average fluid flow velocity in a given physical geometry. The equations of motion have been solved for the standard rheological models in the most obvious geometries (e.g., flow in circular tubes, annuli, and between thin-gap parallel plates). The solution is often presented as a relation between average linear velocity (flow rate per unit area) and pressure drop. In calculations, it is convenient to use the equivalent Newtonian viscosity (μ_e), that is, the viscosity that would be used in the equation of the Newtonian fluid to obtain the same pressure drop under the same flow conditions. While apparent viscosity (at a given local shear rate) is the property of the fluid, equivalent viscosity depends also on the flow geometry and carries the same information as the pressure drop solution. For more

complex rheological models, there is no closed-form solution (neither for the pressure drop nor for the equivalent Newtonian viscosity), and the calculations involve numerical root-finding.

Of particular interest to hydraulic fracturing is the laminar flow in two limiting geometries. *Slot flow* occurs in a channel of rectangular cross section when the ratio of the longer side to the shorter side is extremely large. Limiting *ellipsoid flow* occurs in an elliptic cross section with extremely large aspect ratio. The former corresponds to the KGD geometry and the latter to the PKN geometry.

Table 4-3 gives the solutions commonly used in hydraulic fracturing calculations. The most familiar equation, valid for Newtonian behavior, is presented first. Then an equivalent viscosity is given for the Power law fluid. The equivalent viscosity can be used in the Newtonian form of the pressure drop equation. Notice that the equivalent viscosity depends on the average velocity (u_{avg}) and on the geometry of the flow channel (in case of slot flow, on the width, w ; in case of elliptical cross section, on the maximum width, w_0). It is interesting to note that the equation for laminar flow of a Power law fluid in the limiting ellipsoid geometry has not been derived. The solution presented here can be obtained by analogy considerations (for details, see Valkó and Economides, 1995).

The friction pressure associated with pumping fracturing fluids through surface lines and tubulars cannot be calculated directly using the classic turbulent flow correlations. Special relations have to be applied to account for the drag reduction phenomena caused by the long polymer chains. Rheological behavior also plays an important role in the proppant carrying capacity of the fluid (Roodhart, 1985; Acharya, 1986).

TABLE 4-3. Pressure Drop and Equivalent Newtonian Viscosity

Rheological model	Newtonian $\tau = \mu\dot{\gamma}$	Power law $\tau = K\dot{\gamma}^n$
Slot flow	$\frac{\Delta p}{L} = \frac{12\mu u_{avg}}{w^2}$	$\mu_e = \frac{2^{n-1}}{3} \left(\frac{1+2n}{n} \right)^n K w^{1-n} u_{avg}^{n-1}$
Ellipsoid flow	$\frac{\Delta p}{L} = \frac{16\mu u_{avg}}{w_0^2}$	$\mu_e = \frac{2^{n-1}}{\pi} \left[\frac{1+(\pi-1)n}{n} \right]^n K w_0^{1-n} u_{avg}^{n-1}$

LEAKOFF AND VOLUME BALANCE IN THE FRACTURE

The polymer content of the fracturing fluid is partly intended to impede the loss of fluid into the reservoir. This phenomenon is envisaged as a continuous build-up of a thin layer of polymer (the filter cake), which manifests an ever-increasing resistance to flow through the fracture face. The actual leakoff is determined by a coupled system that includes not only the filter cake, which is one element, but also flow conditions in the reservoir.

A fruitful approximation dating back to Carter, 1957 (cf. appendix to Howard and Fast, 1957), is to consider the combined effect of the different phenomena as a material property. According to this concept, the leakoff velocity, v_L , is given by the Carter I equation:

$$v_L = \frac{C_L}{\sqrt{t}} \quad (4-4)$$

where C_L is the leakoff coefficient (length/time^{1/2}) and t is the time elapsed since the start of the leakoff process. The integrated form of the Carter equation is

$$\frac{V_{Lost}}{A_L} = 2C_L\sqrt{t} + S_p \quad (4-5)$$

where V_{Lost} is the fluid volume that passes through the surface A_L during the time period from time zero to time t . The integration constant, S_p , is called the *spurt loss coefficient*. It can be considered as the width of the fluid body passing through the surface instantaneously at the very beginning of the leakoff process. Correspondingly, the term $2C_L\sqrt{t}$ can be considered as the leakoff width. (Note that the factor 2 is an artifact of the integration. It has nothing to do with the “two wings” and/or “two faces” introduced later.) The two coefficients, C_L and S_p , can be determined from laboratory tests or, preferably, from evaluation of a fracture calibration test.

Formal Material Balance: The Opening-Time Distribution Factor

Consider the fracturing treatment shown schematically in Figure 4-3. The volume V_i injected into one wing during the injection time t_e consists of two parts: the volume of one fracture wing at the end of

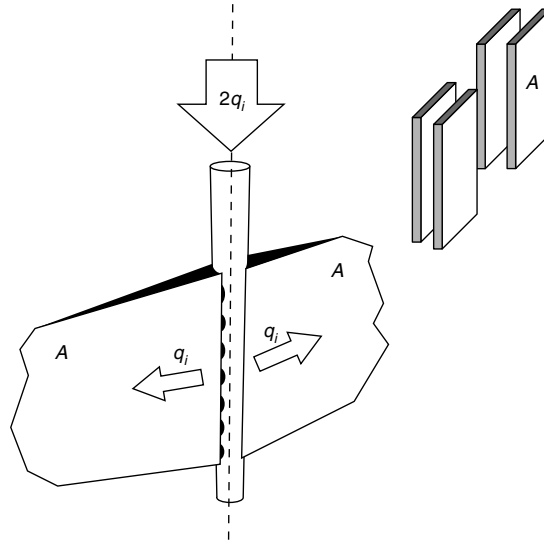


FIGURE 4-3. Notation for material balance.

pumping (V_e) and the volume lost (leakoff volume). The subscript e denotes that a given quantity is being measured or referenced at the end of pumping. Note that all the variables are defined with respect to one wing. The area A_e denotes the surface of one face of one fracture wing. Fluid efficiency η_e is defined as the fraction of the fluid remaining in the fracture: $\eta_e = V_e/V_i$. The average width, \bar{w} , is defined by the relation, $V = A\bar{w}$.

A hydraulic fracturing operation may last from tens-of-minutes up to several hours. Points on the fracture face near the well are “opened” at the beginning of pumping while the points near the fracture tip are younger. Application of Equation 4-5 necessitates the tracking of the opening-time of the different fracture face elements.

If only the overall material balance is considered, it is natural to rewrite the injected volume as the sum of the fracture volume, leakoff volume, and spurt volume using the formalism,

$$V_i = V_e + K_L(2A_e C_L \sqrt{t_e}) + 2A_e S_p \quad (4-6)$$

where the variable K_L is the opening-time distribution factor. It reflects the history of the evolution of the fracture surface, or rather the distribution of the opening-time, hence the name. In particular, if all the surface is opened at the beginning of the injection, then K_L

reaches its absolute maximum, $K_L = 2$. The fluid efficiency is the ratio of the created volume to the injected volume. Dividing both volumes by the final fracture area, we can consider fracture efficiency as the ratio of the created width to the would-be width, where the would-be width is defined as the sum of the created and lost widths.

Therefore, another form of Equation 4-6 is

$$\eta_e = \frac{\bar{w}_e}{\bar{w}_e + 2K_L C_L \sqrt{t_e} + 2S_p} \quad (4-7)$$

showing that the term $2K_L C_L \sqrt{t_e}$ can be considered as the “leakoff width,” and the term $2S_p$ as the “spurt width.” Equation 4-7 can be rearranged to obtain the opening-time distribution factor in terms of fluid efficiency and average width at the end of pumping:

$$K_L = -\frac{S_p}{C_L \sqrt{t_e}} - \frac{\bar{w}_e}{2C_L \sqrt{t_e}} + \frac{\bar{w}_e}{2\eta_e C_L \sqrt{t_e}} \quad (4-8)$$

Note that these relations are independent of the actual shape of the fracture face or the history of its evolution.

Constant Width Approximation (Carter Equation II)

In order to obtain an analytical solution for constant injection rate, Carter considered a hypothetical case in which the fracture width remains constant during the fracture propagation (the width “jumps” to its final value in the first instant of pumping). Then a closed form expression can be given for the fluid efficiency in terms of the two leakoff parameters and the width:

$$\eta_e = \frac{\bar{w}_e (\bar{w}_e + 2S_p)}{4\pi C_L^2 t_e} \left[\exp(\beta^2) \operatorname{erfc}(\beta) + \frac{2\beta}{\sqrt{\pi}} - 1 \right] \quad (4-9)$$

$$\text{where } \beta = \frac{2C_L \sqrt{\pi t_e}}{\bar{w}_e + 2S_p}.$$

Power Law Approximation to Surface Growth

A basic assumption postulated by Nolte (1979, 1986) leads to a remarkably simple form of the material balance. He assumed that the fracture surface evolves according to a power law,

$$A_D = t_D^\alpha \quad (4-10)$$

where $A_D = A/A_e$ and $t_D = t/t_e$, and the exponent α remains constant during the entire injection period. Nolte realized that, in this case, the opening-time distribution factor is a function of α only. He represented the opening-time distribution factor and its dependence on the exponent of fracture surface growth using the notation $g_0(\alpha)$ and presented g_0 for selected values of α . A simple expression first obtained by Hagel and Meyer (1989) can be used to obtain the value of the opening-time distribution factor for any α :

$$g_0(\alpha) = \frac{\sqrt{\pi\alpha}\Gamma(\alpha)}{\Gamma(\alpha + 2/3)} \quad (4-11)$$

where $\Gamma(\alpha)$ is the Euler gamma function.

In calculations, the following approximation to the g_0 function might be easier to use:

$$g_0(\alpha) = \frac{2 + 2.06798 \alpha + 0.541262 \alpha^2 + 0.0301598 \alpha^3}{1 + 1.6477 \alpha + 0.738452 \alpha^2 + 0.0919097 \alpha^3 + 0.00149497 \alpha^4} \quad (4-12)$$

Nolte assumed that the exponent remains between 0.5 and 1. With this assumption, the factor K_L lies between 4/3 (1.33) and $\pi/2$ (1.57), indicating that for two extremely different surface growth histories, the opening-time distribution factor varies less than 20 percent. Generally, the simple approximation $K_L = 1.5$ should provide enough accuracy for design purposes.

Various practitioners have related the exponent α to fracture geometry, fluid efficiency at the end of pumping, and fluid rheological behavior. None of these relations can be considered as proven theoretically, but they are reasonable engineering approximations, especially because the effect of the exponent on the final results is limited. Our recommendation is to use $\alpha = 4/5$ for the PKN, $\alpha = 2/3$ for the KGD, and $\alpha = 8/9$ for the radial model. These exponents can be derived from the no-leakoff equations shown later in Table 4-4.

Numerically, the original constant-width approximation of Carter and the power law surface growth assumption of Nolte give very similar results when used for design purposes. The g_0 -function approach does, however, have technical advantages when applied to the analysis of calibration treatments.

Detailed Leakoff Models

The bulk leakoff model is not the only possible interpretation of the leakoff process. Several mechanistic models have been suggested in the past (Williams, 1970 and Settari, 1985; Ehlig-Economides, et al., 1994; Yi and Peden, 1994; Mayerhofer, et al., 1995). The total pressure difference between the inside of a created fracture and a far point in the reservoir is written as the sum,

$$\Delta p(t) = \Delta p_{face}(t) + \Delta p_{piz}(t) + \Delta p_{res}(t) \quad (4-13)$$

where Δp_{face} is the pressure drop across the fracture face dominated by the filter cake, Δp_{piz} is the pressure drop across a polymer-invaded zone and Δp_{res} is the pressure drop in the reservoir. Depending on their significance under the given conditions, one or two terms may be neglected. While the first two terms are connected to the leakoff rate at a given time instant, the reservoir pressure drop is transient. It depends on the entire history of the leakoff process, not only on its instant intensity.

The detailed leakoff models hold an advantage in that they are based on physically meaningful parameters, such as permeability and filter cake resistance, and they allow for explicit pressure-dependent simulation of the leakoff process. However, the application of these models is limited by the complexity of the mathematics involved and by the extra input they require.

BASIC FRACTURE GEOMETRIES

Engineering models for the propagation of a hydraulically induced fracture combine elasticity, fluid flow, material balance, and (in some cases) an additional propagation criterion. Given the fluid injection history, a model should predict the evolution with time of the fracture dimensions and the wellbore pressure.

For design purposes, an approximate description of the geometry might be sufficient, so simple models that predict fracture length and average width at the end of pumping are very useful. Models that predict these two dimensions—while the third one, fracture height, is fixed—are referred to as 2D models. If the fracture surface is postulated to propagate in a radial fashion, that is, the height is not fixed, the model is still considered to be 2D (the two dimensions being fracture radius and width).

A further simplification occurs if we can relate fracture length and width, neglecting the details of leakoff for now. This is the basic concept of the early so-called “width equations.” It is assumed that the fracture evolves in two identical wings, perpendicular to the minimum principal stress of the formation. Because the minimum principal stress is usually horizontal (except for very shallow formations), the fracture will be vertical.

Perkins-Kern Width Equation

The PKN model assumes that the condition of plane strain holds in every vertical plane normal to the direction of propagation; however, unlike the rigorous plane-strain situation, the stress and strain state are not exactly the same in subsequent planes. In other words, the model applies a quasi-plane-strain assumption, and the reference plane is vertical, normal to the propagation direction. Neglecting the variation of pressure along the vertical coordinate, the net pressure, p_n , is considered as a function of the lateral coordinate x . The vertically constant pressure at a given lateral location gives rise to an elliptical cross section. Straightforward application of Equation 4-1 provides the maximum width of the ellipse as

$$w_0 = \frac{2h_f p_n}{E'} \quad (4-14)$$

Perkins and Kern (1961) postulated that the net pressure is zero at the tip of the fracture, and they approximated the average linear velocity of the fluid at any location based on the one-wing injection rate (q_i) divided by the cross-sectional area. They obtained the pressure loss equation in the form,

$$\frac{dp_n}{dx} = -\frac{4\mu q_i}{\pi w_0^3 h_f} \quad (4-15)$$

Combining Equations 4-14 and 4-15, and integrating with the zero net pressure condition at the tip, they obtained the width profile:

$$w_0(x) = w_{w,o} \left(1 - \frac{x}{x_f} \right)^{1/4} \quad (4-16)$$

where the maximum width of the ellipse at the wellbore (see Figure 4-4) is given by

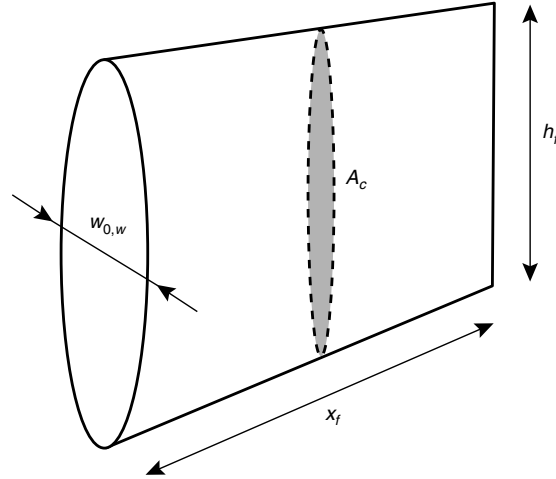


FIGURE 4-4. Basic notation for Perkins-Kern differential model.

$$w_{w,0} = 3.57 \left(\frac{\mu q_i x_f}{E'} \right)^{1/4} \quad (4-17)$$

In reality, the flow rate in the fracture is less than the injection rate, not only because part of the fluid leaks off, but also because the increase of width with time “consumes” another part of the injected fluid. In fact, what is more or less constant along the lateral coordinate at a given time instant, is not the flow rate, but rather the flow velocity, u_{avg} . However, repeating the Perkins-Kern derivation with a constant flow velocity assumption has very little effect on the final results.

Equation 4-17 is the Perkins-Kern width equation. It shows the effect of the injection rate, viscosity, and shear modulus on the width, once a given fracture length is achieved. Knowing the maximum width at the wellbore, we can calculate the average width, multiplying it by a constant shape factor, γ :

$$\bar{w} = \gamma w_{w,0}, \quad \text{where } \gamma = \frac{\pi}{4} \frac{4}{5} = \frac{\pi}{5} = 0.628 \quad (4-18)$$

The shape factor contains two elements. The first one is $\pi/4$, which takes into account that the vertical shape is an ellipse. The second element is $4/5$, which accounts for lateral variation in the maximum width.

In the petroleum industry, a version of Equation 4-17 with a slightly different constant is used more often, and is referred to as the Perkins-Kern-Nordgren (PKN) width equation (Nordgren, 1972):

$$w_{w,0} = 3.27 \left(\frac{\mu q_i x_f}{E'} \right)^{1/4} \quad (4-19)$$

Khristianovich-Zheltoy-Geertsma-deKlerk Width Equation

The first model of hydraulic fracturing, elaborated by Khristianovich and Zheltoy (1955), envisioned a fracture with the same width at any vertical coordinate within the fixed height, h_f . The underlying physical hypothesis is that the fracture faces slide freely at the top and bottom of the layer. The resulting fracture cross section is a rectangle. The width is considered as a function of the coordinate x . It is determined from the plane-strain assumption, now applied in the (every) horizontal plane. The Khristianovich and Zheltoy model contained another interesting assumption: the existence of a non-wetted zone near the fracture tip. Geertsma and deKlerk (1969) accepted the main assumptions of Khristianovich and Zheltoy and reduced the model into an explicit width formula. The KGD width equation is

$$w_w = \left(\frac{336}{\pi} \right)^{1/4} \left(\frac{\mu q_i x_f^2}{E' h_f} \right)^{1/4} = 3.22 \left(\frac{\mu q_i x_f^2}{E' h_f} \right)^{1/4} \quad (4-20)$$

In this case, the shape factor, relating the average width to the wellbore width, has no vertical component. Then, because of the elliptical horizontal shape, we obtain

$$\bar{w} = \gamma w_w, \quad \text{where } \gamma = \frac{\pi}{4} = 0.785 \quad (4-21)$$

Daneshy's (1978) extension of the KGD model considers a non-constant pressure distribution along the fracture length, and a non-Newtonian fracturing fluid whose properties can change with time and temperature. Numerical computations yield the specific leakoff, increase in width, and flow rate at points along the fracture length during fracture extension.

For short fractures, where $2x_f < h_f$, the horizontal plane-strain assumption (KGD geometry) is more appropriate, and for $2x_f > h_f$,

the vertical plane-strain assumption (PKN geometry) is physically more sound. Interestingly, for the special case when the total fracture length and height are equivalent, the two equations give basically the same average width and, hence, fracture volume.

Radial (Penny-shaped) Width Equation

This situation corresponds to horizontal fractures from vertical wells, vertical fractures extending from horizontal wells, or when fracturing relatively thick homogeneous formations—from a limited perforation interval in all cases. While the computations of fracture width are sensitive to how the fluid enters the fracture (a true point source would give rise to infinite pressure), a reasonable model can be postulated by analogy, which results in the same average width as the Perkins-Kern equation when $R_f = x_f = h_f/2$.

The result is

$$\bar{w} = 2.24 \left(\frac{\mu q_i R_f}{E'} \right)^{1/4} \quad (4-22)$$

The real significance of the simple models presented in this section is the insight they provide—helping us to consider the effect of input data on the evolving fracture. Additional insight can be gained by comparing the fracture geometry and net pressure behavior of the models. Table 4-4 provides a direct side-by-side comparison of the basic fracture models (no-leakoff case).

The last row in Table 4-4 deserves particular attention. For the no-leakoff case, net pressure increases with time for the Perkins-Kern model, but decreases with time for the other two models. This is a well-known result that raises some questions. For example, in massive hydraulic fracturing, the net treating pressure most often increases with time, so net pressures derived from the Geertsma-deKlerk and radial models are of limited practical value. A more startling (and less well-known) observation is that the net pressures provided by the Geertsma-deKlerk and radial models are independent of injection rate. The KGD (and radial) view implies that when the fracture extent becomes large, very low net pressures are required to maintain a certain width. While this is a consequence of linear elasticity theory and the way that the plane-strain assumption is applied, it leads to absurd

TABLE 4-4. No-Leakoff Solutions of the Basic Fracture Models

Model	Perkins and Kern	Geertsma and deKlerk	Radial
Fracture Extent	$x_f = c_1 t^{4/5}$	$x_f = c_1 t^{2/3}$	$R_f = c_1 t^{4/9}$
	$c_1 = c'_1 \left(\frac{q_i^3 E'}{\mu h_f^4} \right)^{1/5}$	$c_1 = c'_1 \left(\frac{q_i^3 E'}{\mu h_f^3} \right)^{1/6}$	$c_1 = c'_1 \left(\frac{q_i^3 E'}{\mu} \right)^{1/9}$
	$c'_1 = \left(\frac{625}{512 \pi^3} \right)^{1/5} = 0.524$	$c'_1 = \left(\frac{16}{21 \pi^3} \right)^{1/6} = 0.539$	$c'_1 = 0.572$
Width	$w_{w,0} = c_2 t^{1/5}$	$w_w = c_2 t^{1/3}$	$w_{w,0} = c_2 t^{1/9}$
	$c_2 = c'_2 \left(\frac{q_i^2 \mu}{E' h_f} \right)^{1/5}$	$c_2 = c'_2 \left(\frac{q_i^3 \mu}{E' h_f^3} \right)^{1/6}$	$c_2 = c'_2 \left(\frac{q_i^3 \mu^2}{E'^2} \right)^{1/9}$
	$c'_2 = \left(\frac{2560}{\pi^2} \right)^{1/5} = 3.04$	$c'_2 = \left(\frac{5376}{\pi^3} \right)^{1/6} = 2.36$	$c'_2 = 3.65$
	$\bar{w} = \gamma w_{w,0}$	$\bar{w} = \gamma w_w$	$\bar{w} = \gamma w_{w,0}$
	$\gamma = 0.628$	$\gamma = 0.785$	$\gamma = 0.533$
Net Pressure	$p_{n,w} = c_3 t^{1/5}$	$p_{n,w} = c_3 t^{-1/3}$	$p_{n,w} = c_3 t^{-1/3}$
	$c_3 = c'_3 \left(\frac{E'^4 \mu q_i^2}{h_f^6} \right)^{1/5}$	$c_3 = c'_3 (E'^2 \mu)^{1/3}$	$c_3 = c'_3 (E'^2 \mu)^{1/3}$
	$c'_3 = \left(\frac{80}{\pi^2} \right)^{1/4} = 1.52$	$c'_3 = \left(\frac{21}{16} \right)^{1/3} = 1.09$	$c'_3 = 2.51$

results in the large scale. It is safe to say that the PKN model captures the physical fracturing process better than the other two models.

While many investigations have been performed during the last half century, the same ingredients must always appear in the “mix” of any suggested fracture model: material balance, relating injection rate and fracture volume; linear elasticity, relating fracture width to fracture extent; and fluid mechanics, relating width and pressure loss along the fracture. Additionally, an explicit fracture propagation criterion may be or may not be present.

5

Fracturing of High Permeability Formations

THE EVOLUTION OF THE TECHNIQUE

As recently as the early 1990s, hydraulic fracturing was used almost exclusively for low permeability reservoirs. The large fluid leakoff and unconsolidated sands associated with high permeability formations would ostensibly prevent the initiation and extension of a single, planar fracture with sufficient width to accept a meaningful proppant volume. Moreover, such fracture morphology, even if successfully created and propped, would be incompatible with the defined needs of moderate to high permeability reservoirs, that is, large conductivity (width).

A key breakthrough tied to the advance of high permeability fracturing (HPF) is the tip screenout (TSO), which arrests lateral fracture growth and allows for subsequent fracture inflation and packing. The result is short but wide to exceptionally wide fractures. While in traditional, unrestricted fracture growth an average fracture width of 0.25 in. would be considered normal, in TSO treatments, widths of one inch or even larger are commonly expected.

The role of hydraulic fracturing has expanded to encompass oil wells with permeabilities greater than 50 md and gas wells with over 5 md of permeability (Table 5-1). These wells clearly require a TSO design. Because of these developments, hydraulic fracturing has

TABLE 5-1. Fracturing Role Expanded

Permeability	Gas	Oil
Low	$k < 0.5$ md	$k < 5$ md
Moderate	$0.5 < k < 5$ md	$5 < k < 50$ md
High	$k > 5$ md	$k > 50$ md

captured an enormous share of all well completions, and further gains are certain, only tempered by the economy of scale affecting many petroleum provinces. In places such as the United States and Canada, hydraulic fracturing is poised to be applied to almost all petroleum wells drilled, as was shown in Figure 1-2.

It is interesting that HPF, which is often referred to as *frac & pack* or *fracpac*, did not necessarily originate as an extension of hydraulic fracturing—although HPF borrowed heavily from established techniques—but rather as a means of sand production control.

In controlling the amount of sand production to the surface, there are two distinctly different activities that can be done downhole: *sand exclusion* and *sand deconsolidation control*. Sand exclusion refers to all filtering devices such as screens and gravel packs. Gravel packing, the historically preferred well completion method to remedy sand production, is one such technique. These techniques do not prevent sand migration in the reservoir, so fines migrate and lodge in the gravel pack and screen, causing large damage skin effects. Well performance progressively deteriorates and often is not reversible with matrix stimulation treatments. Attempts to stem the loss in well performance by increasing the pressure drawdown often aggravates the problem further and may potentially lead to wellbore collapse.

A more robust approach is the control of sand deconsolidation, (i.e., prevention of fines migration at the source). It is widely perceived that the use of HPF accomplishes this by mating with the formation in its (relative) undisturbed state and reducing fluid velocities or “flux” at the formation face.

There are actually three factors that contribute to sand deconsolidation: (1) pressure drawdown and the “flux” created by the resulting fluid production, (2) the strength of the rock and integrity of the natural cementation, and (3) the state of stress in the formation. Of these three, the only factor that can be readily altered is the distribution of flow and pressure drawdown. By introducing formation

fluids to the well along a more elongated path (e.g., a hydraulic fracture or horizontal well), it is entirely possible to reduce the fluid flux and, in turn, control sand production.

Consider a simple example by assuming a well that penetrates a 100 ft thick reservoir. If the well has a diameter equal to 1 ft, then the area for incoming radial flow in an open hole completion would be about 300 ft². However, for a fracture half-length of 100 ft, the area of flow would be $(2 \times 100 \times 100 \times 2)$ 40,000 ft². (Note: the second 2 accounts for the two walls of the fracture.) Remember that in a fractured well almost all fluid flow would be from the reservoir into the fracture, and then along the fracture into the well. For the same production rate, this calculation suggests the fluid flux in a fractured well would be less than 1/100th the fluid flux in an unfractured well.

Of course, not a great deal can be done to affect the state of stress or formation competence. The magnitude of earth stresses depends primarily on reservoir depth and to some extent pressure, with the situation becoming more complicated at depths of 3,000 ft or less. Pressure maintenance with gas or water flooding may be counter-productive unless maintenance of reservoir pressure allows economic production at a smaller drawdown. Various innovations have been suggested to remedy incompetent formations or improve on natural cementation—for example, by introducing complex well configurations or various exotic chemical treatments—but there is little that can be done to control this factor either.

In light of the discussion above, it should not be surprising that HPF has replaced gravel packs in many petroleum provinces susceptible to sand production, especially in operations where more sophisticated engineering is done. As with any stimulation technique that results in a productivity index improvement (defined as the production rate divided by the pressure drawdown), it is up to the operator to allocate this new productivity index either to a *larger rate* or a *lower drawdown*, or any combination of the two.

HPF indicates a marked departure from the heritage of gravel packing, incorporating more and more from hydraulic fracture technology. This trend can be seen, for instance, in the fluids and proppants applied. While the original *fracpack* treatments involved sand sizes and “clean” fluids common to gravel packing, the typical proppant sizes for hydraulic fracturing (20/40 mesh) now dominate. The increased application of crosslinked fracturing fluids also illustrates the trend.

For this reason, the terminology of “high permeability fracturing,” or HPF, seems more appropriate than *fracpack*, and is used throughout this book.

In the following section, HPF is considered in a semi-quantitative light in view of competing technologies. This is followed by a discussion of the key issues in high permeability fracturing, including design, execution, and evaluation.

HPF IN VIEW OF COMPETING TECHNOLOGIES

Gravel Pack

Gravel pack refers to the placement of gravel (actually, carefully selected and sized sand) between the formation and the well in order to filter out (retain) reservoir particles that migrate through the porous medium. A “screen” is employed to hold the gravel pack in place. This manner of excluding reservoir fines from flowing into the well invariably causes an accumulation of fines in the near-well zone and a subsequent reduction in the gravel pack permeability (i.e., damage is caused).

The progressive deterioration of gravel pack permeability (increased skin effect) leads, in turn, to a decline in well production. Increasing pressure drawdown to counteract production losses can result in accelerated pore-level deconsolidation and additional sand production.

Any productivity index relationship (e.g., the steady-state expression for oil) can be used to demonstrate this point:

$$J = \frac{q}{p_e - p_{wf}} = \frac{kh}{141.2B\mu \left(\ln \frac{0.472r_e}{r_w} + s \right)} \quad (5-1)$$

Assuming $k = 50$ md, $h = 100$ ft, $B = 1.1$ res bbl/STB, $\mu = 0.75$ cp and $\ln r_e/r_w = 8.5$, the productivity indexes for an ideal (undamaged), a relatively damaged (e.g., $s = 10$), and a typical gravel packed well (e.g., $s = 30$) would be 5, 2.3, and 1.1 STB/d/psi, respectively. For a drawdown of 1,000 psi, these productivity indexes would result in production rates of 5,000, 2,300, and 1,100 STB/d, respectively. Clearly, the difference in production rates between the ideal and gravel packed wells can be considerable and very undesirable.

Consider for a moment the use of high permeability fracturing under the same scenario. This technology combines the advantages of propped fracturing to bypass the near-wellbore damage and gravel packing to provide effective sand control. Figure 5-1 is the classic presentation (compare Figure 3-6) of the equivalent skin effect (Cinco and Samaniego, 1978) in terms of dimensionless fracture conductivity, C_{fD} ($= k_f w / k x_f$), and fracture half-length, x_f .

It can be seen from Figure 5-1 that even with a hydraulic fracture of less than optimum conductivity (e.g., $C_{fD} = 0.5$) and short fracture length (e.g., $x_f = 50$ ft), the skin effect, s_f (again using $r_w = 0.328$ ft), would be equal to -3 .

A negative skin effect equal to -3 applied to Equation 5-1 yields a productivity index of 7.7 STB/d/psi, more than a 50 percent increase over the ideal PI and seven times the magnitude of a damaged gravel-packed well. Even with a damaged fracture (e.g., leakoff-induced damage as described by Mathur et al., 1995) and a skin equal to -1 , the productivity index would be 5.6 STB/d/psi, a five-fold increase over a damaged gravel-packed well.

This calculation brings forward a simple, yet frequently overlooked, issue. Small negative skin values have a much greater impact on well performance than comparable magnitudes (absolute value) of

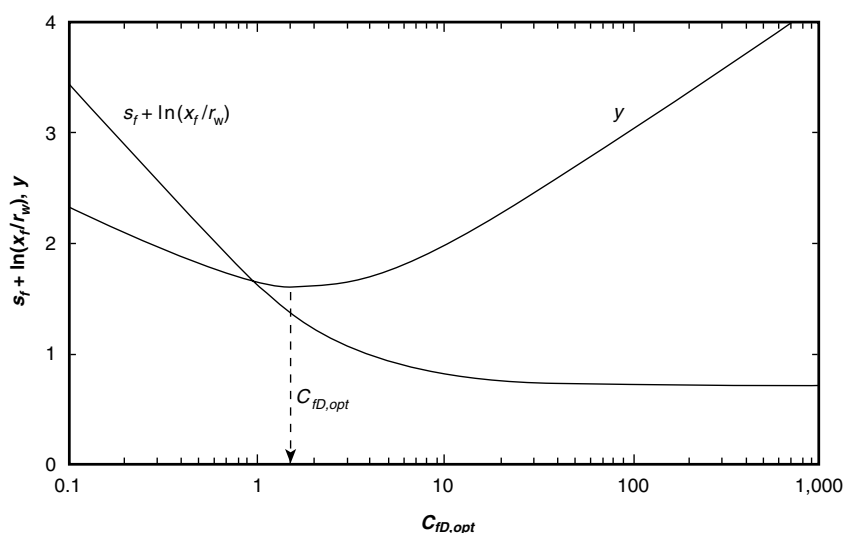


FIGURE 5-1. Pseudoskin factor for a vertical well intersected by a finite conductivity fracture.

positive skin. Furthermore, in the example calculation here, a five-fold increase in the productivity index suggests that the production rate would increase by the same amount if the drawdown is held constant. Under an equally possible scenario, the production rate could be held constant and the drawdown reduced to one-fifth its original value. Any other combination between these two limits can be envisioned.

The utility of high permeability fracturing is, thus, compelling—not just for production rate improvement, but also for the remedy of undesirable drawdown-dependent phenomena.

High-Rate Water Packs

Empirical data reported by Tiner et al. (1996), as distilled and presented in Table 5-2, support the frequent notion that high-rate water packs have an advantage over gravel packs, but do not afford the productivity improvement of HPF. This improvement over gravel packs is reasonable by virtue of the additional proppant placed in the perforation tunnels.

While not shown in the table, the performance of these completions over time is also of interest. It is commonly reported that production from high-rate water packs (as in the case of gravel packs) deteriorates with time. By contrast, Stewart et al. (1995), Mathur et al. (1995), and Ning et al. (1995) all report that production may progressively improve (skin values decrease) during the first several months following a HPF treatment.

PERFORMANCE OF FRACTURED HORIZONTAL WELLS IN HIGH PERMEABILITY FORMATIONS

Two of the most important developments in petroleum production in the last 15 years are horizontal wells and high permeability fracturing. Considerable potential is possible by combining the two.

TABLE 5-2. Skin Values Reported by Tiner et al. (1996)

Gravel Pack	High-Rate Water Pack	HPF
+5 to +10 excellent	+2 to +5 reported	0 to +2 normally
+40 and higher are reported		0 to -3 in some reports

Horizontal wells can be drilled either transverse or longitudinal to the fracture azimuth. The transverse configuration is appropriate for low permeability formations and has been widely used and documented in the literature. The longitudinally fractured horizontal well warrants further attention, specifically in the case of high permeability formations. HPF often results in hydraulic fractures with low dimensionless conductivities. Yet, such fractures installed longitudinally in horizontal wells in high permeability formations can have the net effect of installing a (relative) high conductivity streak in an otherwise limited conductivity flow conduit. Using a generic set of input data, Valkó and Economides (1996) showed discounted revenues for 15 cases that demonstrate this point.

Table 5-3 shows that for a given permeability, the potential for the longitudinally fractured horizontal well is always higher than that of a fractured vertical well and, with realistic fracture widths, may approach the theoretical potential of an infinite conductivity fracture.

Furthermore, the horizontal well fractured with 10-fold less proppant ($C_{fD} = 0.12$) still outperforms the fractured vertical well for $k = 1$ and 10 md, and is competitive at 100 md. The longitudinal configuration may provide the additional benefit of avoiding excess breakdown pressures and tortuosity problems during execution.

DISTINGUISHING FEATURES OF HPF

The Tip Screenout Concept

The critical elements of HPF treatment design, execution, and interpretation are substantially different than for conventional fracture

TABLE 5-3. Discounted Revenue in US\$ (1996) Millions

Configuration	$k = 1$ md	$k = 10$ md	$k = 100$ md
Vertical well	0.73	6.4	57.7
Horizontal well	3.48	14.2	78.8
Fractured vertical well, $C_{fD} = 1.2$	2.59	13.4	89.6
Fractured horizontal well, $C_{fD} = 1.2$	3.88	16.3	95.8
Infinite-conductivity fracture (upper bound for both horizontal and vertical well cases)	3.91	16.3	103.3

treatments. In particular, HPF relies on a carefully timed tip screenout to limit fracture growth and to allow for fracture inflation and packing. This process is illustrated in Figure 5-2.

The TSO occurs when sufficient proppant has concentrated at the leading edge of the fracture to prevent further fracture extension. Once fracture growth has been arrested (and assuming the pump rate is larger than the rate of leakoff to the formation), continued pumping will inflate the fracture (increase fracture width). This TSO and fracture inflation is generally accompanied by an increase in net fracture pressure. Thus, the treatment can be conceptualized in two distinct stages: fracture creation (equivalent to conventional designs) and fracture inflation/packing (after tip screenout).

Figure 5-3 after Roodhart et al. (1994) compares the two-stage HPF process with the conventional single-stage fracturing process. Creation of the fracture and arrest of its growth (tip screenout) is accomplished by injecting a relatively small pad and a 1–4 lbm/gal sand slurry. Once fracture growth has been arrested, further injection builds fracture width and allows injection of higher concentration (e.g., 10–16 lbm/gal) slurry. Final areal proppant concentrations of 20 lbm/ft² are possible. The figure also illustrates the common practice of retarding injection rate near the end of the treatment (coincidental with opening the annulus to flow) to dehydrate/pack the well annulus and near-well fracture. Rate reductions may also be used to force tip screenout in cases where no TSO event is observed on the downhole pressure record.

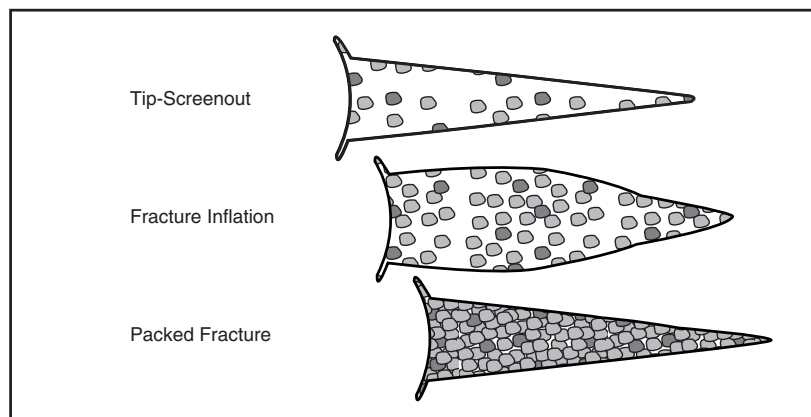


FIGURE 5-2. Width inflation with the tip screenout technique.

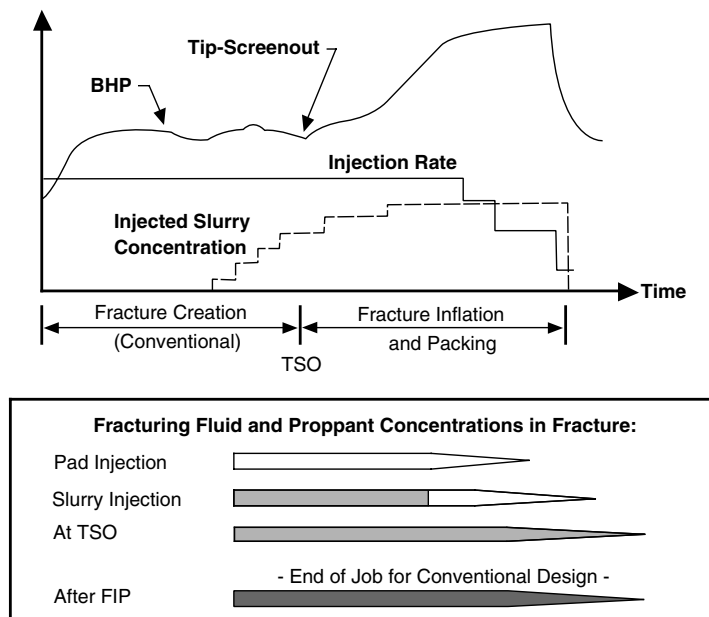


FIGURE 5-3. Comparison of conventional and HPF design concepts.

The tip screenout can be difficult to model, affect, or even detect. There are many reasons for this, including a tendency toward overly conservative design models (resulting in no TSO), partial or multiple tip screenout events, and inadequate pressure monitoring practices.

It is well accepted that accurate bottomhole measurements are imperative for meaningful treatment evaluation. Calculated bottomhole pressures are unreliable because of the dramatic friction pressure effects associated with pumping high sand concentrations through small diameter tubulars and service tool crossovers. Surface data may indicate that a TSO event has occurred when the bottomhole data shows no evidence, and vice versa. Even in the case of downhole pressure data, there has been some discussion of where measurements should be taken. Friction and turbulence concerns have caused at least one operator to conclude that bottomhole pressure data should be collected from below the crossover tool (washpipe gauges) in addition to data collected from the service tool bundle (Mullen et al., 1994).

The detection of tip screenout is discussed further in Chapter 10 along with the introduction of a simple screening tool to evaluate bottomhole data.

Net Pressure and Fluid Leakoff

The entire HPF process is dominated by net pressure and fluid leakoff considerations, first because high permeability formations are typically soft and exhibit low elastic modulus values, and second, because the fluid volumes are relatively small and leakoff rates high (high permeability, compressible reservoir fluids, and non-wall-building fracturing fluids). Also, as described previously, the tip screenout design itself affects the net pressure. While traditional practices applicable to design, execution, and evaluation in MHF continue to be used in HPF, these are frequently not sufficient.

Net Pressure, Closure Pressure, and Width in Soft Formations

Net pressure is the difference between the pressure at any point in the fracture and that of the fracture closure pressure. This definition involves the existence of a unique closure pressure. Whether the closure pressure is a constant property of the formation or depends heavily on the pore pressure (or rather on the disturbance of the pore pressure relative to the long term steady value) is an open question.

In high permeability, soft formations it is difficult (if not impossible) to suggest a simple recipe to determine the closure pressure as classically derived from shut-in pressure decline curves (see Chapter 10). Furthermore, because of the low elastic modulus values, even small, induced uncertainties in the net pressure are amplified into large uncertainties in the calculated fracture width.

Fracture Propagation

Fracture propagation, the availability of sophisticated 3D models notwithstanding, presents complications in high permeability formations, which are generally soft and have low elastic modulus values. For example, Chudnovsky (1996) emphasized the stochastic character of this propagation. Also, because of the low modulus values, an inability to predict net pressure behavior may lead to a significant departure between predicted and actual treatment performance.

It is now a common practice to “predict” fracture propagation and net pressure features using a computer fracture simulator. This trend of substituting clear models and physical assumptions with “knobs”—such as arbitrary stress barriers, friction changes (attributed to erosion,

if decreasing, and sand resistance, if increasing) and less-than-well understood properties of the formation expressed as dimensionless “factors”—does not help to clarify the issue.

LEAKOFF MODELS FOR HPF

Considerable effort has been expended on laboratory investigation of the fluid leakoff process for high permeability cores. A comprehensive report can be found in Vitthal and McGowen (1996) and McGowen and Vitthal (1996). The results raise some questions about how effectively fluid leakoff can be limited by filter cake formation.

In all cases, but especially in high permeability formations, the quality of the fracturing fluid is only one of the factors that influence leakoff, and often not the determining one. Transient fluid flow in the formation might have an equal or even larger impact. Transient flow cannot be understood by simply fitting an empirical equation to laboratory data. The use of models based on solutions to the fluid flow equation in porous media is an unavoidable step.

In the following, three models are considered that describe fluid leakoff in the high permeability environment. The traditional Carter leakoff model requires some modification for use in HPF as shown. (Note: While this model continues to be used across the industry, it is not entirely sufficient for the HPF application.) An alternate, filter cake leakoff model has been developed based on the work by Mayerhofer, et al. (1993). The most appropriate leakoff model for high permeability formations may be that of Fan and Economides (1995), which considers the series resistance caused by the filter cake, the polymer-invaded zone, and the reservoir. While the Carter model is in common use, the models of Mayerhofer, et al. and Fan and Economides represent important building blocks and provide a conceptual framework for understanding the key issue of leakoff in high permeability fracturing.

Fluid Leakoff and Spurt Loss as Material Properties: The Carter Leakoff Model with Nolte’s Power Law Assumption

There are two main schools of thought concerning leakoff. The first considers the phenomenon as a *material property* of the fluid/rock system. The basic relation (called the integrated Carter equation, given also in Chapter 4) is given in consistent units as

$$\frac{V_L}{A_L} = 2C_L\sqrt{t} + S_p \quad (5-2)$$

where A_L is the area and V_L is the total volume lost during the time period from time zero to time t . To make use of material balance, the term V_L must be described. For rigorous theoretical development, V_L is the volume of liquid entering the formation through the two created fracture surfaces of one wing. The integration constant, S_p , is called the spurt loss coefficient and is measured in units of length. It can be considered as the *width* of the fluid body passing through the surface instantaneously at the very beginning of the leakoff process, while $2C_L\sqrt{t}$ is the width of the fluid body following the first slug. The two coefficients, C_L and S_p , can be determined from laboratory or field tests.

As discussed in more detail in Chapter 4, Equation 5-2 can be visualized assuming that the given surface element “remembers” when it has been opened to fluid loss and has its own “zero” time that is likely different from that of other elements along the fracture surface. Points on the fracture face near the well are opened at the beginning of pumping while the points at the fracture tip are younger. Application of Equation 5-2 or its differential form necessitates tracking the opening time for different fracture-face elements, as discussed in Chapter 4.

The second school of thought considers leakoff as a consequence of flow mechanisms in the porous medium, and employs a corresponding mathematical description.

Filter Cake Leakoff Model According to Mayerhofer, et al.

The method of Mayerhofer, et al. (1993) describes the leakoff rate using two parameters that are physically more realistic than the leakoff coefficient: (1) filter cake resistance at a reference time and (2) reservoir permeability. It is assumed that these parameters (R_0 , the reference resistance at a reference time t_0 , and k_r , the reservoir permeability) have been identified from a minifrac diagnostic test. In addition, reservoir pressure, reservoir fluid viscosity, porosity, and total compressibility are assumed to be known.

Total pressure gradient from inside a created fracture out into the reservoir, Δp , at any time during the injection, can be written as

$$\Delta p(t) = \Delta p_{face}(t) + \Delta p_{piz}(t) + \Delta p_{res}(t) \quad (5-3)$$

where Δp_{face} is the pressure drop across the fracture face dominated by the filtercake, Δp_{piz} is the pressure drop across a polymer invaded zone, and Δp_{res} is the pressure drop in the reservoir. This concept is shown in Figure 5-4.

In a series of experimental works using typical hydraulic fracturing fluids (e.g., borate and zirconate crosslinked fluids) and cores with less than 5 md of permeability, no appreciable polymer invaded zone was detected. This simplifying assumption is not valid for linear gels such as HEC (which do not form a filter cake) and may break down for crosslinked fluids at higher permeabilities (e.g., 200 md). Yet, at least for crosslinked fluids in a broad range of applications, the second term in the right-hand side of Equation 4-21 can reasonably be ignored, so

$$\Delta p(t) = \Delta p_{face}(t) + \Delta p_{res}(t) \quad (5-4)$$

The filter cake pressure term can be expressed as a function of, and is proportional to, R_0 , the characteristic resistance of the filter cake. The transient pressure drop in the reservoir can be re-expressed as a series expansion of p_D , a dimensionless pressure function describing the behavior (unit response) of the reservoir. Dimensionless time, t_D , is calculated with the maximum fracture length reached at time

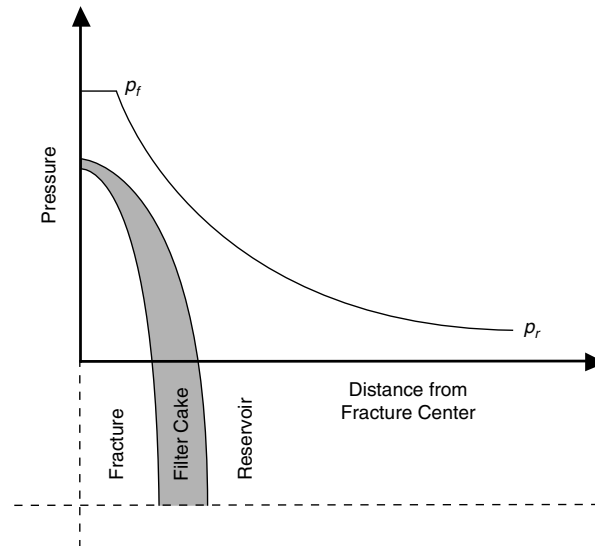


FIGURE 5-4. Filter cake plus reservoir pressure drop in the Mayerhofer et al. (1993) model.

t_n . And r_p is introduced as the ratio of permeable height to the total height (h_p/h_f).

With rigorous introduction of these variables and considerable rearrangement (not shown), an expression for the leakoff rate can be written that is useful for both hydraulic fracture propagation and fracture-closure modeling:

$$q_n = \frac{\Delta p(t_n) - \frac{\mu_r}{\pi k_r r_p h_f} \left[-q_{n-1} p_D(t_{Dn} - t_{Dn-1}) + \sum_{j=1}^{n-1} (q_j - q_{j-1}) p_D(t_{Dn} - t_{Dj-1}) \right]}{\frac{R_0}{2r_p A_n} \sqrt{\frac{t_n}{t_e}} + \frac{\mu_r p_D(t_{Dn} - t_{Dn-1})}{\pi k_r r_p h_f}} \quad (5-5)$$

This expression allows for the determination of the leakoff rate at any time instant, t_n , if the total pressure difference between the fracture and the reservoir is known, as well as the *history* of the leakoff process. The dimensionless pressure solution, $p_D(t_{Dn} - t_{Dj-1})$, must be determined with respect to a dimensionless time that takes into account the *actual* fracture length at t_n .

The model can be used to analyze the pressure fall-off subsequent to a fracture injection (minifrac) test, as described by Mayerhofer, et al. (1995). The method requires more input data than the similar analysis based on Carter leakoff, but it offers the distinct advantage of differentiating between the two major factors in the leakoff process, filter cake resistance and reservoir permeability.

Polymer-Invaded Zone Leakoff Model of Fan and Economides

The leakoff model of Fan and Economides (1995) concentrates on the additional resistance created by the polymer-invaded zone.

The total driving force behind fluid leakoff is the pressure difference between the fracture face and the reservoir, $p_{frac} - p_i$, which is equivalent to the sum of three separate pressure drops—across the filter cake, the polymer-invaded zone, and in the reservoir:

$$p_{frac} - p_i = \Delta p_{cake} + \Delta p_{inv} + \Delta p_{res} \quad (5-6)$$

The fracture treating pressure is equivalent to the net pressure plus fracture closure pressure (minimum horizontal stress).

When a non-cake building fluid is used, the pressure drop across the filter cake is negligible. This is the case for many HPF treatments.

The physical model of this situation (i.e., fluid leakoff controlled by polymer invasion and transient reservoir flow) is depicted in Figure 5-5. The polymer invasion is labeled in the figure as region 1, while the region of reservoir fluid compression (transient flow) is denoted as 2.

By employing conservation of mass, a fluid flow equation, and an appropriate equation of state, a mathematical description of this fluid leakoff scenario can be written. As a starting point, Equation 5-7 describes the behavior of a Power law fluid in porous media:

$$\frac{\partial^2 p}{\partial x^2} = \frac{n\phi\mu_{eff}c_t}{k} \left(\frac{1}{u}\right)^{1-n} \frac{\partial p}{\partial t} \quad (5-7)$$

where c_t is the system compressibility, k is the formation permeability, u is the superficial flow rate, n is the fluid flow behavior index, ϕ is the formation porosity, and $\mu_{eff} = \frac{K'}{12} \left(9 + \frac{3}{n}\right)^n (150k\phi)^{\frac{1-n}{2}}$ is the fluid effective viscosity (K' is the power law fluid consistency index).

Combining the description of the polymer-invaded zone and the reservoir, the total pressure drop is given by Fan and Economides (1995) as

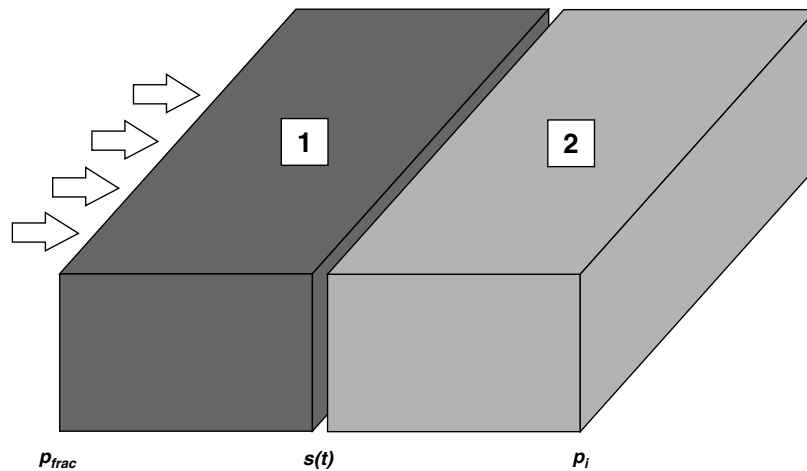


FIGURE 5-5. Fluid leakoff model with polymer invasion and transient reservoir flow.

$$p_{frac} - p_r = \frac{\sqrt{\pi} \phi \eta}{2} \frac{k}{k} \left\{ \begin{array}{l} \mu_{app} \sqrt{\alpha_1} e^{\left(\frac{\eta}{\sqrt{4\alpha_1}}\right)^2} \operatorname{erf}\left(\frac{\eta}{\sqrt{4\alpha_1}}\right) \\ + \mu_r \sqrt{\alpha_2} e^{\left(\frac{\eta}{\sqrt{4\alpha_2}}\right)^2} \operatorname{erfc}\left(\frac{\eta}{\sqrt{4\alpha_2}}\right) \end{array} \right\} \quad (5-8)$$

$$\text{where } a_1 = \frac{k}{n\phi\mu_{eff}\left(\frac{1}{u}\right)^{1-n} c_t} \text{ and } a_2 = \frac{k}{\phi\mu c_t}.$$

At given conditions, Equation 5-8 can be solved iteratively for the parameter η (not to be confused with fluid efficiency). Once the value of η is found for a specified total pressure drop, the leakoff rate is calculated from

$$q_L = A \left(\frac{\eta}{2\phi} \right) \frac{1}{\sqrt{t}} \quad (5-9)$$

In other words, the factor $\eta/(2\phi)$ can be considered a *pressure-dependent apparent leakoff coefficient*.

FRACTURING HIGH PERMEABILITY GAS CONDENSATE RESERVOIRS

In gas condensate reservoirs, a situation emerges very frequently that is tantamount to fracture face damage. Because of the pressure gradient that is created normal to the fracture, liquid condensate is formed, which has a major impact on the reduction of the relative permeability to gas. Such a reduction depends on the phase behavior of the fluid and the penetration of liquid condensate, which in turn, depends on the pressure drawdown imposed on the well. These phenomena cause an apparent damage that affects the performance of all fractured wells, but especially those with high reservoir permeability.

Wang, et al. (2000) presented a model that predicts the fractured well performance in gas condensate reservoirs, quantifying the effects of gas permeability reduction. Furthermore, they presented fracture treatment design for condensate reservoirs. The distinguishing feature

primarily affects the required fracture length to offset the problems associated with the emergence of liquid condensate.

Gas relative permeability curves were derived using a pore-scale network model and are represented by a weighted linear function of immiscible and miscible relative permeability curves:

$$k_{rg} = fk_{rgI} + (1-f)k_{rgM} \quad (5-10)$$

where k_{rg} is the gas relative permeability, and f is a weighing factor that is a function of the capillary number,

$$f = \frac{1}{1 + \left(\frac{N_c}{a}\right)^{1/b}} \quad (5-11)$$

The numerical values for a and b are 1.6×10^{-3} and 0.324, respectively, and N_c is the capillary number, defined as

$$N_c = \frac{k\nabla p}{\sigma} \quad (5-12)$$

In Equation 5-12, k is the permeability, ∇p is the pressure gradient, and σ is the interfacial tension. The conventional relative permeability for capillary dominated (immiscible) flow in Equation 5-10, k_{rgI} , is defined as

$$k_{rgI} = \left(\frac{S_g}{1 - S_{wi}}\right)^{n_g} \quad (5-13)$$

where S_g is the gas saturation, S_{wi} is the connate water saturation, and n_g is a constant equal to 5.5. The relative permeability function in the limit of viscous dominated (miscible) flow, k_{rgM} , is defined as

$$k_{rgM} = \frac{S_g}{1 - S_{wi}} \quad (5-14)$$

Recall that Cinco and Samaniego (1981) provided an expression of the fracture face skin effect that is additive to the dimensionless pressure for the finite conductivity fracture performance:

$$s_{fs} = \frac{\pi b_s}{2x_f} \left(\frac{k}{k_s} - 1\right) \quad (5-15)$$

where b_s is the penetration of damage and k_s is the damaged permeability.

An analogy can readily be made for a hydraulically fractured gas condensate reservoir. Liquid condensate that drops out normal to the fracture face can also result in a skin effect, in this case reflecting a reduction in the relative permeability to gas. The penetration of damage would be the zone inside which liquid condensate exists (i.e., the dew point pressure establishes the boundary).

The permeability ratio reduces to the ratio of the relative permeabilities, and because at the boundary k_{rg} is equal to 1, Equation 5-15 becomes simply,

$$s_{fs} = \frac{\pi b_s}{2x_f} \left(\frac{1}{k_{rg}} - 1 \right) \quad (5-16)$$

Optimizing Fracture Geometry in Gas Condensate Reservoirs

In gas condensate reservoirs, the fracture performance is likely to be affected greatly by the presence of liquid condensate, tantamount to fracture face damage. An assumption for the evaluation is that the reservoir pressure at the boundary of this “damaged” zone must be exactly equal to the dew point pressure.

For any fracture length and a given flowing bottomhole pressure inside the retrograde condensation zone of a two-phase envelope, the pressure profile normal to the fracture phase and into the reservoir will delineate the points where the pressure is equal to the dew point pressure. From this pressure profile, the distribution of fracture face skin can be determined. The depth of the affected zone is determined from Equation 5-16, the modified Cinco-Ley and Samaniego expression. An additional necessary element is the relative permeability impairment given by the correlation presented in Equations 5-10 to 5-14.

Two example case studies are presented below. The first represents a reservoir with 5 md permeability and a gas condensate with a dew point pressure of 2,545 psi. The flowing bottomhole pressure is 1,800 psi. First, a standard hydraulic fracture optimization—ignoring the effects of the fracture face skin—using a proppant number, N_{prop} , equal to 0.02, results in an expected dimensionless fracture conductivity of 1.6 and a fracture half-length of 220 ft for a 4,000 ft square reservoir. (The value of the proppant number, assuming $k_f = 50,000$ md, $h = 50$ ft, $\rho_p = 165$ lb/ft³ and $\phi_p = 0.4$, implies a proppant mass approximately equal to 80,000 lb_m.) The dimensionless productivity index would be 0.35.

A series of simulations based on the work of Wang, et al. shows the maximum productivity index that can be achieved when the gas condensate skin is introduced, and indicates appropriate changes to the fracture design. The fracture length is progressively increased, while the proppant number (i.e., the mass of proppant injected) is held constant. This, of course, causes an unavoidable reduction in the fracture conductivity, even while maximizing the productivity index.

The results, shown in Figure 5-6, indicate an optimum fracture half-length of 255 ft (16 percent increase from the zero-skin optimum) and an optimum dimensionless conductivity of 1.2 instead of 1.6. Much more significant is the drop in the optimum productivity index to 0.294.

Meeting the expected zero-skin productivity index of 0.35 would necessitate raising the proppant number to approximately 0.045—and more than double the required mass of proppant.

For a much higher permeability reservoir (200 md)—again, ignoring the fracture face skin initially—the same calculation results in an optimum fracture half-length equal to 35 ft ($C_{fD} = 1.6$). The proppant number for this case is 0.0005 (for the same 80,000 lb_m of proppant). The corresponding dimensionless productivity index is 0.21.

Figure 5-7 is the optimization for the fracture dimensions with gas condensate damage, showing an optimum half-length of 45 ft (a 30

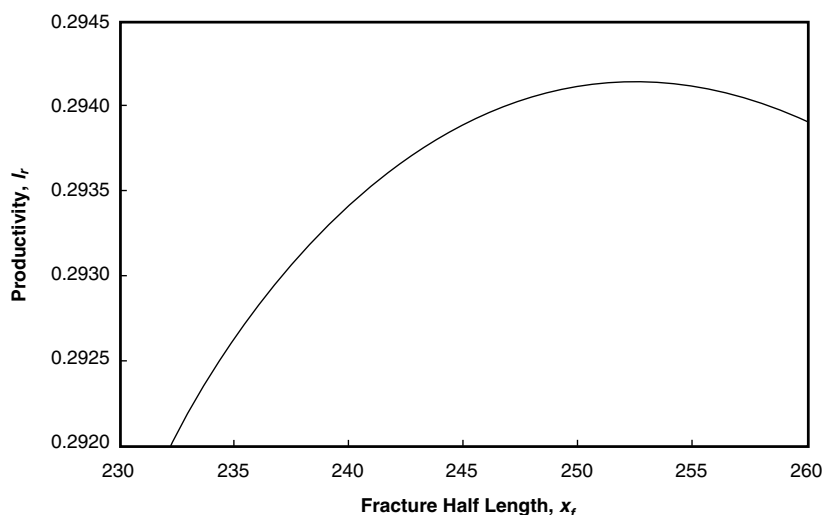


FIGURE 5-6. Optimized fracture geometry in a gas-condensate reservoir ($k = 5$ md).

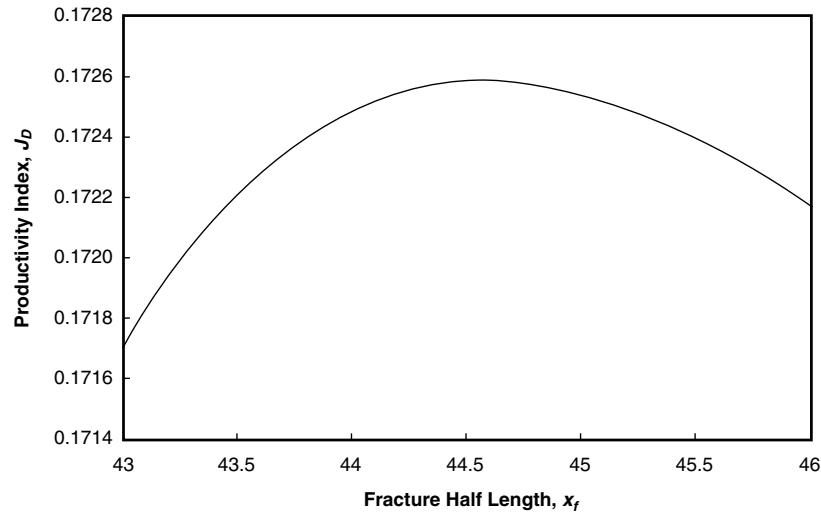


FIGURE 5-7. Optimized fracture geometry in a gas-condensate reservoir ($k = 200$ md).

percent increase over the zero-skin optimum). The new optimum C_{fD} is 1 and the corresponding productivity index is 0.171.

Here the impact of gas condensate damage on the productivity index expectations and what would be needed to counteract this effect is far more serious. The required proppant number would be 0.003—suggesting 6 times the mass of proppant originally contemplated! In most cases, such a fracture treatment would be highly impracticable, so the expectations for well performance would need to be pared down considerably.

EFFECT OF NON-DARCY FLOW IN THE FRACTURE

Non-Darcy flow is another important issue that deserves specific consideration in the context of HPF. Non-Darcy flow in gas reservoirs causes a reduction of the productivity index by at least two mechanisms. First, the apparent permeability of the formation may be reduced (Wattenbarger and Ramey, 1969) and second, the non-Darcy flow may decrease the conductivity of the fracture (Guppy et al., 1982).

Consider a closed gas reservoir producing under pseudosteady-state conditions, and apply the concept of pseudoskin effect determined by dimensionless fracture conductivity.

Definitions and Assumptions

Gas production is calculated from the pseudosteady-state deliverability equation:

$$q = \frac{\pi khT_{sc} [m(\bar{p}) - m(p_{wf})]}{p_{sc}T} \times \frac{k_{r,app}}{k_r \left[f_1(C_{fD,app}) + \ln \left(\frac{0.472r_e}{x_f} \right) \right]} \quad (5-17)$$

where $m(p)$ is the pseudopressure function, $k_{f,app}$ is the apparent permeability of the proppant in the fracture, and $k_{r,app}$ is the apparent permeability of the formation. (All equations in this subsection are given for a consistent system of units, such as SI.) The function f was introduced by Cinco-Ley and Samaniego (1981) and was presented in Chapter 3 as

$$f_1(C_{fD}) = s_f + \ln \frac{x_f}{r_w} = \frac{1.65 - 0.328u + 0.116u^2}{1 + 0.18 \ln u + 0.064u^2 + 0.005u^3} \quad (5-18)$$

where $u = \ln C_{fD}$.

The apparent dimensionless fracture conductivity is defined by

$$C_{fD,app} = \frac{k_{f,app}w}{k_{r,app}x_f} \quad (5-19)$$

The apparent permeabilities are flow-rate dependent; therefore, the deliverability equation becomes implicit in the production rate.

Proceeding further requires a model of non-Darcy flow. Almost exclusively, the Forcheimer equation is used:

$$-\frac{dp}{dx} = \frac{\mu}{k}v + \beta\rho|v|v \quad (5-20)$$

where $v = q_a/A$ is the Darcy velocity and β is a property of the porous medium.

A popular correlation was presented by Firoozabadi and Katz (1979) as

$$\beta = \frac{c}{k^{1.2}} \quad (5-21)$$

where $c = 8.4 \times 10^{-8} \text{ m}^{1.4}$ ($= 2.6 \times 10^{10} \text{ ft}^{-1} \text{ md}^{1.2}$).

78 ■ Unified Fracture Design

To apply the Firoozabadi and Katz correlation, we write

$$-\frac{dp}{dx} = \mu v \frac{1}{k} \left(1 + \frac{\beta k \rho |v|}{\mu} \right) = \mu v \frac{1}{k} \left(1 + \frac{c \rho |v|}{k^{0.2} \mu} \right) \quad (5-22)$$

showing that

$$\frac{k_{app}}{k} = \frac{1}{1 + \frac{c \rho |v|}{k^{0.2} \mu}} \quad (5-23)$$

The equation above can be used both for the reservoir and for the fracture if correct representative linear velocity is substituted. In the following, it is assumed that $h = h_f$.

A representative linear velocity for the reservoir can be given in terms of the gas production rate as

$$v = \frac{q_a}{4hx_f} \quad (5-24)$$

where q_a is the in-situ (actual) volumetric flow rate; hence, for the reservoir non-Darcy effect,

$$\left(\frac{c \rho v}{k^{0.2} \mu} \right)_r = \left(\frac{c \rho q_a}{2h\mu} \right) \frac{1}{2x_f k_r^{0.2}} \quad (5-25)$$

A representative linear velocity in the fracture can be given in terms of the gas production rate as

$$v = \frac{q_a}{2hw} \quad (5-26)$$

Thus, for the non-Darcy effect in the fracture, one can use

$$\left(\frac{c \rho v}{k^{0.2} \mu} \right)_f = \left(\frac{c \rho q_a}{2h\mu} \right) \frac{1}{wk_f^{0.2}} \quad (5-27)$$

The term ρq_a is the mass flow rate and is the same in the reservoir and in the fracture; $c \rho q_a$ is expressed in terms of the gas production rate as

$$\frac{c \rho q_a}{2h\mu} = \frac{c \rho_a \gamma_g}{2h\mu} q = c_0 q \quad (5-28)$$

where q is the gas production rate in standard volume per time, γ_g is the specific gravity of gas with respect to air, and ρ_a is the density of

air at standard conditions. The factor c_0 is constant for a given reservoir-fracture system.

The final form of the apparent permeability dependence on production rate is

$$\left(\frac{k_{app}}{k}\right)_r = \frac{1}{1 + \frac{c_0 q}{2x_f k_r^{0.2}}} \quad (5-29)$$

for the reservoir and

$$\left(\frac{k_{app}}{k}\right)_f = \frac{1}{1 + \frac{c_0 q}{wk_f^{0.2}}} \quad (5-30)$$

for the fracture. As a consequence, the deliverability equation becomes

$$q = \frac{\pi kh T_{sc} [m(\bar{p}) - m(p_{wf})]}{p_{sc} T} \times \frac{1}{\left(1 + \frac{c_0 q}{2x_f k_r^{0.2}}\right) \left[f_1(C_{fD,app}) + \ln\left(\frac{0.472r_e}{x_f}\right) \right]} \quad (5-31)$$

where

$$C_{fD,app} = \frac{k_f w}{k_r x_f} \frac{1 + \frac{c_0 q}{wk_f^{0.2}}}{1 + \frac{c_0 q}{2x_f k_r^{0.2}}} \quad (5-32)$$

The *additional* skin effect, s_{ND} , appearing because of non-Darcy flow, can be expressed as

$$s_{ND} = \left(1 + \frac{c_0 q}{2x_f k_r^{0.2}}\right) \left[f_1(C_{fD,app}) + \ln\left(\frac{0.472r_e}{x_f}\right) \right] - \left[f_1(C_{fD}) + \ln\left(\frac{0.472r_e}{x_f}\right) \right] \quad (5-33)$$

The additional non-Darcy skin effect is always positive and depends on the production rate in a nonlinear manner.

Equations 5-31 and 5-33 are of primary importance to interpret post-fracture well testing data and to forecast production. If the mechanism responsible for the post-treatment skin effect is not understood clearly, the evaluation of the treatment and the production forecast might be severely erroneous.

Case Study for the Effect of Non-Darcy Flow

As previously discussed, non-Darcy flow in a gas reservoir causes a reduction of the productivity index by at least two mechanisms. First, the apparent permeability of the formation may be reduced, and second, the non-Darcy flow may decrease the fracture conductivity. In this case study, the effect of non-Darcy flow on production rates and observed skin effects is investigated.

Reservoir and fracture properties are given in Table 5-4.

A simplified form of Equation 5-30 in field units is

$$q = \frac{\bar{p}^2 - p_{wf}^2}{1424\mu ZT} \times \frac{1}{\left(1 + \frac{c_0 q}{2x_f k_r^{0.2}}\right) \left[f_1(C_{fD,app}) + \ln\left(\frac{0.472r_e}{x_f}\right) \right]} \quad (5-34)$$

where $c_0 = \frac{c\rho_a\gamma_g}{2h\mu}$ must be expressed in ft-md^{0.2}/MMSCF/day. In the given example, $c_0 = 73$ ft-md^{0.2}/MMSCF/day and

$$C_{fD,app} = \left(\frac{k_f w}{k_r x_f}\right) \frac{1 + \frac{c_0}{2x_f k_r^{0.2}} q}{1 + \frac{c_0}{w k_f^{0.2}} q} = \left(\frac{k_f w}{k_r x_f}\right) \frac{1 + c_{0r} q}{1 + c_{0f} q} \quad (5-35)$$

where $c_{0r} = 2.34 \times 10^{-3} \text{ m}^3/\text{s} = 7.67 \times 10^{-2} \text{ (MSCF/day)}^{-1}$
 $c_{0f} = 6.14 \times 10^{-1} \text{ m}^3/\text{s} = 2.78 \times 10^2 \text{ (MSCF/day)}^{-1}$

Therefore, in field units

$$C_{fD,app} = 1.39 \frac{1 + 0.76q}{1 + 280q} \quad \text{and} \quad (5-36)$$

$$q = \frac{4000^2 - p_{wf}^2}{21.645} \times \frac{1}{(1 + 0.76q) \left[f_1(C_{fD,app}) + 3.16 \right]} \quad (5-37)$$

The non-Darcy component of the skin effect can be calculated as

$$s_{ND} = (1 + 0.00076q) \left[f_1(C_{fD,app}) + 3.16 \right] - 4.619 \quad (5-38)$$

The results are shown graphically in Figures 5-8 to 5-10.

TABLE 5-4. Data for Fractured Well in Gas Reservoir

r_e	ft	1,500
μ	cp	0.02
Z	N/A	0.95
T	°R	640
k_r	md	10
h	ft	80
h_f	ft	80
k_f	md	10,000
x_f	ft	30
w	inch	0.5
γ_g	N/A	0.65
\bar{p}	psi	4,000
r_w	ft	0.328

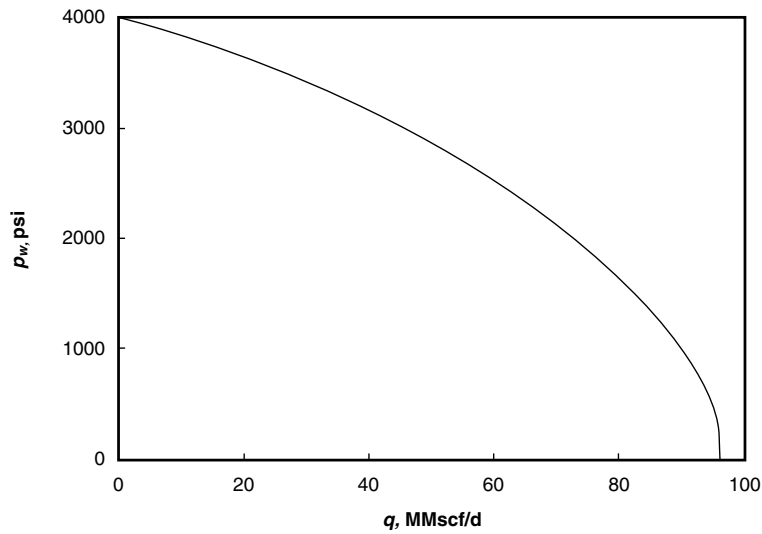


FIGURE 5-8. Inflow performance of fractured gas reservoir, non-Darcy effect from Firoozabadi-Katz correlation.

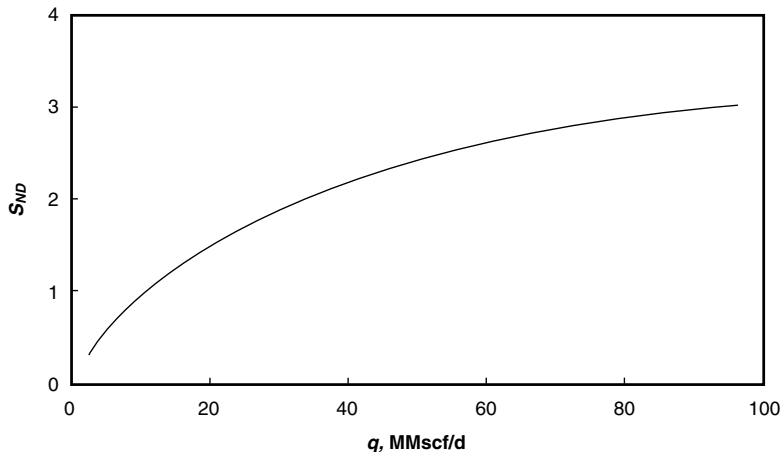


FIGURE 5-9. Additional skin effect from non-Darcy flow in the fracture.

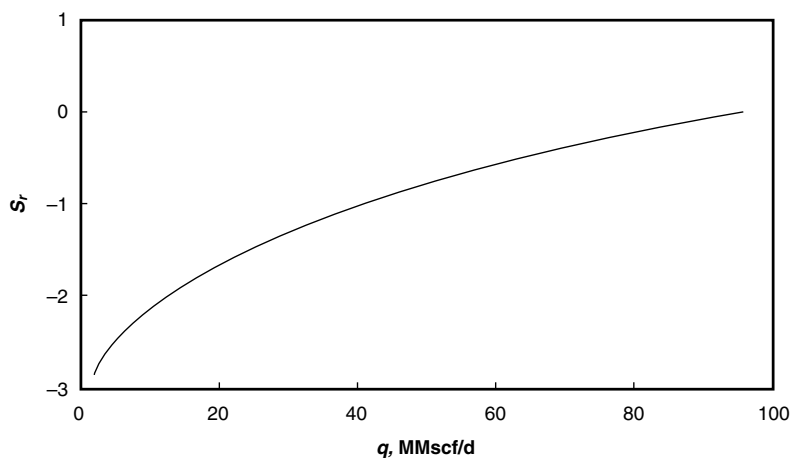


FIGURE 5-10. Observable pseudoskin, the resulting effect of fracture with non-Darcy flow effects.

It is apparent that the effect of the fracture (negative skin on the order of -3) is hidden by the positive skin effect induced by non-Darcy flow. The zero or positive observable skin effect, while directly attributable to the (inevitable) effect of non-Darcy flow, might be interpreted as an unsuccessful HPF job.

6

Fracturing Materials

Materials used in the fracturing process include fracturing fluids, fluid additives, and proppants. The fluid and additives act together, first to create the hydraulic fracture, and second, to transport the proppant into the fracture. Once the proppant is in place and trapped by the earth stresses (“fracture closure”), the carrier fluid and additives are degraded in-situ and/or flowed back out of the fracture (“fracture cleanup”), establishing the desired highly-productive flow path.

Proppants and chemicals constitute a large share of the total cost to fracture treat a well. The relative value of fracturing materials and pumping costs for treatments performed in the United States are estimated as follows: 45 percent for pumping (pump rental and horsepower charges), 25 percent for proppants, 20 percent for fracturing chemicals, and 10 percent for acid.

Materials and proppants used in hydraulic fracturing have undergone tremendous changes since the first commercial fracturing treatment was performed in 1949 with a few sacks of coarse sand and gelled gasoline as the carrier fluid.

FRACTURING FLUIDS

The fracturing fluid transmits hydraulic pressure from the pumps to the formation, which creates a fracture, and then transports proppant (hence the name *carrier fluid*) into the created fracture. The invasive fluids are then removed (or cleaned up) from the formation, allowing the production of hydrocarbons. Factors to consider when selecting the fluid include availability, safety, ease of mixing and use, viscosity characteristics, compatibility with the formation, ability to be cleaned up from the fracture, and cost.

Fracturing fluids can be categorized as (1) oil- or water-base, usually “crosslinked” to provide the necessary viscosity, (2) mixtures of oil and water, called emulsions, and (3) foamed oil- and water-base systems that contain nitrogen or carbon dioxide gas. Oil-based fluids were used almost exclusively in the 1950s. By the 1990s, more than 90 percent of fracturing fluids were crosslinked water-based systems. Today, nitrogen and carbon dioxide systems in water-based fluids are used in about 25 percent of fracture stimulation jobs.

Table 6-1 lists the most common fracturing fluids in order of current usage. The choice of which crosslinking method to use is based

TABLE 6-1. Crosslinked Fluid Types

Crosslinker	Gelling Agent	pH Range	Application Temperature
B, non-delayed	Guar, HPG	8–12	70–300 °F
B, delayed	Guar, HPG	8–12	70–300 °F
Zr, delayed	Guar	7–10	150–300 °F
Zr, delayed	Guar	5–8	70–250 °F
Zr, delayed	CMHPG, HPG	9–11	200–400 °F
Zr-a, delayed	CMHPG	3–6	70–275 °F
Ti, non-delayed	Guar, HPG, CMHPG	7–9	100–325 °F
Ti, delayed	Guar, HPG, CMHPG	7–9	100–325 °F
Al, delayed	CMHPG	4–6	70–175 °F
Sb, non-delayed	Guar, HPG	3–6	60–120 °F

a—compatible with carbon dioxide

on the capability of a fluid to yield high viscosity while meeting cost and other performance requirements.

Viscosity is perhaps the most important property of a fracturing fluid. Guar gum, produced from the guar plant, is the most common gelling agent used to create this viscosity. Guar derivatives called hydroxypropyl guar (HPG) and carboxymethyl-hydroxypropyl guar (CMHPG) are also used because they provide lower residue, faster hydration, and certain rheological advantages. For example, less gelling agent is required if the guar is crosslinked.

The base guar or guar derivative is reacted with a metal that couples multiple strands of gelling polymer. Crosslinking effectively increases the size of the base guar polymer, increasing the viscosity in the range of shear rates important for fracturing from 5- to 100-fold. Boron (B) is often used as the crosslinking element, followed by organometallic crosslinkers such as zirconium (Zr) and titanium (Ti), and to a lesser extent antimony (Sb) and aluminum (Al).

Foams are especially useful in water-sensitive or depleted (low pressure) reservoirs (Chambers, 1994). Their application minimizes fracture face damage and eases the clean-up of the wellbore after the treatment.

FLUID ADDITIVES

Gelling agent, crosslinker, and pH control (buffer) materials define the specific fluid type and are not considered to be additives. Fluid additives are materials used to produce a specific effect independent of the fluid type. Table 6-2 lists commonly used additives.

Biocides control bacterial contamination. Most waters used to prepare fracturing gels contain bacteria that originate either from contaminated source water or the storage tanks on location. The bacteria produce enzymes that can destroy viscosity very rapidly. Bacteria can be effectively controlled by raising the pH to greater than 12, adding bleach, or employing a broad-spectrum biocide.

Fluid loss control materials provide spurt loss control. The material consists of finely ground particles ranging from 0.1 to 50 microns. The most effective low-cost material is ground silica sand. Starches, gums, resins, and soaps can also be used, with the advantage that they allow some degree of post-treatment cleanup by virtue of their solubility in water. Note that the guar polymer itself eventually controls leakoff, once a filter cake is established.

TABLE 6-2. Fracturing Fluid Additives

Additive	Concentration, gal or lb _m added per 1,000 gallons of clean fluid	Purpose
Biocide	0.1–1.0 gal	Prevents guar polymer decomposition by bacteria
Fluid loss	10–50 lb _m	Decreases leakoff of fluid during fracturing
Breakers	0.1–10 lb _m	Provides controlled fluid viscosity reduction
Friction reducers	0.1–1.0 gal	Reduces wellbore frictional pressure loss while pumping
Surfactants	0.05–10 gal	Reduces surface tension, prevents emulsions, and changes wettability
Foaming agents	1–10 gal	Provides stable foam with nitrogen and carbon dioxide
Clay control	1–3% KCl typical	Provides temporary or permanent clay (water compatibility)

Breakers reduce viscosity by reducing the size of the guar polymer, thereby having the potential to dramatically improve post-treatment cleanup and production. Table 6-3 summarizes several breaker types and application temperatures.

Surfactants prevent emulsions, lower surface tension, and change wettability (i.e., to water wet). Reduction of surface tension allows improved fluid recovery. Surfactants are available in cationic, nonionic, and anionic forms, and are included in most fracturing treatments. Some specialty surfactants provide improved wetting and fluid recovery.

Foaming agents provide the surface-active stabilization required to maintain finely divided gas dispersion in foam fluids. These ionic materials also act as surfactants and emulsifiers. Stable foam cannot be prepared without a surfactant for stabilization.

Clay control additives produce temporary compatibility in water-swelling clays. Solutions containing 1 to 3 percent KCl or other salts are typically employed. Organic chemical substitutes are now available, which are used at lower concentrations.

The type of additives and concentrations used depend greatly on the reservoir temperature, lithology, and fluids. Tailoring of additives for specific applications and advising clients is a main function of the QA/QC chemist.

TABLE 6-3. Fracturing Fluid Breakers

Breaker	Application Temperature	Comments
Enzyme	60–200 °F	Efficient breaker; limit use to pH less than 10
Encapsulated enzyme	60–200 °F	Allows higher concentrations for faster breaks
Persulfates (sodium, ammonium)	120–200 °F	Economical; very fast at higher temperatures
Activated persulfates	70–120 °F	Low temperature and high pH applications
Encapsulated persulfates	120–200 °F	Allows higher concentrations for faster breaks
High temperature oxidizers	200–325 °F	Used where persulfates are too fast-acting

PROPPANTS

Because proppants must oppose earth stresses to hold open the fracture after release of the fracturing fluid hydraulic pressure, material strength is of crucial importance. The propping material must be strong enough to bear the closure stress, otherwise the conductivity of the (crushed) proppant bed will be considerably less than the design value (both the width and permeability of the proppant bed decrease). Other factors considered in proppant selection are size, shape, composition, and, to a lesser extent, density.

The two main categories of proppants are naturally occurring sands and manmade ceramic or bauxite proppants. Sands are used for lower-stress applications, in formations approximately 8,000 ft and (preferably, considerably) less. Manmade proppants are used for high-stress situations in formations generally deeper than 8,000 ft. For high permeability fracturing, where a high conductivity is essential, using high-strength proppants may be justified at practically any depth.

There are three primary ways to increase fracture conductivity: (1) increase the proppant concentration, that is, to produce a wider fracture, (2) use a larger (and hence, higher permeability) proppant, or (3) employ a higher-strength proppant, to reduce crushing and improve conductivity. Figures 6-1, 6-2, and 6-3 illustrate the three methods of increasing conductivity through proppant choice.

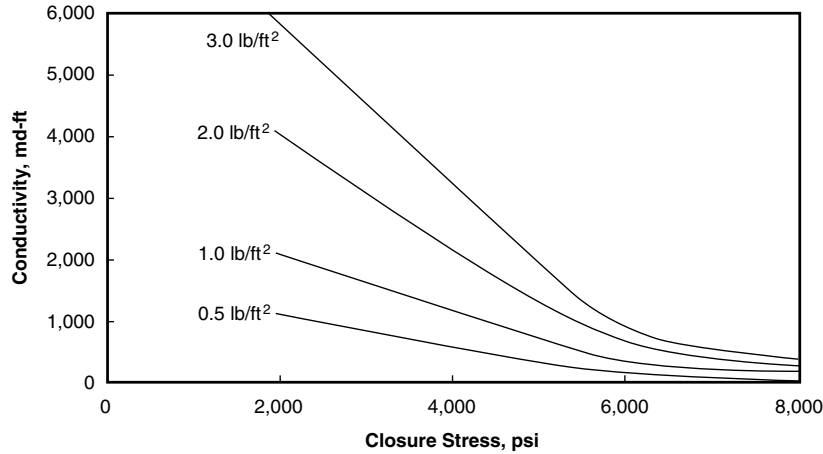


FIGURE 6-1. Fracture conductivity for various areal proppant concentrations (20/40 mesh).

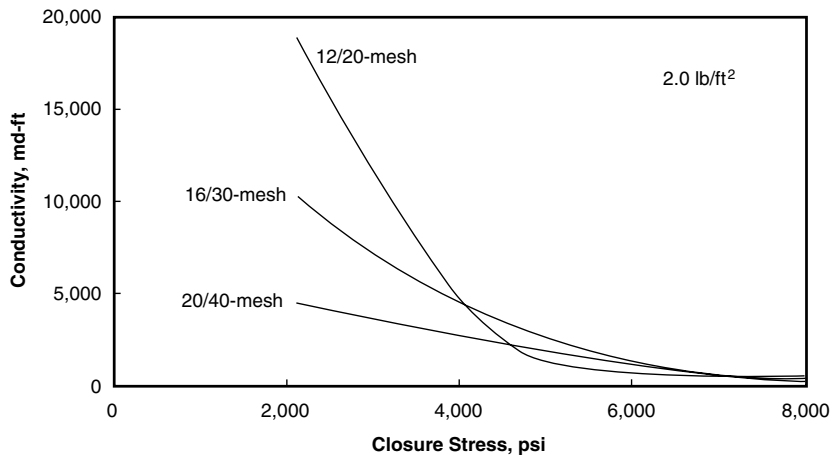


FIGURE 6-2. Fracture conductivity for various mesh sizes.

Figure 6-4 is a selection guide for popular proppant types based on the dominant variable of closure stress.

Calculating Effective Closure Stress

In the course of proppant selection, it is necessary to estimate the magnitude of the closure stress acting on the proppant. The most

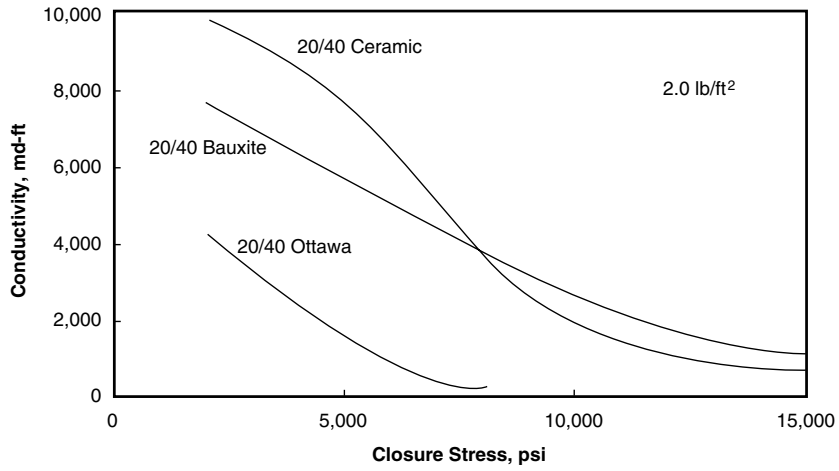


FIGURE 6-3. Fracture conductivity for various proppants.

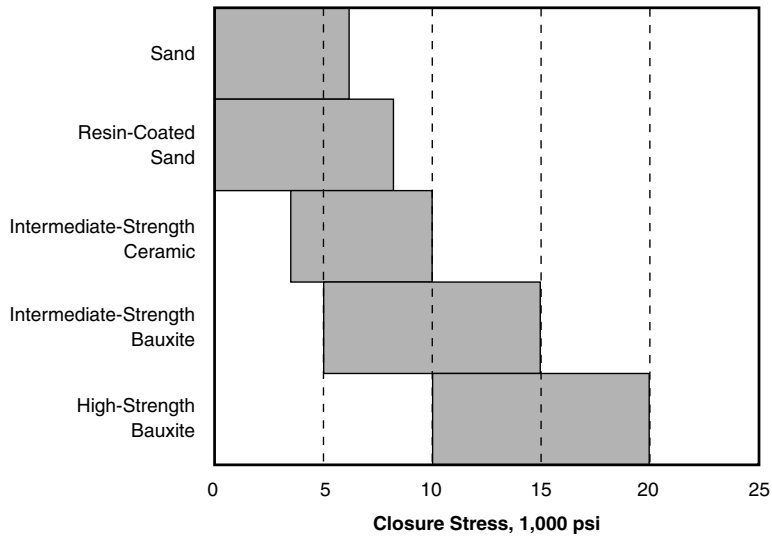


FIGURE 6-4. Proppant selection guide.

common equation used to estimate the closure stress (i.e., the minimum horizontal stress at depth in the reservoir) is known as Eaton's equation. It is commonly given in the form:

$$S_h = \frac{\nu}{1-\nu}(S_v - p_p) + p_p \quad (6-1)$$

where ν is the Poisson ratio, S_v is the absolute vertical stress, and p_p is the reservoir pore pressure. It is worthwhile to understand the forward development of this relationship.

The absolute vertical stress, S_v , is essentially equal to the force exerted by the weight of the overburden per unit area. Formally, it is the integral of the formation density of the various layers overlying the reservoir. In practice, this value is found to range from 0.95 to 1.1 psi per foot of depth, and in the (typical) absence of specific information, is taken to be equal to 1 psi/ft.

To obtain the effective vertical stress (i.e., the weight of the overburden supported by the rock matrix), the total vertical stress must be reduced by an amount equal to the reservoir pore pressure, giving

$$\sigma_v = S_v - \alpha p_p \quad (6-2)$$

where the coefficient α , called Biot's constant or the *poroelastic* constant, is added to the pore pressure term to account for the fact that reservoir fluids are locally free to move out of the control volume under consideration (not a closed box). This situation is depicted in Figure 6-5.

Biot's constant is typically a value between 0.7 and 1, but most often is taken as unity in order to simplify the already rather approximate calculation.

Now, we know that the *longitudinal strain* that results when a linear elastic solid is placed under a uniaxial load translates to a *lateral strain* according to classic mechanics of materials, that is, the two quantities being related by (in fact defining) the Poisson ratio of the solid, $\nu = \partial e_x / \partial e_z$. In a similar way, the vertical stress created by the soil layers overlying an oilfield will induce a horizontal stress in the reservoir rock (through the solid matrix). The magnitude of this horizontal stress is calculated by:

$$\sigma_h = \frac{\nu}{1-\nu} \sigma_v \quad (6-3)$$

where σ_h is of course the *effective* horizontal stress.

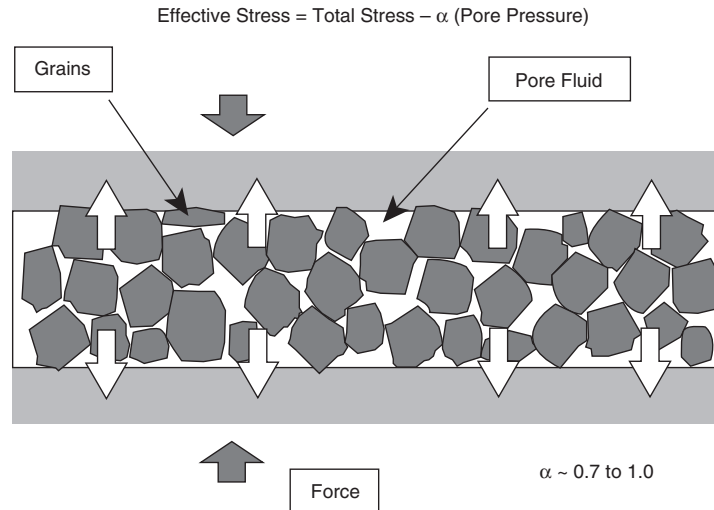


FIGURE 6-5. Poroelasticity.

Combining Equations 6-2 and 6-3 and rearranging slightly,

$$S_h = \frac{\nu}{1-\nu}(S_v - \alpha p_p) + \alpha p_p \quad (6-4)$$

which, taking Biot's constant to be equal to 1, yields the common form of Eaton's equation.

Now, it is important to recognize that, unless the producing bottom-hole pressure in the fracture treated well is drawn down to somewhere near zero, the entire burden of this horizontal stress will not be borne by the proppant. Another important observation is that the horizontal stress in the reservoir is itself a function of reservoir pore pressure, so the closure stress on the proppant is nominally reduced with reservoir depletion.

FRACTURE CONDUCTIVITY AND MATERIALS SELECTION IN HPF

Fracture Width as a Design Variable

A great deal has been published concerning optimum fracture dimensions in HPF. While there are debates regarding the optimum, fracture

width is largely regarded as more important than fracture length. Of course, this is an intuitive statement and only recognizes the first principle of fracture optimization: higher permeability formations require higher fracture conductivity to maintain an acceptable value of the dimensionless fracture conductivity, C_{fD} .

A “rule of thumb” is that fracture length should be equal to 1/2 of the perforation height (thickness of producing interval). Hunt et al. (1994) showed that cumulative recovery from a well in a 100 md reservoir with a 10 ft damage radius is optimized by extending a fixed 8,000 md-ft conductivity fracture to any appreciable distance beyond the damaged zone. This result implies that there is little benefit to a 50 ft fracture length compared to a 10 ft fracture length. Two observations may be in order. First, the Hunt et al. evaluation is based on cumulative recovery. Second, their assumption of a fixed fracture conductivity implies a decreasing dimensionless fracture conductivity with increasing fracture length (i.e., less than optimal placement of the proppant).

It is generally true that if an acceptable C_{fD} is maintained—this may require an increase in areal proppant concentration from 1.5 lb_m/ft², which is common in hard-rock fracturing, to 20 lb_m/ft² or more—additional length will provide additional production. As explained in Chapter 3, the optimum fracture conductivity of 1.6 corresponds to the best compromise between the capacity of the fracture to conduct and the capacity of the reservoir to deliver fluids. This applies to high permeability and low permeability formations alike.

The problem, in practice, has been that fracture extent and width are difficult to influence separately. Historically, once a fracturing fluid and injection rate are selected, the fracture width evolves with increasing length according to strict relations (at least in the well-known PKN and KGD design models). Therefore, the key decision variable has been the fracture extent. After the fracture extent is determined, the width is calculated as a consequence of technical limitations (e.g., maximum realizable proppant concentration). Knowledge of the leakoff process helps to determine the necessary pumping time and pad volume.

The tip screenout technique has brought a significant change to this design philosophy. Through TSO, fracture width can be increased without increasing the fracture extent. Now we have a very effective means to design and execute fractures that satisfy the optimum condition.

The ultimate decision requires optimizing the mass of proppant based on economics or, in cases where total fluid and proppant

volumes are physically limited (e.g., in offshore environments), optimizing placement of a finite proppant volume

Proppant Selection

The primary and unique issue relating to proppant selection for high permeability fracturing, beyond maintaining a high permeability at any stress, is *proppant sizing*. While specialty proppants such as intermediate strength and resin-coated proppants have certainly been employed in HPF, the majority of treatments are pumped with standard graded-mesh sand.

When selecting a proppant size for HPF, the engineer faces competing priorities: size the proppant to address concerns with sand exclusion, or use maximum proppant size to ensure adequate fracture conductivity.

As with equipment choices and fluids selection, the gravel-packing roots of *frac & pack* are also evident when it comes to proppant selection. Engineers initially focused on sand exclusion and a gravel pack derived sizing criteria such as that proposed by Saucier (1974). Saucier recommends that the mean gravel size (D_{g50}) be five to six times the mean formation grain size (D_{f50}). The so-called “4-by-8 rule” implies minimum and maximum grain-size diameters that are distributed around Saucier’s criteria (i.e., $D_{g,min} = 4D_{g50}$ and $D_{g,max} = 8D_{g50}$, respectively). Thus, many early treatments were pumped with standard 40/60 mesh or even 50/70 mesh sand. The somewhat limited conductivity of these gravel pack mesh sizes under in-situ formation stresses is not adequate in many cases. Irrespective of sand mesh size, *frac & packs* tend to reduce concerns with fines migration by virtue of reducing fluid flux at the formation face.

The current trend in proppant selection is to use fracturing-size sand. A typical HPF treatment now employs 20/40 proppant (sand). Maximizing the fracture conductivity can itself help prevent sand production by virtue of reducing drawdown. Results with the larger proppant have been encouraging, both in terms of productivity and limiting or eliminating sand production (Hannah et al., 1993).

It is interesting to note that the topics of formation competence and sanding tendency, major issues in the realm of gravel pack technology, have not been widely studied in the context of HPF. It seems that in many cases HPF is providing a viable solution to completion failures in spite of the industry’s primitive understanding of (soft) rock mechanics.

This move away from gravel pack practices toward fracturing-type practices is common to many aspects of HPF with the exception (so far) of downhole tools, and it seems to justify the migration in our terminology from *frac & pack* to high permeability fracturing. The following discussion of fluid selection is consistent with this perspective.

Fluid Selection

Fluid selection for HPF has always been driven by concerns with damaging the high permeability formation, either by filter cake buildup or (especially) polymer invasion. Most early treatments were carried out using HEC, the classic gravel pack fluid, as it was perceived to be less damaging than guar-based fracturing fluids. While the debate has lingered on and while some operators continue to use HEC fluids, the fluid of choice is increasingly borate-crosslinked HPG.

Based on a synthesis of reported findings from several practitioners, Aggour and Economides (1996) provide a rationale to guide fluid selection in HPF. Their findings suggest that if the extent of fracturing fluid invasion is minimized, the degree of damage (i.e., permeability impairment caused by filter cake or polymer invasion) is of secondary importance. They employ the effective skin representation of Mathur et al. (1995) to show that if fluid leakoff penetration is small, even severe permeability impairments can be tolerated without exhibiting positive skin effects. In this case, the obvious recommendation in HPF is to use high polymer concentration, cross-linked fracturing fluids with fluid-loss additives, and an aggressive breaker schedule. The polymer, crosslinker, and fluid-loss additives limit polymer invasion, and the breaker ensures maximum fracture conductivity, a critical factor which cannot be overlooked.

Experimental work corroborates these contentions. Linear gels have been known to penetrate cores of very low permeability (1 md or less) whereas crosslinked polymers are likely to build filter cakes at permeabilities two orders of magnitude higher (Roodhart, 1985; Mayerhofer et al., 1991). Filter cakes, while they may damage the fracture face, clearly reduce the extent of polymer penetration into the reservoir normal to the fracture face. At extremely high permeabilities, even crosslinked polymer solutions may invade the formation.

Cinco-Ley and Samaniego (1981) and Cinco-Ley et al. (1978) described the performance of finite-conductivity fractures and delineated three major types of damage affecting this performance.

- **Reduction of proppant pack permeability** resulting from either proppant crushing or (especially) unbroken polymer chains leads to fracture conductivity impairment. This can be particularly problematic in moderate to high permeability reservoirs. Extensive progress in breaker technology has dramatically reduced concerns with this type of damage.
- **Choke damage** refers to the near-well zone of the fracture, which can be accounted for by a skin effect. This damage can result from either over-displacement at the end of a treatment or by fines migration during production. In the latter case, one can envision fines from the formation or proppant accumulating near the well but within the fracture.
- **Fracture face damage** implies permeability reduction normal to the fracture face, including permeability impairments caused by the filter cake, polymer-invaded, and filter cake-invaded zones.

Composite Skin Effect

Mathur et al. (1995) provide the following representation for effective skin resulting from radial wellbore damage and fracture face damage:

$$s_d = \frac{\pi}{2} \left[\frac{b_2 k_r}{b_1 k_3 + (x_f - b_1) k_2} + \frac{(b_1 - b_2) k_r}{b_1 k_1 + (x_f - b_1) k_r} - \frac{b_1}{x_f} \right] \quad (6-5)$$

Figure 6-6 depicts the two types of damage accounted for in s_d (i.e., fracture-face and radial wellbore damage).

The b - and k - terms are defined graphically in Figure 6-7 and represent the dimensions and permeabilities of various zones included in the finite conductivity fracture model of Mathur et al.

The equivalent damage skin can be added directly to the undamaged Cinco and Samaniego fracture skin effect to obtain the total skin,

$$s_t = s_d + s_f \quad (6-6)$$

Parametric Studies

Aggour and Economides (1996) employed the Mathur et al. model (with no radial wellbore damage) to evaluate total skin and investigate the relative effects of different variables. Their results related the total skin in a number of discrete cases to (1) the depth of fluid invasion normal to the fracture face and (2) the degree of permeability reduction

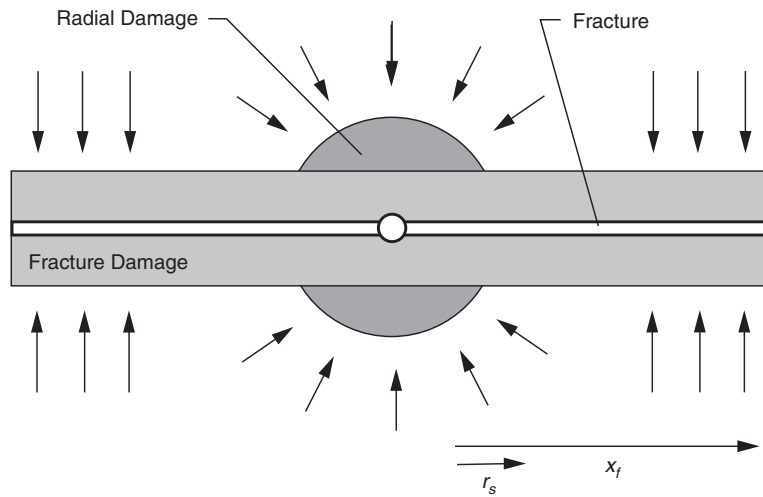


FIGURE 6-6. Fracture face damage.

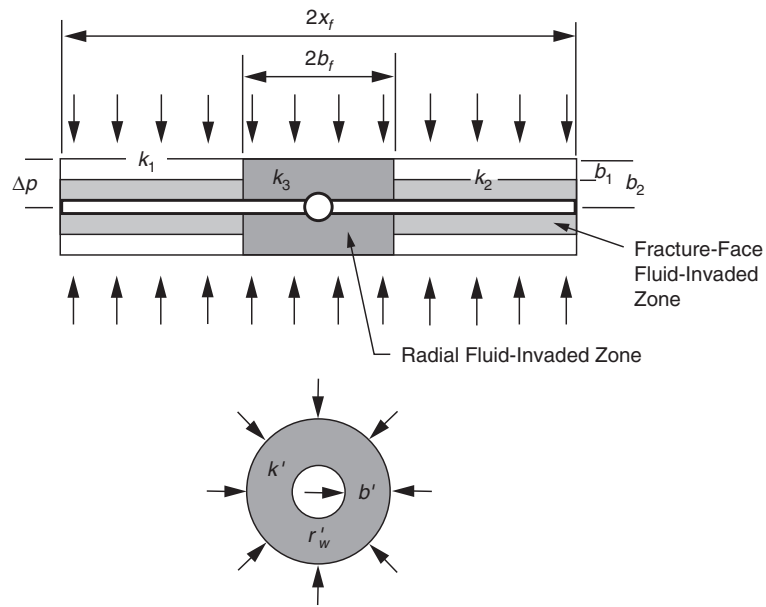


FIGURE 6-7. Fluid invaded zones.

in the polymer-invaded zone. A sample of their results (for $x_f = 25$ ft, $C_{fD} = 0.1$, and $k_f = 10$ md), expressed initially in terms of damage penetration ratios, b_2/x_f , and permeability impairment ratios, k_2/k_f , are re-expressed in real units in Table 6-4. Under each of these conditions, the total skin is equal to zero.

These results suggest that for a (nearly impossible) 2.5 ft penetration of damage, a positive skin is obtained only if the permeability impairment in the invaded zone is more than 90 percent. For a damage penetration of 1.25 ft, the permeability impairment would have to be over 95 percent to achieve positive skins. If the penetration of damage can be limited to 0.25 ft, even a 99 percent permeability reduction in the invaded zone would not result in positive skins. At a higher dimensionless conductivity equal to 1, even higher permeability impairments can be tolerated without suffering positive skins. Thus, if the fracturing fluid leads to a clean and wide proppant pack, penetration and damage to the reservoir can be tolerated.

It is also clear from this work that the extent of damage normal to the fracture face is more important than the degree of damage. If fluid invasion can be minimized, even 99 percent damage can be tolerated. The importance of maximizing C_{fD} is also illustrated; certainly, a good proppant pack should not be sacrificed in an attempt to minimize the fracture face damage.

This points toward the selection of appropriate fracturing fluids:

- Linear gels by virtue of their considerable leakoff penetration are not recommended.
- Crosslinked polymer fluids with high gel loadings appear to be much more appropriate.
- Aggressive breaker schedules are imperative.
- Filter cake building additives may also be considered to minimize the spurt loss and total leakoff.

TABLE 6-4. Fluid Invasion Damage Tolerated for Zero Skin

Depth of Fluid Invasion Normal to Fracture Face	Permeability Reduction in Invaded Zone
2.5 ft	90%
1.25 ft	95%
0.25 ft	99%

Source: Aggour and Economides (1996).

Work by Mathur et al. (1995) and Ning et al. (1995) further support the conclusion that fracture face damage should not significantly alter long-term HPF performance. The Mathur et al. study of Gulf Coast wells assumed a linear cleanup of the fracture and observed an improvement of the production rate at early time. The Ning et al. study of gas wells in Alberta, Canada, showed that fracture conductivity has the greatest effect on long-term production rates, whereas the effects of polymer invasion were minimal.

Experiments in Fracturing Fluid Penetration

McGowen et al. (1993) presented a series of experiments showing the extent of fracturing fluid penetration in cores of various permeabilities. Fracturing fluids used were 70 lb_m per 1,000-gal HEC and 30 or 40 lb_m per 1,000 gal borate-crosslinked HPG. Filtrate volumes were measured in ml per cm² of leakoff area (i.e., cm of penetration) for a 10 md limestone and 200 and 1,000 md sandstones at 120°F and 180°F.

Several conclusions can be drawn from the work:

- Crosslinked fracturing fluids are far superior to linear gels in controlling fluid leakoff. For example, 40 lb_m per 1,000 gal borate-crosslinked HPG greatly outperforms 70 lb_m per 1,000 gal HEC in 200 md core at 180°F.
- Linear gel performs satisfactorily in 10 md rock but fails dramatically at 200 md. Even aggressive use of fluid loss additives (e.g., 40 lb_m per 1,000 gal silica flour) does not appreciably alter the leakoff performance of HEC in 200 md core.
- Increasing crosslinked gel concentrations from 30 to 40 lb_m per 1,000 gal has a major impact on reducing leakoff in 200 md core. Crosslinked borate maintains excellent fluid loss control in 200 md sandstone and performs satisfactorily even at 1,000 md.

This experimental work strongly corroborates the modeling results of Aggour and Economides (1996) and points toward the use of higher-concentration crosslinked polymer fluids with, of course, an appropriately designed breaker system.

Viscoelastic Carrier Fluids

HEC and borate-crosslinked HPG fluids are the dominant fluids currently employed in HPF. However, there is a third class of fluid that deserves to be mentioned, the so-called viscoelastic surfactant, or VES fluids. There is little debate that these fluids exhibit excellent rheological properties and are non-damaging, even in high permeability formations. The elegance of VES fluids is that they do not require the use of chemical breaker additives; the viscosity of this fluid conveniently breaks (leaving considerably less residue than polymer-based fluids) either when it contacts formation oil or condensate or when its salt concentration is reduced. Brown et al. (1996) present typical VES fluid performance data and case histories.

The vulnerability of VES fluids is in their temperature limitation and much higher costs per unit volume. The maximum application temperature for VES fluids has only recently been extended from 130°F up to 240°F.

VES fluids have great potential when considered in a holistic manner: treatments may cost more than polymer fluids, but the resulting appropriately sized fracture could be a far superior producer.

7

Fracture Treatment Design

Fracture treatment goes well beyond the sizing of a fracture, as important as that is for production enhancement, to include the calculation of a pumping schedule that will realize the goals set for the treatment. This chapter also includes discussion of pre-treatment diagnostics that are often incorporated with fracture treatments to determine or at least place bounds on parameters that are critical to the design procedure and execution.

MICROFRACTURE TESTS

The microfracture stress test (“microfrac”) determines the magnitude of the minimum principal in-situ stress of a target formation. The test usually involves the injection of pressurized fluid into a small, isolated zone (4 to 15 ft, 1.2 to 4.6 m) at low injection rates (1 to 25 gal/min, 0.010 to 0.095 m³/min). The minimum principal in-situ stress can be determined from the pressure decline after shut-in or the pressure increase at the beginning of an injection cycle. The fracture closure pressure and fracture reopening pressure provide good approximations for the minimum principal in-situ stress.

MINIFRACS

The most important test on location before the main treatment is known as a “minifrac,” or a fracture calibration test. The minifrac is a pump-in/shut-in test that employs full-scale pump rates and relatively large fluid volumes, on the order of thousands of gallons. Information gathered from a minifrac includes the closure pressure, p_c , net pressure, entry conditions (perforation and near-wellbore friction), and possibly evidence of fracture height containment. The falloff portion of the pressure curve is used to obtain the leakoff coefficient for a given fracture geometry. Figure 7-1 illustrates the strategic locations on a typical pressure response curve registered during the calibration activities.

A minifrac design should be performed along with the initial treatment design. The design goal for the minifrac is to be as representative as possible of the main treatment. To achieve this objective, sufficient geometry should be created to reflect the fracture geometry of the main treatment and to obtain an observable closure pressure from the pressure decline curve. The most representative minifrac would have an injection rate and fluid volume equal to the main treatment, but this is often not practical. In reality, several conflicting design criteria must be balanced, including minifrac volume, created

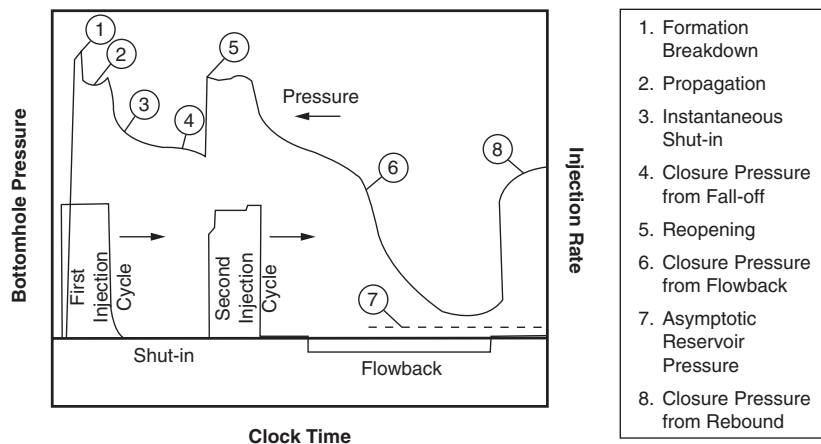


FIGURE 7-1. Key elements on minifrac pressure response curve.

fracture geometry, damage to the formation, a reasonable closure time, and the cost of materials and personnel.

Fracture closure is typically determined from one or more constructions of the pressure decline curve while taking into consideration any available prior knowledge (e.g., that obtained from microfrac tests). Some of the most popular plots used to identify fracture closure pressure are:

- $p_{shut-in}$ vs. t
- $p_{shut-in}$ vs. \sqrt{t}
- $p_{shut-in}$ vs. g -function (and variations)
- $\log(p_{ISIP} - p_{shut-in})$

The origin and use of these various plots is sometimes more intuitive than theoretical, which can lead to spurious results. The theoretical basis and limitations of pressure decline analysis must be understood in the context of individual applications. An added complication is that temperature and compressibility effects may cause pressure deviations. In this case, temperature-corrected decline curves can be generated to permit the normal interpretations of the different plot types (Soliman, 1984).

The original concept of pressure decline analysis is based on the observation that the rate of pressure decline during the closure process contains useful information on the intensity of the leakoff process (Nolte, 1979, Soliman and Daneshy, 1991). This stands in contrast to the pumping period, when the pressure is affected by many other factors.

If we assume that the fracture area has evolved with a constant exponent α and remains constant after the pumps are stopped, at time $(t_e + \Delta t)$ the volume of the fracture is given by

$$V_{t_e+\Delta t} = V_i - 2A_e S_p - 2A_e g(\Delta t_D, \alpha) C_L \sqrt{t_e} \quad (7-1)$$

where the dimensionless delta time is defined as

$$\Delta t_D = \Delta t / t_e \quad (7-2)$$

and the two-variable function $g(\Delta t_D, \alpha)$ can be obtained by integration. Its general form is given by (Valkó and Economides, 1995):

$$g(\Delta t_D, \alpha) = \frac{4\alpha\sqrt{\Delta t_D} + 2\sqrt{1+\Delta t_D} \times F\left[\frac{1}{2}, \alpha; 1+\alpha; (1+\Delta t_D)^{-1}\right]}{1+2\alpha} \quad (7-3)$$

The function $F[a, b; c; z]$ is the “Hypergeometric function” available in the form of tables or computing algorithms. For computational purposes (e.g., the included MF Excel spreadsheet for minifrac analysis), the g -function approximations given in Table 7-1 are useful.

Dividing Equation 7-1 by the area, the fracture width at time Δt after the end of pumping is given by

$$\bar{w}_{t_e+\Delta t} = \frac{V_i}{A_e} - 2S_p - 2C_L\sqrt{t_e}g(\Delta t_D, \alpha) \quad (7-4)$$

Hence, the time variation of the width is determined by the $g(\Delta t_D, \alpha)$ function, the length of the injection period, and the leakoff coefficient, but is not affected by the fracture area.

The decrease of average width cannot be observed directly, but the net pressure during closure is already directly proportional to the average width according to

$$p_{net} = S_f \bar{w} \quad (7-5)$$

simply because the formation is described by linear elasticity theory (i.e., Equation 4-2). The coefficient S_f is the *fracture stiffness*, expressed in Pa/m (psi/ft). Its inverse, $1/S_f$, is called the *fracture compliance*. For the basic fracture geometries, expressions of the fracture stiffness are given in Table 7-2.

TABLE 7-1. Approximation of the g -Function for Various Exponents α

$g\left(d, \frac{4}{5}\right) = \frac{1.41495 + 79.4125 d + 632.457 d^2 + 1293.07 d^3 + 763.19 d^4 + 94.0367 d^5}{1. + 54.8534 d^2 + 383.11 d^3 + 540.342 d^4 + 167.741 d^5 + 6.49129 d^6}$
$g\left(d, \frac{2}{3}\right) = \frac{1.47835 + 81.9445 d + 635.354 d^2 + 1251.53 d^3 + 717.71 d^4 + 86.843 d^5}{1. + 54.2865 d + 372.4 d^2 + 512.374 d^3 + 156.031 d^4 + 5.95955 d^5 - 0.0696905 d^6}$
$g\left(d, \frac{8}{9}\right) = \frac{1.37689 + 77.8604 d + 630.24 d^2 + 1317.36 d^3 + 790.7 d^4 + 98.4497 d^5}{1. + 55.1925 d + 389.537 d^2 + 557.22 d^3 + 174.89 d^4 + 6.8188 d^5 - 0.0808317 d^6}$

TABLE 7-2. Proportionality Constant, S_f , and Suggested α for Basic Fracture Geometries

	PKN	KGD	Radial
S_f	$\frac{2E'}{\pi h_f}$	$\frac{E'}{\pi x_f}$	$\frac{3\pi E'}{16R_f}$
α	4/5	2/3	8/9

The combination of Equations 7-4 and 7-5 yields the following (Nolte, 1979):

$$p = \left(p_C + \frac{S_f V_i}{A_e} - 2S_f S_p \right) - (2S_f C_L \sqrt{t_e}) \times g(\Delta t_D, \alpha) \quad (7-6)$$

Equation 7-6 shows that the pressure falloff in the shut-in period will follow a straight line trend,

$$p = b_N - m_N \times g(\Delta t_D, \alpha) \quad (7-7)$$

if plotted against the g -function (i.e., transformed time, Castillo, 1987). The g -function values should be generated with the exponent α considered valid for the given model. The slope of the straight line, m_N , is related to the unknown leakoff coefficient by

$$C_L = \frac{-m_N}{2\sqrt{t_e} S_f} \quad (7-8)$$

Substituting the relevant expression for fracture stiffness, the leakoff coefficient can be estimated as given in Table 7-3. This table shows that the estimated leakoff coefficient for the PKN geometry does not depend on unknown quantities because the pumping time, fracture height, and plain strain modulus are assumed to be known. For the other two geometries considered, the procedure results in an estimate of the leakoff coefficient that is strongly dependent on the fracture extent (x_f or R_f).

From Equation 7-6 we see that the effect of the spurt loss is concentrated in the intercept of the straight line with the $g = 0$ axis:

$$S_p = \frac{V_i}{2A_e} - \frac{b_N - p_C}{2S_f} \quad (7-9)$$

TABLE 7-3. Leakoff Coefficient and No-Spurt Fracture Extent for Various Fracture Geometries

	PKN	KGD	Radial
Leakoff coefficient, C_L	$\frac{\pi h_f}{4\sqrt{t_e} E'}(-m_N)$	$\frac{\pi x_f}{2\sqrt{t_e} E'}(-m_N)$	$\frac{8R_f}{3\pi\sqrt{t_e} E'}(-m_N)$
Fracture Extent	$x_f = \frac{2E'V_i}{\pi h_f^2(b_N - p_C)}$	$x_f = \sqrt{\frac{E'V_i}{\pi h_f(b_N - p_C)}}$	$R_f = \sqrt[3]{\frac{3E'V_i}{8(b_N - p_C)}}$

As suggested by Shlyapobersky (1987), Equation 7-9 can be used to obtain the unknown fracture extent if we assume there is no spurt loss. The second row of Table 7-3 shows the estimated fracture extent for the three basic models. Note that the no-spurt-loss assumption results in an estimated fracture length for the PKN geometry, but this value is not used to obtain the leakoff coefficient. For the KGD and radial models, fracture extent is calculated first and then used to interpret the slope (i.e., to determine C_L). Once the fracture extent and the leakoff coefficient are known, the lost width at the end of pumping can be easily obtained from

$$w_{Le} = 2g_0(\alpha)C_L\sqrt{t_e} \quad (7-10)$$

The fracture width is

$$\bar{w}_e = \frac{V_i}{x_f h_f} - w_{Le} \quad (7-11)$$

for the two rectangular models and

$$\bar{w}_e = \frac{V_i}{R_f^2 \pi / 2} - w_{Le} \quad (7-12)$$

for the radial model.

Often the fluid efficiency is also determined:

$$\eta_e = \frac{\bar{w}_e}{\bar{w}_e + w_{Le}} \quad (7-13)$$

Note that the fracture extent and the efficiency are *state variables*, which is to say that they will have different values in the minifrac

and main treatment. Only the leakoff coefficient is a *model parameter* that can be transferred from the minifrac to main treatment, but even then some caution is needed in its interpretation. The bulk leakoff coefficient determined from the above method is “apparent” with respect to the fracture area. If we have information on the permeable height, h_p , and it indicates that only part of the fracture area falls into the permeable layer, the apparent leakoff coefficient should be converted into a “true” value that corresponds to the permeable area only. This is done by simply dividing the apparent value by r_p (see Equation 7-14).

While adequate for many low permeability treatments, the outlined procedure might be misleading for higher permeability reservoirs. The conventional minifrac interpretation determines a single effective fluid loss coefficient, which usually slightly overestimates the fluid loss when extrapolated to the full job volume (Figure 7-2).

This overestimation typically provides an extra factor of safety in low permeability formations to prevent a screenout. However, this same technique applied in high permeability, or when the differential pressure between the fracture and the formation is high, can significantly overestimate the fluid loss for wall-building fluids (Figure 7-3, Dusterhoft, 1995).

Overestimating fluid leakoff can be highly detrimental when the objective is to achieve a carefully timed tip screenout. In this case,

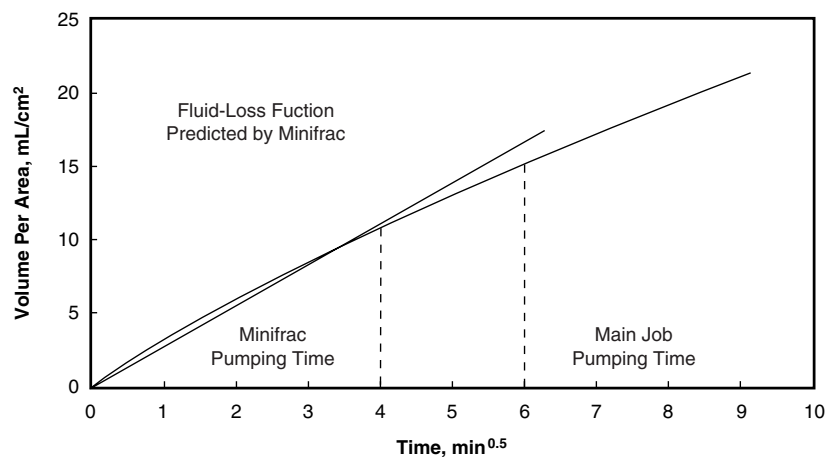


FIGURE 7-2. Fluid leakoff extrapolated to full job volume, low permeability.

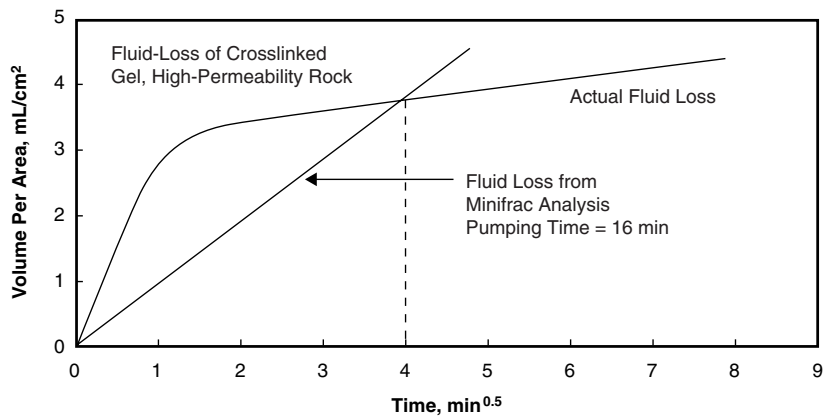


FIGURE 7-3. Overestimation of fluid leakoff extrapolated to full job volume, high permeability.

modeling both the spurt loss and the combined fluid loss coefficient by performing a net pressure match in a 3D simulator is an alternative to classical falloff analysis. This approach is illustrated in Figure 7-4.

Note that the incorporation of more than one leakoff parameter (and other adjustable variables) increases the *degrees of freedom*.

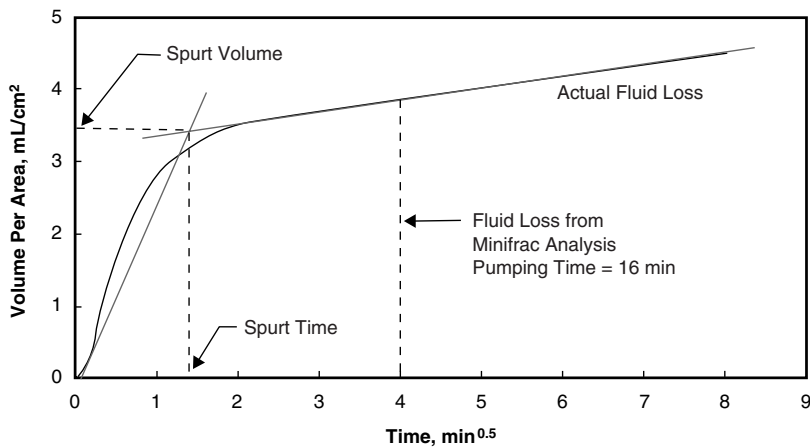


FIGURE 7-4. Leakoff estimate based on a net-pressure match in a 3D simulator (Source: Dusterhot et al., 1995).

While a better match of the observed pressure can usually be achieved, the solution often becomes *non-unique* (i.e., other values of the same parameters may provide a similar fit).

TREATMENT DESIGN BASED ON THE UNIFIED APPROACH

We ended Chapter 3 by delineating a certain design logic: for a given amount of proppant reaching the pay layer, we can determine the optimum length (and width). One of the main results was that, for low or moderate proppant numbers (relatively low proppant volumes and/or moderate-to-high formation permeabilities), the optimal compromise occurs at $C_{fd} = 1.6$.

When the formation permeability is above 50 md, it is practically impossible to achieve a proppant number larger than 0.1. Typical proppant numbers for HPF range from 0.0001 to 0.01. Thus, for moderate and high permeability formations, the optimum dimensionless fracture conductivity is always $C_{fDopt} = 1.6$.

In “tight gas” it is possible to achieve large dimensionless proppant numbers, at least in principle. If we assume a limited drainage area and do not question whether the proppant actually reaches the pay layer, a dimensionless proppant number equal to 1 or even 5 can be *calculated*. However, proppant numbers larger than one are not likely in practice.

When the propped volume becomes very large, the optimal compromise happens at larger dimensionless fracture conductivities simply because the fracture penetration ratio cannot exceed unity (i.e., fracture length becomes constrained by the well spacing or limits of the reservoir).

A crucial issue in the design is the assumed fracture height. The relation of fracture height to pay thickness determines the volumetric proppant efficiency. The actual proppant number depends on that part of the proppant that is placed into the pay. It is calculated as the volume of injected proppant multiplied by the volumetric proppant efficiency. Therefore, strictly speaking, an optimum target length can be obtained only if the fracture height is already known. In the following, we assume that the fracture height is known. Later we will return to this issue.

Pump Time

Armed with a target length and assuming that h_f , E' , q_i , μ , C_L , and S_p are known, we can design a fracture treatment. The first problem is to determine the pumping time, t_e , using the combination of a width equation and material balance. The first part of a typical design procedure is shown in Table 7-4. Notice that the injection rate, q_i , refers to the slurry (not clean fluid) injected into one wing.

Techniques used to refine K_L are delineated in Tables 7-5 to 7-7.

If the permeable height, h_p , is less than the fracture height, it is convenient to use exactly the same method, but with “apparent” leakoff and spurt loss coefficients. The apparent leakoff coefficient is the “true” leakoff coefficient (the value with respect to the permeable layer) multiplied by the factor r_p , defined as the ratio of permeable to fracture surface (cf. Figures 7-5 and 7-6).

TABLE 7-4. Determination of the Pumping Time

1. Calculate the wellbore width at the end of pumping from the PKN (or any other) width equation: $w_{w,0} = 3.27 \left(\frac{\mu q_i x_f}{E'} \right)^{1/4}$ (or rather the non-Newtonian form shown later)
2. Convert wellbore width into average width: $\bar{w}_e = 0.628 w_{w,0}$
3. Assume an opening time distribution factor, $K_L = 1.5$ (techniques to refine this value are described below)
4. Solve the following equation for t_e : $\frac{q_i t}{h_f x_f} - 2K_L C_L \sqrt{t} - (\bar{w}_e + 2S_p) = 0$ (Quadratic Equation for $x = \sqrt{t}$) Selecting \sqrt{t} as the new unknown, a simple quadratic equation must be solved: $at + b\sqrt{t} + c = 0$ where $a = \frac{q_i}{h_f x_f}; \quad b = -2K_L C_L; \quad c = -(\bar{w}_e + 2S_p)$
5. Calculate injected volume: $V_i = q_i t_e$, and fluid efficiency: $\eta_e = \frac{h_f x_f \bar{w}_e}{V_i}$

TABLE 7-5. Refinement of K_L using the Carter II Equation

Calculate an improved estimate of K_L from:

$$K_L = -\frac{S_p}{C_L \sqrt{t_e}} - \frac{\bar{w}_e}{2C_L \sqrt{t_e}} + \frac{\bar{w}_e}{2\eta_e C_L \sqrt{t_e}},$$

where $\eta_e = \frac{\bar{w}_e(\bar{w}_e + 2S_p)}{4\pi C_L^2 t_e} \left[\exp(\beta^2) \operatorname{erfc}(\beta) + \frac{2\beta}{\sqrt{\pi}} - 1 \right]$ and $\beta = \frac{2C_L \sqrt{\pi t_e}}{\bar{w}_e + 2S_p}$.

If K_L is near enough to the previous guess, stop; otherwise, iterate by repeating the material balance calculation using the new estimate of K_L .

TABLE 7-6. Refinement of K_L by Linear Interpolation According to Nolte

Estimate the next K_L from

$$K_L = 1.33\eta_e + 1.57(1 - \eta_e),$$

where $\eta_e = \frac{\bar{w}_e x_f h_f}{i t_e}$.

If K_L is near enough to the previous guess, stop; otherwise, iterate by repeating the material balance calculation using the new estimate of K_L .

TABLE 7-7. K_L from the α Method

Assume a power law exponent α (Table 7-2) and calculate $K_L = g_0(\alpha)$ using equations in Table 7-1. Use the obtained K_L instead of 1.5 in the material balance. (Note that this is not an iterative process.)

For the PKN and KGD geometries, it is the ratio of permeable to the fracture height,

$$r_p = \frac{h_p}{h_f} \quad (7-14)$$

while for the radial model it is given by

$$r_p = \frac{2}{\pi} \left[x(1-x^2)^{0.5} + \arcsin(x) \right] \quad \text{where} \quad x = \frac{h_p}{2R_f} \quad (7-15)$$

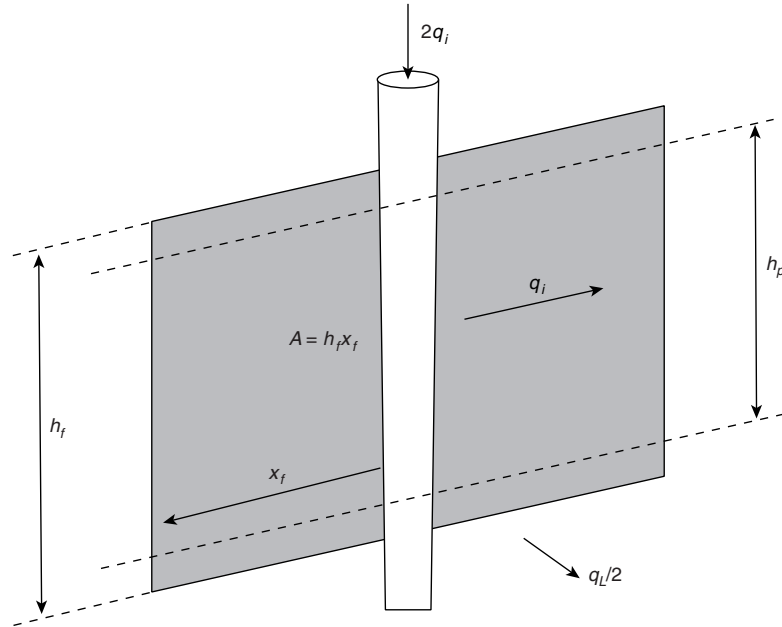


FIGURE 7-5. Ratio of permeable to total surface area, KGD, and PKN geometry.

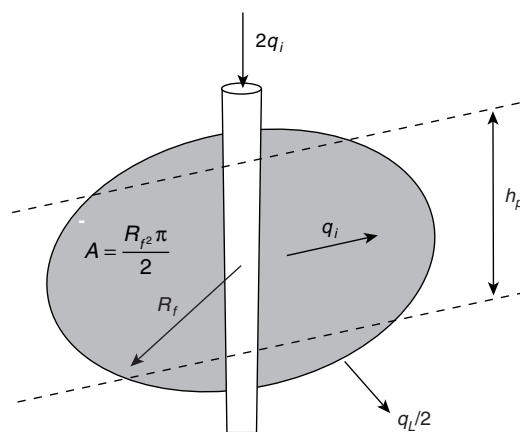


FIGURE 7-6. Ratio of permeable to total surface area, radial geometry.

There are several ways to incorporate non-Newtonian behavior into the width equations. A convenient procedure is to add one additional equation connecting the equivalent Newtonian viscosity with the flow rate. Assuming power law fluid behavior, the equivalent Newtonian viscosity can be calculated for the average cross section using the appropriate entry from Table 4-3. After substituting the equivalent Newtonian viscosity into the PKN width equation, we obtain

$$w_{w,0} = 9.15^{\frac{1}{2n+2}} \times 3.98^{\frac{n}{2n+2}} \left[\frac{1 + 2.14n}{n} \right]^{\frac{n}{2n+2}} K^{\frac{1}{2n+2}} \left(\frac{i^n h_f^{1-n} x_f}{E'} \right)^{\frac{1}{2n+2}} \quad (7-16)$$

Proppant Schedule

Given the total pumping time and slurry volume, a stepwise pump schedule (more specifically, a proppant addition schedule, or just *proppant schedule*) is still needed that will yield the designed, propped fracture geometry.

Fluid injected at the beginning of the job without proppant is called the “pad.” It initiates and opens up the fracture. Typically, 30 to 60 percent of the fluid pumped during a treatment leaks off into the formation while pumping; the pad provides much of this necessary extra fluid. The pad also generates sufficient fracture length and width to allow proppant placement. Too little pad results in premature bridging of proppant and shorter-than-desired fracture lengths. Too much pad results in excessive fracture height growth and created fracture length. For a fixed slurry volume, excessive pad may result in a final propped length that is considerably shorter than the created (desired) fracture length. Even if the fluid loss were zero, a minimum pad volume would be required to open sufficient fracture width to admit proppant. Generally, a fracture width equal to three times the proppant diameter is felt to be necessary to avoid bridging.

After the specified pad is pumped, the proppant concentration of the injected slurry is ramped up step-by-step until a maximum value is reached at end of the treatment.

Figure 7-7 conceptually illustrates the proppant distribution in the fracture after the first proppant-carrying stage. Most fluid loss occurs in the pad, near the fracture tip. However, some fluid loss occurs along the fracture, and in fact, fluid loss acts to dehydrate the proppant-laden stages. Figure 7-8 shows the concentration of the initial proppant stage climbing from 1 up to 3 lb_m of proppant per gallon of fluid (ppg) as

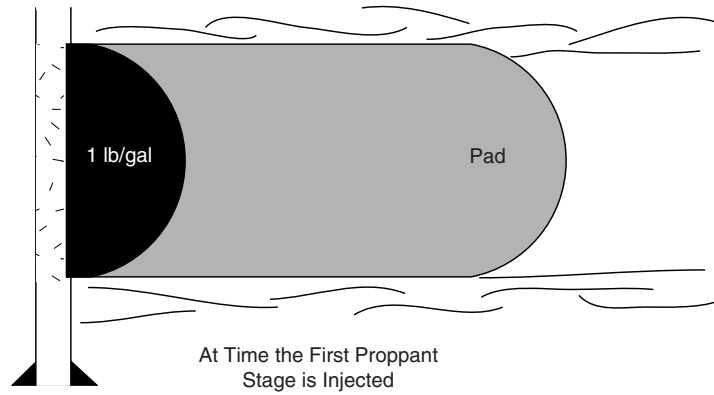


FIGURE 7-7. Beginning of proppant distribution during pumping.

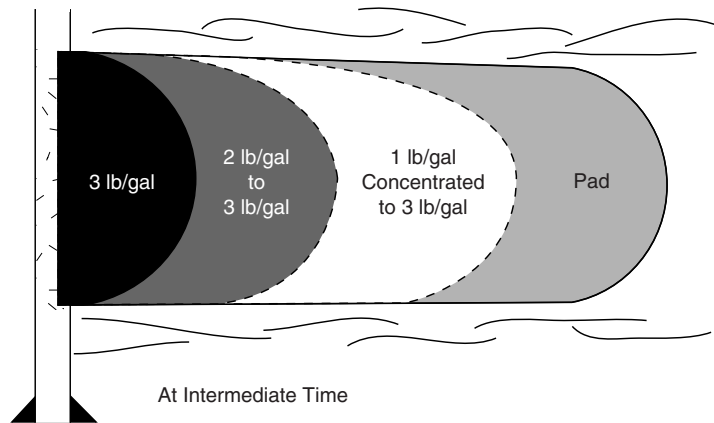


FIGURE 7-8. Evolution of slurry proppant distribution during pumping.

the treatment progresses. Later stages are pumped at higher initial proppant concentrations because they suffer less fluid leakoff (i.e., shorter exposure time and reduced leakoff rates near the well).

Figure 7-9 completes the ideal sequence in which the pad is depleted just as pumping ends and the first proppant stage has concentrated to a final designed value of 5 ppg. The second proppant stage has undergone less dehydration, but also has concentrated to the same

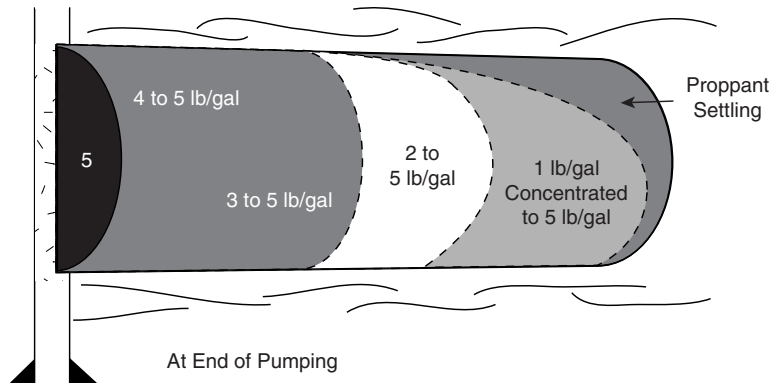


FIGURE 7-9. Proppant concentration in the injected slurry.

final value. If done properly, the entire fracture is filled with a *uniform proppant concentration* at the end of the treatment.

If proppant bridges in the fracture prematurely during pumping, a situation known as a “screen-out,” the treating pressure will rise rapidly to the technical limit of the equipment. In this case, pumping must cease immediately (both for the safety of personnel on location and to avoid damaging the equipment), effectively truncating the treatment before the full proppant volume has been placed. Making things worse, the treatment string is often left filled with sand, which then requires incremental rig time and expense to clean out.

TSO designs for highly permeable and soft formations are specifically *intended* to screen out. In this case, it is often possible to continue pumping and inflate the fracture width without exceeding the pressure limits of the equipment because these formations tend to be highly compliant.

While more sophisticated methods are available to calculate the ramped proppant schedule, the simple design technique given in Table 7-8 using material balance and a prescribed functional form (e.g., power law, Nolte 1986) is satisfactory.

One additional parameter must be specified: c_e , the maximum proppant concentration of the injected slurry at the end of pumping. The physical capabilities of the fracturing equipment being used provides one limit to the maximum proppant concentration, but rarely should this be specified as the value for c_e . Ideally, the proppant schedule should be designed to result in a uniform proppant concentration in the fracture at the end of pumping, with the value of the

TABLE 7-8. Proppant Schedule

-
1. Calculate the exponent of the proppant concentration curve:

$$\varepsilon = \frac{1 - \eta_e}{1 + \eta_e}$$

2. Calculate the pad volume and the time needed to pump it:

$$V_{pad} = \varepsilon V_i \quad t_{pad} = \varepsilon t_e$$

3. The required proppant concentration (mass per unit of injected slurry volume) curve is given by the following:

$$c = c_e \left(\frac{t - t_{pad}}{t_e - t_{pad}} \right)^\varepsilon,$$

where c_e is the maximum end-of-job proppant concentration in the injected slurry.

4. Convert the proppant concentration from *mass per unit of injected slurry volume* into *mass added per unit volume of base fluid* (or “neat” fluid), denoted by c_a , and usually expressed in ppga (pounds added per gallon added of neat fluid).
-

concentration equal to c_e . Therefore, the proppant concentration, c_e , at the end of pumping should be determined from material balance:

$$M = \eta_e c_e V_i \quad (7-17)$$

where V_i is the volume of slurry injected in one wing, η_e is the fluid efficiency (or more accurately, slurry efficiency), and M is the mass of injected proppant (one wing).

According to Nolte (1986), the schedule is derived from the requirement that (1) the whole length created should be propped; (2) at the end of pumping, the proppant distribution in the fracture should be uniform; and (3) the proppant schedule should be of the form of a delayed power law with the exponent, ε , and fraction of pad being equal (Table 7-8). More complex proppant scheduling calculations attempt to account for the movement of the proppant both in the lateral and the vertical directions; variations of the viscosity of the slurry with time and location (due to temperature, shear rate and changes in solid content); width requirements for free proppant movement; and other phenomena (Babcock et al. 1967, Daneshy 1974, Shah 1982).

Note that in the above schedule the injection rate q_i refers to the slurry (not clean fluid) injected into one wing. The obtained proppant mass M also refers to one wing.

Continuing our previous example, assume that the target fracture length (152.4 m or 500 ft) was obtained from the requirement to place optimally $M = 8,760$ kg (19,400 lb_m) of proppant into each wing. Using Equation 7-17, we obtain that $c_e = 875$ kg/m³ (7.3 lb_m/gal). Note that this is still expressed in mass per slurry volume. This means that 12.5 lb_m of proppant must be added to one gallon of neat fracturing fluid (i.e., the added proppant concentration is 12.5 ppga).

The conversion from mass/slurry-volume to mass/neat-fluid-volume is

$$c_a = \frac{c}{1 - \frac{c}{\rho_p}} \quad (7-18)$$

where ρ_p is the density of the proppant material.

In our example the fluid efficiency is 19.3 percent, so the proppant exponent and the fraction of pad volume is $\varepsilon = 0.677$. Therefore, the pad injection time is 27.8 min, and after the pad, the proppant concentration of the slurry should be continuously elevated according to the schedule: $c = 875 \left(\frac{t-1666}{795} \right)^{0.677}$, where c is in kg/m³ and t is in seconds, or $c = 7.3 \left(\frac{t-27.8}{13.3} \right)^{0.677}$, where c is in lb_m/gal of slurry volume and t is in minutes. The obtained proppant curve is shown in Figure 7-10.

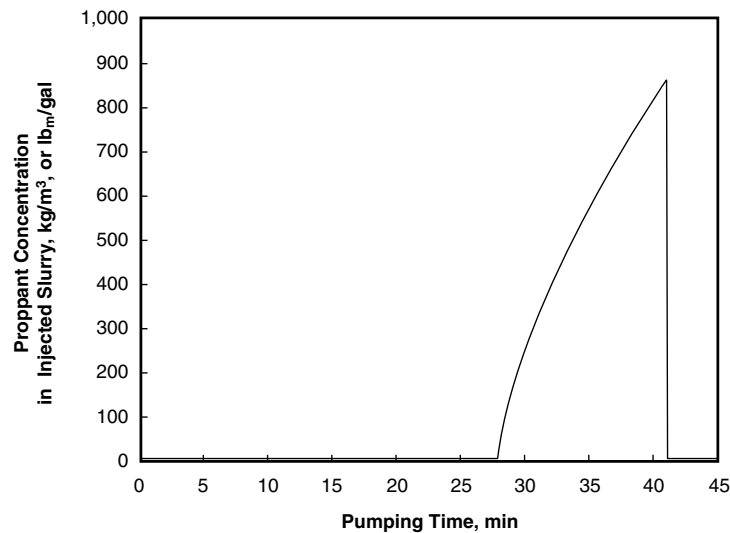


FIGURE 7-10. Evolution of proppant distribution during pumping.

At the end of pumping, the proppant concentration is equal to c_e everywhere in the fracture. Thus, the mass of proppant placed into one wing is $M = V_e \times c_e = \eta_e \times V_i \times c_e$, or in our case, $M = 8,760$ kg (19,400 lb_m). The average propped width after closure can be determined if the porosity of the proppant bed is known. Assuming $\phi_p = 0.3$, the propped volume is $V_p = M/[(1 - \phi_p)\rho_p]$, or in our case, 6.0 m³. The average propped width is $w_p = V_p/(x_f \times h_f)$, that is, 2 mm (0.078 in.).

A quick check of the dimensionless fracture conductivity, substituting the propped width, shows that $C_{fD} = (60 \times 10^{-12} \times 0.002)/(5 \times 10^{-16} \times 152) = 1.6$, as it should be for a treatment with a relatively low proppant number.

In the above example, we assumed that the optimum target length and width can be realized without any problem. Of course, it is possible that certain physical or technical constraints (e.g., maximum possible proppant concentration in the slurry) do not allow optimal placement.

Departure from the Theoretical Optimum

In case of conflict, the design engineer has several options. One possibility is to overcome technical limitations by, for example, choosing another type of fluid, proppant and/or equipment.

More often, however, we choose to depart from the theoretical optimum. The art of fracture design is to depart from the theoretical optimum dimensions, but in a reasonable manner and only as much as necessary. In practical terms, this means that the optimum fracture length or pad volume should be reduced or increased by a “factor.”

For low permeability formations, the first design attempt often results in very long but narrow fracture. Because there is a certain minimum propped width that is required to maintain continuity of the fracture (e.g., 3 times the proppant diameter), the design engineer should reduce the target length—multiplying it by a factor of 0.5 or sometimes even 0.1. In a careful design procedure, the engineer departs from the theoretical optimum only as much as necessary to satisfy another technical limitation, such as a required minimum width.

In high permeability formations, the first attempt may result in a short fracture with insufficient conductivity (width). This portends a move from the conventional to TSO design, which can produce extremely large fracture widths.

TSO Design

It is the tip screenout or TSO design which clearly differentiates high permeability fracturing from conventional massive hydraulic fracturing. While HPF introduces other identifiable differences (e.g., higher permeability, softer rock, smaller proppant volumes, and so on), it is the tip screenout that makes these fracturing treatments unique. Conventional fracture treatments are designed to propagate laterally and achieve TSO at the end of pumping. In high permeability fracturing, pumping continues beyond the TSO to a second stage of fracture width inflation and packing. It is this two-stage treatment that gives rise to the vernacular of *frac & pack*. The conventional and HPF design concepts were illustrated and compared in Figures 5-3 and 5-4.

Early TSO designs commonly called for 50 percent pad (similar to conventional fracturing) and proppant schedules that ramped-up aggressively; then it became increasingly common to reduce the pad to 10 to 15 percent of the treatment and extend the 0.5 to 2 lb_m/gal stages (which combined may constitute 50 percent of the total slurry volume, for example). Notionally, this was intended to “create width” for the higher concentration proppant addition (e.g., 12 to 14 lb_m/gal).

In our design model (included HF2D Excel spreadsheet), the TSO design procedure differs from the conventional procedure in one basic feature: it uses a “TSO criterion” to separate the lateral fracture propagation period from the width inflation period. This criterion is based on a “dry-to-wet” average width ratio, that is, the ratio of dry width (assuming only the “dry” proppant is left in the fracture) to wet width (dynamically achieved during pumping). According to our assumptions, the screen-out occurs and arrests fracture propagation when the *dry-to-wet width ratio* reaches a critical value.

After the TSO is triggered, injection of additional slurry only serves to inflate the width of the fracture. Thus, it is important to schedule the proppant such that the critical dry-to-wet width ratio is reached at the same time (pumping time) that the *created* fracture length matches the *optimum* fracture length. With the TSO design, practically any width can be achieved—at least in principle. In addition, the first part of any TSO design very much resembles a traditional design, only the target length is reached in a relatively short time, and the dry-to-wet width ratio must reach its critical value during this first part of the treatment.

We suggest a critical dry-to-wet ratio of 0.5 to 0.75 as the TSO criterion (representing quite dehydrated sand in the fracture). Unfortunately, there is no good theoretical or practical method to refine this value. Engineering intuition and previous experience are critical to judging whether a significant arrest of fracture propagation is even possible in a given formation.

There is also no clear procedure to predict if TSO width inflation will be possible in a given formation, though rock mechanics laboratory investigations can suggest the answer. The formation needs to be “soft enough”; in other words, the elasticity modulus cannot be too high. On the other hand, soft formations are often unconsolidated, lacking significant cohesion between the formation grain particles. The main technical limitation to keep in mind is the net pressure, which increases during width inflation. The design engineer should be prepared to depart from the theoretical optimum placement if necessary to keep the fracture treating pressure below critical limits imposed by the equipment.

Another consideration in TSO design is that the created fracture must bypass the assumed damaged region near the wellbore. As such, the design should specify a minimum target length, even if the theoretical optimum calls for a shorter fracture. Often the minimum length is on the order of 50 ft, while the nature of the damage and the length of the perforated interval may dictate other values. Note that this departure from the optimum again can be realized by specifying the “multiply optimum length by a factor” parameter in the provided design software.

PUMPING A TSO TREATMENT

Anecdotal observations related to real-time HPF experiences are abundant in the literature and are not the focus of an engineering-operations text such as this. However, some observations related to treatment execution are in order:

- Most treatments are pumped using a gravel pack service tool in the “circulate” position with the annulus valve closed at the surface. This allows for live annulus monitoring of bottomhole pressure (annulus pressure + annulus hydrostatic head) and real-time monitoring of the progress of the treatment.

- When there is no evidence of the planned TSO on the real-time pressure record, the late treatment stages can be pumped at a reduced rate to effect a tip screenout. Obviously, this requires reliable bottomhole pressure data and direct communication by the frac unit operator.
- Near the end of the treatment, the pump rate is slowed to gravel packing rates and the annulus valve is opened to begin circulating a gravel pack. The reduced pump rate is maintained until tubing pressure reaches an upper limit, signaling that the screen-casing annulus is packed.
- Because very high proppant concentrations are employed, the sand-laden slurry used to pack the screen-casing annulus must be displaced from surface with clean gel, well before the end of pumping. Thus, proppant addition and slurry volumes must be metered carefully to ensure there is sufficient proppant left in the tubing to place the gravel pack (i.e., to avoid over-displacing proppant into the fracture).
- Conversely, if an HPF treatment sands out prematurely (i.e., with proppant in the tubing), the service tool can be moved into the “reverse” position and the excess proppant circulated out.
- Movement of the service tool from the squeeze/circulating position to the reverse position can create a sharp instantaneous drawdown effect and should be done carefully to avoid swabbing unstabilized formation material into the perforation tunnels and annulus.

Swab Effect Example

The following simple equation, given by Mullen et al. (1994) can be used to convert swab volumes into oilfield unit flow rates:

$$q_s = 2,057 \frac{V_s}{t_m} \quad (7-19)$$

where q_s is the instantaneous swab rate in bbl/day, V_s is the swabbed volume of fluid in gal, t_m is the time of tool movement in seconds, and 2,057 is the conversion factor for gal/sec to bbl/day.

The volume of swabbed fluid is calculated from the service tool diameter and the length of stroke during which the sealed service tool does not allow fluid bypass. The average swab volume of a 2.68 in. service tool is 2.8 gal when the service tool is moved from the squeeze position to the reverse-circulation position. Assuming a rather normal movement time of 5 sec, this represents an instantaneous production rate of 1,100 bbl/day.

Perforations for HPF

It is widely agreed that establishing a conductive connection between the fracture and wellbore is critical to the success of HPF, but no consensus or study has emerged that gives definitive direction.

With an eye toward maximizing conductivity and fluid flow rate, many operators shoot the entire target interval with high shot density and large holes (e.g., 12 shots per foot with “big hole” charges). Other operators—more concerned with multiple fracture initiations, near-well tortuosity, and perforations that are not packed with sand—take the extreme opposite approach, perforating just the middle of the target interval with a limited number of 0° or 180° phased perforations. Arguments are made for and against underbalanced versus overbalanced perforating: underbalanced may cause formation failure and “sticking the guns;” overbalanced eliminates a cleanup trip but may negatively impact the completion efficiency.

Solvent or other scouring pills are commonly circulated to the bottom of the workstring and then reversed out to remove scale, pipe dope, or other contaminants prior to pumping into the formation. Several hundred gallons (e.g., 10 to 25 gallons per foot) of 10 to 15 percent HCl acid will then be circulated or bullheaded down to the perforations and be allowed to soak (i.e., to improve communication with the reservoir by cleaning up the perforations and dissolving debris in the perforation tunnel). Some operators are beginning to forego the solvent and acid cleanup (obviously to reduce rig time and associated costs). Their presumption is that the damaging material is pumped deep into the formation and will not seriously impact well performance.

PRE-TREATMENT DIAGNOSTIC TESTS FOR HPF

There are several features unique to high permeability fracturing which make pre-treatment diagnostic tests and well-specific design strategies

highly desirable if not essential: fracture design in soft formations is very sensitive to leakoff and net pressure; the controlled nature of the sequential tip screenout/fracture inflation and packing/gravel packing process demands relatively precise execution strategies; and the treatments are very small and typically “one-shot” opportunities. Furthermore, methods used in hard-rock fracturing to determine critical fracture parameters *a priori* (e.g., geologic models, log and core data, or Poisson ratio computational models based on poroelasticity) are of limited value or not yet adapted to the unconsolidated, soft, high permeability formations.

There are three tests (with variations) that form the current basis of pre-treatment testing in high permeability formations: step-rate tests, minifrac tests, and pressure falloff tests.

Step-Rate Tests

The step-rate test (SRT), as implied by the name, involves injecting clean gel at several stabilized rates, beginning at matrix rates and progressing to rates above fracture extension pressure. In a high permeability environment, a test may be conducted at rate steps of 0.5, 1, 2, 4, 8, 10, and 12 barrels per minute, and then at the maximum attainable rate. The injection is held steady at each rate step for a uniform time interval (typically 2 or 3 minutes at each step).

In principle, the test is intended to identify the fracture extension pressure and rate. The stabilized pressure (ideally bottomhole pressure) at each step is classically plotted on a Cartesian graph versus injection rate. Two straight lines are drawn, one through those points that are obviously *below* the fracture extension pressure (dramatic increase in bottomhole pressure with increasing rate), and a second through those points that are clearly *above* the fracture extension pressure (minimal increase in pressure with increasing rate). The point at which the two lines intersect is interpreted as the fracture extension pressure. The dashed lines on Figure 7-11 illustrate this classic approach.

While the conventional SRT is operationally simple and inexpensive, it is not necessarily accurate. A Cartesian plot of bottomhole pressure versus injection rate, in fact, does not generally form a straight line for radial flow in an unfractured well. Simple pressure transient analysis of SRT data using desuperposition techniques shows that with no fracturing the pressure versus rate curve should exhibit upward concavity. Thus, the departure of the real data from ideal behavior may occur at a pressure and rate well below that indicated by the classic intersection of the straight lines (see Figure 7-11).

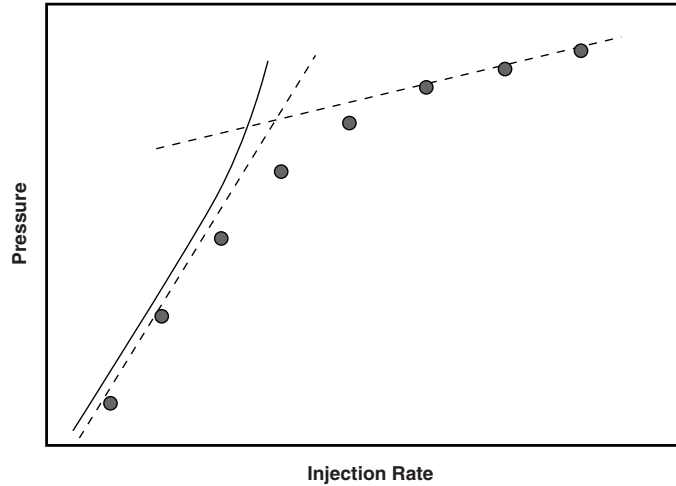


FIGURE 7-11. Ideal SRT—radial flow with no fracturing.

The two-SRT procedure of Singh and Agarwal (1988) is more fundamentally sound. However, given the relatively crude objectives of the SRT in high permeability fracturing, the conventional test procedure and analysis may be sufficient.

The classic test does provide an indication of several things:

- Upper limit for fracture closure pressure (useful in analysis of minifrac pressure falloff data).
- Surface treating pressure that must be sustained during fracturing (or whether sustained fracturing is even possible with a given fluid).
- Reduced rates that will ensure no additional fracture extension and packing of the fracture and near-wellbore with proppant (aided by fluid leakoff).
- Perforation and/or near wellbore friction, which is seldom a problem in soft formations with large perforations and high shot densities.
- Casing pressure that can be expected if the treatment is pumped with the service tool in the circulating position.

A step-down option to the normal SRT is sometimes used specifically to identify near-wellbore restrictions (tortuosity or perforation friction). This test is done immediately following a minifrac or other pump-in stage. By observing bottomhole pressure variations with decreasing rate, near-wellbore restrictions can be immediately detected (i.e., bottomhole pressures that change only gradually as injection rate is reduced sharply in steps is indicative of *no restriction*).

Minifrac

Following the SRT, a minifrac should be performed to tailor the HPF treatment with well-specific information. This is the critical diagnostic test. The minifrac analysis and treatment design modifications can typically be done on-site in less than an hour.

Concurrent with the rise of HPF, minifrac tests, and especially the use of bottomhole pressure information, have become much more common. Otherwise, the classic minifrac procedure and primary outputs as described in the preceding section (i.e., determination of fracture closure pressure and a bulk leakoff coefficient) are widely applied to HPF, this in spite of some rather obvious shortcomings.

The selection of closure pressure, a difficult enough task in hard rock fracturing, can be arbitrary or nearly impossible in high permeability, high-fluid-loss formations. In some cases, the duration of the closure period is so limited (one minute or less) that the pressure signal is masked by transient phenomena. Deviated wellbores and laminated formations (common in offshore U.S. Gulf Coast completions), multiple fracture closures, and other complex features are often evident during the pressure falloff. The softness of these formations (i.e., low elastic modulus) means very subtle fracture closure signatures on the pressure decline curve. Flowbacks are not used to accent closure features because of the high leakoff and concerns with production of unconsolidated formation sand.

New guidelines and diagnostic plots for determining closure pressure in high-permeability formations are being pursued by various practitioners and will eventually emerge to complement or replace the standard analysis and plots.

The shortcomings of classic minifrac analysis are further exposed when used (commonly) to select a single effective fluid loss coefficient for the treatment. As described above, in low permeability formations this approach results in a slight overestimation of fluid loss and actually provides a factor of safety to prevent screenout. In high

permeability formations, the classic approach can dramatically underestimate spurt loss (zero spurt loss assumption) and overestimate total fluid loss. This uncertainty in leakoff behavior makes the controlled timing of a tip screenout very difficult. Entirely new procedures based on sound fundamentals of leakoff in HPF (as outlined in Chapter 5) are ultimately needed. The traditional practice of accounting for leakoff with a bulk leakoff coefficient is simply not sufficient for this application.

Pressure Falloff Tests

A third class of pre-treatment diagnostics for HPF has emerged that is *not* common to MHF: pressure falloff tests. Owing to the high formation permeability, common availability of high quality bottom-hole pressure data, and multiple pumping and shut-in cycles, matrix formation properties including k_h and skin can be determined from short duration pressure falloff tests using the appropriate transient flow equation. Chapman et al. (1996) and Barree et al. (1996) propose pre-frac or matrix injection/falloff tests that involve injecting completion fluid below fracturing rates for a given period of time, and then analyzing the pressure decline using a Horner plot.

The test is performed using standard pumping equipment and poses little interruption to normal operations. A test can normally be completed within one hour or may even make use of data from unplanned injection/shut-in cycles.

The resulting permeability certainly relates to fluid leakoff as described in Chapter 5 and allows the engineer to better anticipate fluid requirements. An initial skin value is useful in “benchmarking” the HPF treatment and for comparison with post-treatment pressure transient analysis.

Bottomhole Pressure Measurements

A discussion of pre-treatment diagnostic tests requires a discussion of the source of pressures used in the analysis. Implicit to the discussion is that the only meaningful pressures are those adjacent to the fracture face, whether measured directly or translated to that point. There are at least four different types of bottomhole pressure data, depending on the location at which the real data are taken:

- Calculated bottomhole pressure—implies bottomhole pressure calculated from surface pumping pressure.
- Deadstring pressure—open annulus, bottomhole pressure deduced knowing density of fluid in annulus; tubing may also be used as dead string when treatment is pumped down the casing.
- Bundle carriers in the workstring—measured downhole, but above the service tool crossover.
- Washpipe data—attached to washpipe below service tool crossover.

Washpipe pressure data is the most desirable for HPF design and analysis based on its location adjacent to the fracture and downstream of all significant flowing pressure drops. Workstring bundle carrier data can introduce serious error in many cases because of fluid friction generated through the crossover tool and in the casing-screen annulus. Without detailed friction pressure corrections that account for specific tool dimensions and annular clearance, there is a possibility for a significant departure between washpipe and workstring bundle carrier pressures. Deadstring pressures are widely used and considered acceptable by most practitioners; some others suggest that redundant washpipe pressure data has shown that the deadstring can mask subtle features of the treatment. The use of bottomhole transducers with real-time surface readouts is suggested in cases where a dead string is not feasible or when well conditions (e.g., transients) may obscure important information.

Reliance on bottomhole pressures calculated from surface pumping pressure is not recommended in HPF. The combination of heavy sand-laden fluids, constantly changing proppant concentrations, very high pump rates, and short pump times makes the estimation of friction pressures nearly impossible.

